

Sheffield Hallam University

Electrical studies on new generations of oxide cathodes for CRT applications.

HASHIM, Abbass A.

Available from the Sheffield Hallam University Research Archive (SHURA) at:

<http://shura.shu.ac.uk/19767/>

A Sheffield Hallam University thesis

This thesis is protected by copyright which belongs to the author.

The content must not be changed in any way or sold commercially in any format or medium without the formal permission of the author.

When referring to this work, full bibliographic details including the author, title, awarding institution and date of the thesis must be given.

Please visit <http://shura.shu.ac.uk/19767/> and <http://shura.shu.ac.uk/information.html> for further details about copyright and re-use permissions.

CITY CAMPUS, HOWARD STREET
SHEFFIELD S1 1WB



REFERENCE

ProQuest Number: 10697069

All rights reserved

INFORMATION TO ALL USERS

The quality of this reproduction is dependent upon the quality of the copy submitted.

In the unlikely event that the author did not send a complete manuscript and there are missing pages, these will be noted. Also, if material had to be removed, a note will indicate the deletion.



ProQuest 10697069

Published by ProQuest LLC (2017). Copyright of the Dissertation is held by the Author.

All rights reserved.

This work is protected against unauthorized copying under Title 17, United States Code
Microform Edition © ProQuest LLC.

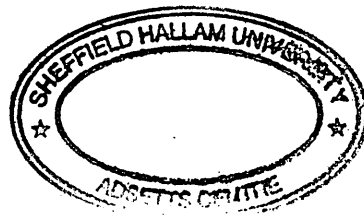
ProQuest LLC.
789 East Eisenhower Parkway
P.O. Box 1346
Ann Arbor, MI 48106 – 1346

**ELECTRICAL STUDIES ON NEW GENERATIONS OF
OXIDE CATHODES FOR CRT APPLICATIONS**

ABBASS A HASHIM

B.Sc., M.Sc.

**A thesis submitted in partial fulfilment of the requirements of
Sheffield Hallam University
for the degree of Doctor of Philosophy**



June, 2005

Declaration

I certify that this thesis submitted for the degree of Ph.D. is a result of my own research, except where otherwise acknowledged, and that this thesis has not been submitted for a higher degree to any other university or institution.

Signed:-----

ABBASS A HASHIM

Date: 29 /06/2005

ABSTRACT

A systematic study has been made of two novel types of BaO/SrO oxide cathode with 5% and 2.5% addition of Ni powder by weight on a Ni cap containing an activating impurity. The emission and conductivity characteristics of oxide cathodes depend largely on the activation process. In this thesis the electrical properties of these new types of oxide cathodes, supplied by LG Philips Displays, have been investigated in relation to the different activation processes. Scanning electron microscopic techniques were employed to study the surface morphological changes of the oxide cathodes and nickel caps as a result of cathode activation extending over periods of 1–12 *hrs*. Elemental analysis of barium, strontium, tungsten, magnesium and aluminum was obtained from the energy dispersion x-ray spectroscopy.

The conductivity and the electron activation energy were studied as a function of temperature in the range 300–1200 *K* after conversion and activation of the cathode at 1200 *K* for one hour and accelerated up to 600 *hrs* at a temperature of 1100 *K*. Experimental results yield three values for the electron activation energy of 1.49, 2.38 *eV* and 3.3 *eV*. The conduction mechanisms observed a metallic conduction at low temperature (300–500) *K* after operation for several hundred hours due to improvements in the Ba coverage layer on the grains of oxide layer. The influence of different durations on the activation process has been investigated at three activation temperatures (1125 *K*, 1200 *K*, 1425 *K*). SEM and EDX analysis show a structural phase transformation in the oxide material. The activator agents W and Al are shown to penetrate the BaO/SrO layer in two different ways.

The formation of compounds associated with the diffusion of reducing elements (Mg, Al and W) to the Ni cap surface of oxide cathode through hundreds of cathode acceleration hours has been studied by a new method. This method used two cathodes, one of them is coated and the other is uncoated, in an attach-contact configuration mounted in a dummy tube.

The D.C electrical characteristics show a very strong rectifying behavior through the Metal-Semiconductor junction (M-S junction) due to the I/V curves. The characteristics are found to be reversible and reproducible, and gave a rectification ratio (r) of 100. The calculated value of ideality factor indicated $n = 9.6$, which is evidence of tunnelling conduction.

ACKNOWLEDGEMENTS

I am deeply indebted to Professor D. S. Barratt, LG Philips Displays-Blackburn, for initially giving me the opportunity to undertake a Ph.D. course in the Material Engineering Research Institute, Centre for Electronic Devices and Materials, Sheffield Hallam University, and for kindness support and supervision throughout my studies. My special appreciation is also to LG Philips Displays components company- Blackburn for their fund and support to this project.

A special thanks to Dr A.K. Hassan and A.V. Nabok Centre for Electronic Devices and Materials, Sheffield Hallam University, for their help and guidance.

I would like to express my gratitude and thanks to MRI (Material Research Institute), Sheffield Hallam University and especially to Mr. D. Horsefield, Miss K. Rhodes, Mr. L. Bowen, Mr. S. Creasey and Mr. A. Williams from Electron Microscopy Support section. My special thanks also go to the senior technicians Mr. Ken Duty and Brian Disbury from School of Engineering, Sheffield Hallam University.

I extend my appreciation to all of my fellow Ph.D. colleagues for their help and friendship during the course of my study and wish them all the best for their future in particular Mr. A. Vale and Mr. A. Holloway for their special help.

A special thank and grateful to my best friend Professor M T Mohammad for more than twenty five years of encouragement and help.

I also wish to express my special thank to my brother Hashim Hashim without him I couldn't be here from the beginning.

Finally I would like to thank my special lady and my wife Mrs Hiam Ahmad for her kindness patience and support all the way through my study and my life.

Contents

Abstract

Acknowledgements

Contents

Key of symbols

Chapter 1

Introduction and the Aims of the Work

| | |
|--|---|
| 1.1 Improvement of the display technology | 1 |
| 1.2 Competition for an advanced cathode | 2 |
| 1.3 The recent emission current density enhancements | 3 |
| 1.4 Aims and objectives of the study | 5 |

Chapter 2

LITERATURE REVIEW AND THE CONDUCTION THEORIES

| | |
|---|----|
| 2.1 The early discovery of the oxide cathode | 7 |
| 2.2 BaO/SrO as a semiconductor | 7 |
| 2.3 The Hall coefficient measurements | 9 |
| 2.4 Direct determination of electrical conductivity of oxide cathodes | 11 |
| 2.5 Elements behavior and structures in the oxide material | 14 |
| 2.6 The emission lifetime studies | 20 |
| 2.7 Element analysis and technique | 23 |
| 2.8 Ba effect on the conductivity and emission of the oxide cathode | 28 |
| 2.9 The addition of Ni powder | 29 |
| 2.10 Phenomena of basic emission | 33 |
| 2.11 The effect of the interface layer | 33 |
| 2.12 Thermionic mechanism models | 35 |
| 2.12.1 Ba mono-atomic layer model | 35 |
| 2.12.2 Donor model | 35 |

| | | |
|--------|--|----|
| 2.13 | The conduction theories of oxide-coated cathode | 36 |
| 2.14 | Conduction mechanism in the oxide cathodes according to Loosjes and Vink | 37 |
| 2.14.1 | Interpretation of I/V measurements (The model) | 38 |
| 2.14.2 | Interpretation of the I/V measurements | 40 |
| 2.15 | Relationship between thermionic emission and electrical conductivity of oxide-coated cathode | 45 |
| 2.15.1 | The characteristics of "N" type and "S" type cathodes | 45 |
| 2.15.2 | M-type conduction | 48 |
| 2.16 | The theory of oxide-coated cathode | 51 |
| 2.16.1 | The characteristics of the oxide coated cathode | 51 |
| 2.16.2 | The theory of the conduction filament | 53 |
| 2.17 | Electronic processes in oxide cathode | 57 |
| 2.17.1 | Ion adsorption effects | 57 |
| 2.17.2 | Simplified analysis of an idealized model | 58 |
| 2.18 | Conduction mechanisms and Narita theory | 64 |

Chapter 3

Industrial cathodes preparation and experimental technique

| | | |
|-------|--|----|
| 3.1 | Introduction | 72 |
| 3.2 | Cathode assembly | 72 |
| 3.3 | Industrial preparation techniques of cathode devices | 74 |
| 3.4. | Cathode Activation | 75 |
| 3.5 | The chemical reaction mechanisms through the cathode operation life time | 76 |
| 3.6 | Accelerated life by increased operating temperature | 77 |
| 3.7 | Experimental technique and the measurement method | 79 |
| 3.7.1 | Cathode to cathode in a vacuum chamber | 79 |
| 3.7.2 | Spectroscopy analysis | 84 |
| 3.7.3 | Coated-non coated cathode assembly in an evacuated dummy tube | 85 |

Chapter 4

Acceleration life time test

| | |
|-------------------------------------|----|
| 4.1 Introduction | 90 |
| 4.2 Experimental measurements | 91 |
| 4.2.1 Acceleration D.C. measurement | 92 |
| 4.2.2 Acceleration A.C. measurement | 99 |

Chapter 5

Formation of an interface layer in thermionic oxide cathodes for CRT applications

| | |
|---|-----|
| 5.1 Introduction | 102 |
| 5.2 The activation of the cathode on the optimized temperature | 104 |
| 5.3 The experimental analysis for the optimized temperature | 105 |
| 5.3.1 Morphological and elemental analysis | 105 |
| 5.3.2 D.C. Electrical characterisation | 113 |
| 5.4 Optimisation of parameters for activation of oxide cathodes | 118 |
| 5.4.1 Structural and elemental analysis | 119 |
| 5.4.2 Electrical properties | 127 |

Chapter 6

Electron conduction associated with the chemical transport of reducing elements in oxide cathode

| | |
|--|-----|
| 6.1 Introduction | 133 |
| 6.2 The metal-semiconductor junction and Schottky effect | 136 |
| 6.3 Result and discussion | 137 |
| 6.3.1 Morphological and elemental analysis | 137 |
| 6.3.2 D.C. Electrical characterization | 142 |

Chapter 7

Conclusions, further work and resistivity network model

| | |
|---|-----|
| 7.1 Oxide cathode characteristics for CRT application | 150 |
| 7.2 Electrical measurement and conduction properties | 151 |
| 7.3 Morphological and elemental analysis | 152 |
| 7.4 Resistivity network model | 154 |
| 7.5 Suggestions and future work | 160 |

References

Appendix

Key of symbols

e : the electron charge.

k : the Boltzman's constant.

Error! Objects cannot be created from editing field codes.: the work function at Error! Objects cannot be created from editing field codes..

τ : the emission life.

J : the current density in general.

α : the temperature coefficient.

E_a : the Activation energy.

N_d : the donor concentration.

E_d : is the donor level from the bottom of the conduction band.

χ : the electron affinity.

A : the Richardson constant (theoretical value is $120.4 \text{ A / cm}^{-2} \text{ K}^{-2}$).

σ : the conductivity in general.

ρ : the resistivity in general.

σ_{el} : the electrical conductivity.

I_e : the DC current.

R : the resistance in general.

Φ_e : the electron work function.

I_s : the saturation current.

σ_o : is the specific conductivity at $T = \infty$.

$e\phi$: the activation energy.

F : the applied field.

a : the electron acceleration.

m : the electron mass.

\bar{v} : the mean velocity.

t : the time.

$\overline{\Delta v}$: is the variation in the mean velocity.

l : the mean free path.

J_s : the saturation current density.

Y : the dimensionless constant.

G : the conductance.

a_i : is the cross-sectional area of the conducting part of the grains.

L : is the thickness of the coating.

λ : the Debye length.

ξ : is the space-charge density in coulombs/cm^3 .

L : is the approximate depth of the surface layer.

D : the grain size.

n_e : the effective electron density.
 X : the coordinate.
 Q : is the total space charge in (coulomb/cm²).
 n_a : the apparent electron density.
 μ, μ_e : the electron mobility.
 n_b : the beginning electron density.
 σ_0 : is the conductivity of the oxide layer.
 σ_i : is the conductivity of the interface layer.
 η : is the thickness ratio of the interface layer t_i to the oxide coating t_o .
 N_e : is the number of excess barium.
 r : the reflection coefficient.
 R_H : the Hall coefficient.
 R_i : the interface resistance.
 R_o : is the activated oxide layer resistance.
 $\sigma_{DC}(T)$: is the direct current (or the static, $\omega = 0$).
 ω : the frequency.
 m^* : the electron effective mass.
 h : the Planck's constant.
 n : is the ideality factor.
 r : is the rectification ratio.
 C : the capacitance.

Chapter 1

Introduction and the Aims of the Work

1.1 Improvement of the display technology

In recent years and despite improvements in alternative technologies (in particular LCD and other flat panel technologies) the cathode ray tube has remained one of the most cost-effective means of displaying moving picture images for television and computer applications. Nonetheless, the requirement from the picture tubes themselves has changed in recent years with the introduction of new applications such as internet TV and game consoles. Thus, modern television tubes face increasing demands for higher resolution and brightness together with reduced depth (slim TV). These, in turn, place additional burdens on the cathodes and the trends are towards higher current densities (ideally at lower operating temperatures), and greater robustness particularly in terms of ion bombardment and poisoning sensitivity.

Despite considerable work over the years on alternative technologies, the oxide cathode remains the workhorse of the cathode ray tube (CRT) industry and has itself been the focus of considerable research activity [Gäertner et al, 2003]. The requirements for improved performance from CRTs in terms of brightness and resolution will certainly continue into the future and the challenge for cathode and gun designers is to meet these performance

demands. In particular, there is a requirement to study new materials and processing methods and these form the basis for the work described herein.

1.2 Competition for an advanced cathode

One of the more significant advances in recent times has involved the work of L.G. Philips Display Components and their development of new compositions for the emissive layer of their oxide cathodes. The Philips Company is one of the largest manufacturers involved in the development of cathode technology, cathode materials and the emitter layers. The industry is continuously looking for high brightness and high resolution cathode ray tubes, by enhancement of the current density of the cathode, which is one of the most important factors. The display market has witnessed the emergence of new technologies such as the flat panel and liquid crystal displays. However, CRTs are anticipated to remain as one of the most dominant display technology for the foreseeable future.

At present there are two principal competing cathode technologies used in CRT displays. One is the well-established oxide cathode which has the lowest manufacturing cost, but with a maximum emission current of order of a few A/cm^2 , and the other is the I (impregnated) or dispenser cathode which offers substantially higher emission performance (of the order $10 A/cm^2$) but with dramatically increased manufacturing costs and complexity.

There is therefore a significant advantage, both for the manufacturers and users of CRT-based display technologies, if an alternative form of cathode

can be developed which allows the emission performance of the cathode to be achieved at substantially reduced cost. This will require a new approach to the cathode design and manufacture, particularly with regard to the materials processing.

As the source of electrons, the cathode is an essential component of all oxide cathode ray tubes.

The mature technology of the oxide cathode in recent years is the emerging requirements for high resolution and readability of displays which have reached the limits of capability for conventionally used materials in the oxide cathode, in particular the long term sustainable emission current and the emission lifetime under high current loading. These limitations are thought to be largely due to the relatively limited conductivity of the oxide and the resultant effects of localized resistive heating within the oxide layer as high emission currents are drawn through it.

1.3 The recent emission current density enhancements

One approach to an enhancement in the emission current density is to reduce the cathode coating resistivity by the incorporation of a conductive metallic phase, which produces a reduction in the surface work function. This has been studied by a number of workers [Uda et al, 1999, Hodgson et al, 1999, Gärtner, 1992 and Narita, 1995].

The provision of a low work function is dependent on the change in the equilibrium rates of Ba formation and deposition. This mechanism is responsible on the high current density. Aside from the requirements of long

life, low power consumption and operation at an acceptably low temperature, an important feature is the cathode emission current density. This current density directly determines the maximum current density that can be obtained in the focused spot of the electron beam and in the CRT image [Hermann et al, 1951].

Also to reduce the cathode coating resistivity, Hayashida and his colleagues [1999] used the dopant of earth alkaline elements of group III, IV or V, which led to an increase in the electrical conductivity of the emitter layer.

There has also been an increasing demand for higher performance cathode for colour picture tubes for computer displays and for wide screen TV. These commercial and economic pressures have demanded that such emission improvements should be associated with increases in raw materials or component costs.

Ba dispenser cathodes are increasingly used in high-resolution TV and monitor tubes due to their copious emission and the absence of load limitations as experienced in the case of oxide cathodes.

Over the years, Barium Oxide composition played the main role in the emission and conduction mechanism of the oxide coated cathode.

For many years oxide cathodes have been almost universally used in the cathode ray and other electronic beam vacuum tubes. At present, the oxide cathode is still of considerable practical importance as an electron emitter. In many papers, simple models are proposed to explain the electronic processes in an oxide cathode through simplified analysis, estimation and correlations of the observed characteristics with the experimentally obtained parameters.

In the case of oxide coatings, several investigations have concluded that the electron emission and the electrical conductivity of an oxide coated cathode are linearly related to each state of cathode activation [Hannay et al, 1949].

1.4 Aims and objectives of the study

LG Philips have brought out a new commercial generation of oxide cathodes, known as oxide cathode, and oxide cathode plus. The aim of the current study is to investigate experimentally, the electrical properties of these novel cathodes and to map the elements contained therein, in order to optimise their material structural composition.

The current project involves a wide range of investigations into two different types of cathodes in order to determine the conductivity and the variation in the structural morphology of the oxide coating and the Ni cap base. These investigations include the different conduction mechanisms studied by employing DC and AC measurement techniques.

In order to fulfil the above aim, the following objectives were achieved:

1. Activation and operation processes were optimized by subjecting the cathodes to heat treatments at different temperatures and for different periods of time.
2. A cathode tube assembly was designed and developed for electrical characterisation under sealed high vacuum conditions with a new interface layer investigation method.
3. Scanning electron microscopy (SEM) and energy dispersion x-ray spectroscopy (EDX) were employed to investigate the effects of different cathode activation processes on the structural properties of the oxide coating.

The reactions that take place inside and between the layers and the Ni-cap were also examined.

4. AC and DC electrical measurements were performed on activated cathodes and a physical interpretation of the results was obtained in terms of transport mechanisms, relative contribution of constituent components (for example pores) and structural morphology.

5. The continuous growth of the interface layer between the oxide layer and the cap was examined by measuring the conductivity of the cathode when operated for a prolonged period of time.

Chapter 2

LITERATURE REVIEW AND THE CONDUCTION THEORIES

2.1 The early discovery of the oxide cathode

It is known from the work of Wehnelt [1904] that the electron emission from a heated platinum wire could be increased by many orders of magnitude if it was coated with a mixture of strontium and barium oxide. Numerous changes were introduced in the structure of the cathode, but these oxide materials still remain the major ingredients of the cathode in almost all present CRTs.

2.2 BaO/SrO as a semiconductor

(Ba, Sr)O was characterised as a reduction semiconductor because of the increase in conductivity obtained [Hannay, 1949]. Hence, very probably as an electronic semiconductor, the conduction electrons originated from a stoichiometric excess of (Ba, Sr) atom in solid solution. The electrical conductivity and the thermionic emission of (Ba, Sr)O cathodes are directly proportional to each other by three orders of magnitude [Chin et al, 1974]. Well-defined chemical and electrical activation and deactivation procedures were used to obtain this result. It was inferred that activation represented an increase in the chemical potential of the electrons in the oxide, with little or no change occurring in the state of the surface. It was also found that a deviation from the proportionality of conductivity and emission was expected under

such conditions leading to inhomogeneity in the oxide. This observation was also in agreement with semi-conductor theory [Hannay, 1949].

Cathode performance when operated for several months was reduced [Leblond et al, 1994]. The photocathode studied was a standard thermionic trioxide cathode, containing a bulk concentration of 4%W ($BaCO_3$, 56%; $CaCO_3$, 31%; $SrCO_3$, 31%). After conditioning in which this type of cathode was held at about $1000^\circ C$ for some minutes, the carbonates were converted into oxides. Free atoms of Ba, Ca and Sr diffuse to the surface leading to small islets of BaO, CaO and SrO covered by atoms of Ba, Ca and Sr. Under these conditions the oxide becomes a highly N-type degenerated semiconductor [Leblond et al, 1994].

The best description of the bulk oxide layer is an impurity n-type semiconductor of high conductivity (only small voltage drops) in its active state. Figure 2.1 shows the energy band diagram for the BaO at thermodynamic equilibrium [Nergaard 1952]. The energy band gap is about $3.8-4.4 eV$, and donor levels lie at $1.4 eV$ and $2 eV$ below the conduction band.

At temperatures $>700 K$ additional pore conductivity by the electron gas contributes to the overall performance.

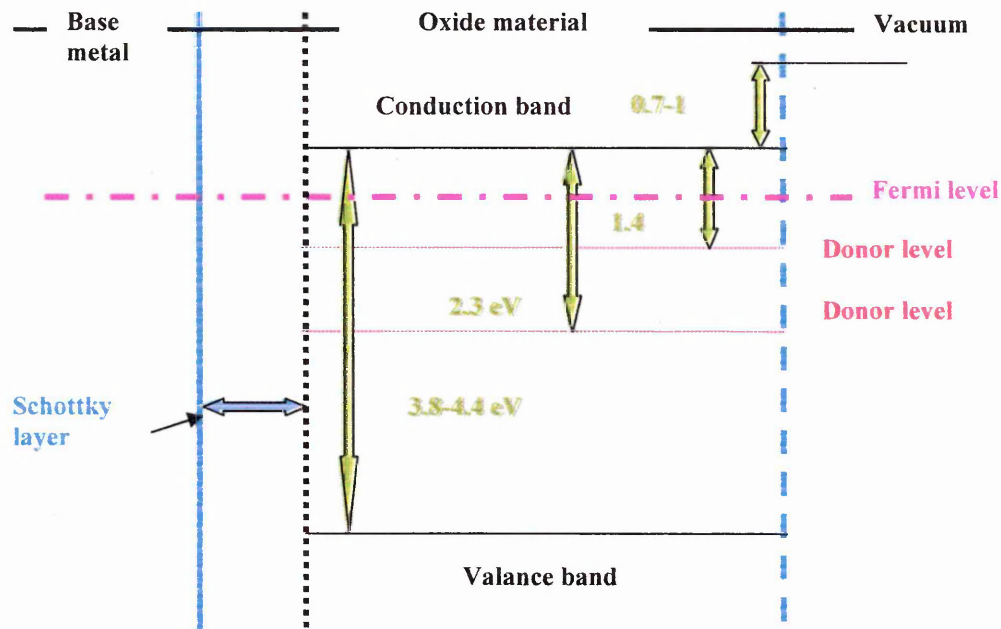


Figure 2.1: Energy band diagram of BaO [Nergaard, 1952]

2.3 Hall Coefficient Measurements

It was found from Hall coefficient R_H measurements, that in the double barium-strontium oxide, the conductivity σ below about 850 K was P-type, and $\log \sigma$ and $\log R_H$ against $1/T$, both had slopes near $0.7 eV$ [Wright, 1949]. Also near this point there was a P-N transition, above which the slope of $\log \sigma$ was $0.8 eV$, while the slope of $\log R_H$ was $1.1 eV$, as shown in Figure 2.2. There was probably, therefore, a change of electron mobility with temperature in this range. The value of σ in this range depended on the activation procedure immediately before measurement. Higher values were obtainable after high current density activation. There were considerable time changes following an activation treatment, especially above 1050 K, which he believed to be due to evaporation of free barium formed during activation.

According to Redington [1952], the diffusion of Ba in BaO took place by two types of mechanisms. Mechanisms involved either were charge-transport or non charge transport and defects were responsible for both processes.

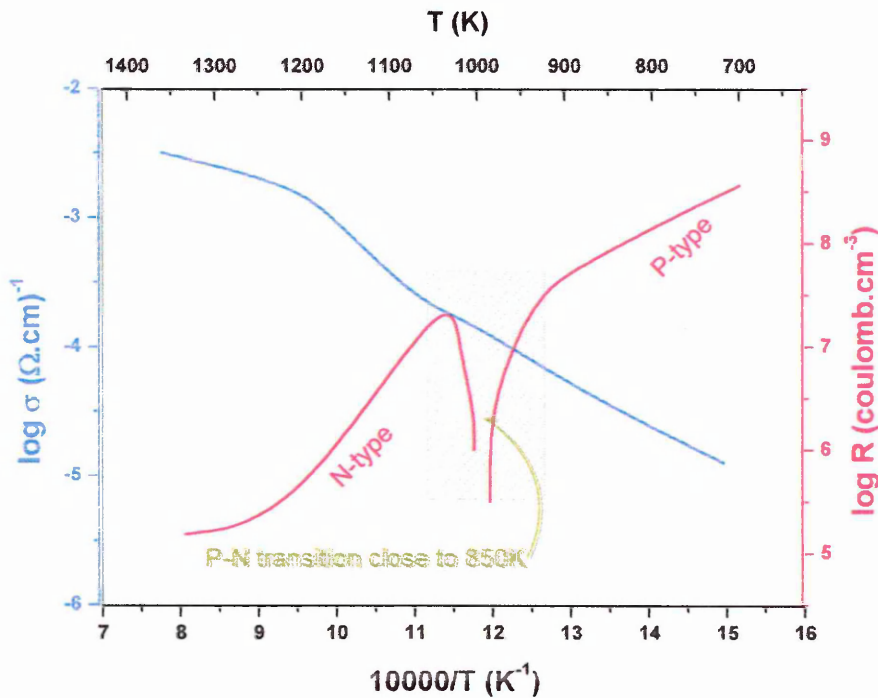


Figure 2.2: Dependence of conductivity and Hall coefficient on temperature [Wright, 1949].

Six types of defects were considered (barium vacancies, interstitial barium atoms, interstitial barium ions, bound pairs of barium, oxygen vacancies, and a linear or laminar defect) only the combination of the interstitial atom and the barium vacancy gave a phenomenologically correct account of the experimental observations [Redington, 1952].

The Hall coefficient of the oxide cathode was negative and had a maximum value in the range 600 to 800 K [Forman, 1954]. Above 700 K the value of

electron mobility was very large, and below $700K$ the mobility decreased rapidly with decreasing temperature. Large magneto-resistive effects were observed, and these were found to be dependent on the temperature and the degree of porosity of the cathode. These results were consistent with the porous semiconductor model for the oxide cathodes as originally suggested by Loosjes and Vink [1949].

2.4 Direct determination of electrical conductivity of oxide cathodes

Using a similar method to Loosjes and Vink, a close correspondence between the high temperature activation energy and the work function of the cathode was found. Shepherd [1953], took that as evidence for a crystal-to-crystal emission process in the coating providing electron transport at high temperature. By considering the effect of oxygen on the electrical properties of oxide cathodes, the formation of singly charged oxygen ions in the cathode coating was found to play a major role in the recovery process.

The electrical conductivity σ_{el} of the oxide layer was determined directly in a new procedure in a close-planar diode configuration in a UHV chamber, together with thermionic emission data. The cathode temperature measured, as a function of continuous dc-load is essentially the result of a superposition of electron emission cooling-proportional to the dc-current and ohmic heating proportional to the square of dc-current. The compensation point between electron emission cooling and ohmic heating σ_{el} can be determined directly from the emission data, as shown in Figure 2.3. At the compensation point

between electron emission cooling [Gärtner et al, 1986] and ohmic heating, σ_{el} can be determined directly from the resistance R of the oxide layer, as in the formula:

$$RI_e^2 = I_e \left[\Phi_e + \frac{kT}{e} \ln \left(\frac{I_s}{I_e} \right) + \frac{2kT}{e} \right] \quad (2.1)$$

After activation, a result of about $10^{-2} (\Omega.cm)^{-1}$ at $780^\circ C$ true temperature was obtained from BaSr oxide cathodes, which was consistent with literature. It was shown that electrical conductivity decreases with operation time in accordance with reducing Ba generation. σ_{el} can be increased with an oxide dopant like Yttrium or Europium [Gärtner et al, 2002].

Loosjes-Vink theory on the high-temperature conduction through the oxide cathode coating was further supported by the work of Tomlinson [1954]. Using a special diode with embedded probes the measured I/V characteristics of such coatings were generally linear for temperatures above $700K$ and curved at lower potentials. The presence of space charge in the pores of the coating was predicted at temperatures above $700K$. The calculated work function in the range of temperature ($T > 700K$) was about $0.8 - 1.17 eV$.

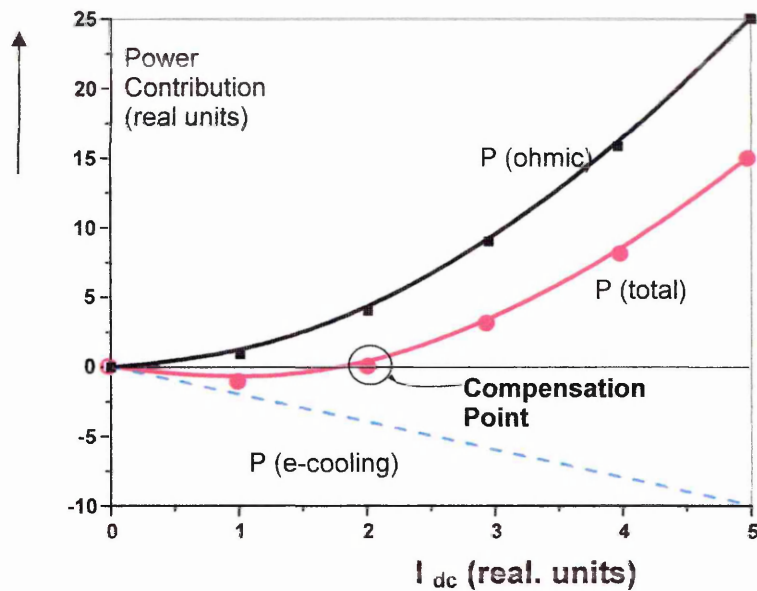


Figure 2.3: Schematic diagram illustrating the superposition of ohmic heating and emission cooling of oxide cathode coating [Gärtner et al, 2002].

The higher temperature conductivity arose in the emission current, which flowed between the granules, the spaces or pores being filled with an electron cloud. This twofold mechanism was a result of the porosity of the coating. The results of his experimental work strongly supported the theory of the activation energy in the high temperature regime being equal to the work function at all stages of activation.

Hensley [1955], performed measurements on a system could be pressed two parallel planar cathodes so arranged that their surfaces could be pressed together or separated by a small gap. Low-field conductivity measurements showed that above approximately 700 K, the conductance of the system was

independent of the physical contact between the cathode surfaces. This result supports the theory that the high temperature conductivity is a property of the electron gas in the cathode pores. The ratio of the conductivity to thermionic emission was measured under conditions designed to preserve the state of activation of the cathode surface. The results agreed with the theoretically predicted ratio and demonstrate that the higher values previously reported were caused by a lower activation of the surface than in the interior of the cathode.

The current-voltage characteristics of a well-activated triple (BaSrCa) oxide coating on O ring nickel core disks were measured in the range $\pm 20V$ by an a.c. method. The variation with temperature of the conductivity of a typical coating is similar to those observed previously by other methods. From 300–600K the current-voltage characteristics are approximately linear, but above 600K (the cross over temperature) a change occurs which is coincident with the change to a higher slope in the $\log\sigma$ versus $1/T$ curve because of the commencement of thermionic emission in the pores of the material [Tomlinson and King, 1956].

2.5 Elements behavior and structures in the oxide material

During the lifetime, both Ba and Sr oxides are being depleted from the coating surface, much as would be expected from known evaporation data [Haas et al, 1979 and Shih et al, 1981]. In contrast, the relative loss of Ba was not so great at the interface, perhaps because it was offset by the electrolytic effect. However, this loss of Ba, compared to Ca at the coating surface during life did not seem to have a major effect on the average work function. By the same

token, examples were found where the distribution in work function was related to the Ba to Ca content, a discrepancy that was not fully understood.

In the case of the O layer, a sintering effect (which is a near-surface process) may be, means of preferential crystal, exist without altering the BaO lattice from which the electron emission predominates. A way by which this additional O appears at the surface, i.e. O^- ions, was mentioned from evidence of possible electrolytic effects. For the case of the apparent Ba-Ca composition discrepancy with work function, it was possible that the compositional change with life might represent a simple decrease in fractional area due to evaporation and hence caused almost no increase in the work function. The change in composition noted within a cathode, on the other hand, may be representing a CaO slag formation due to partial melting of the coating. This could reduce the density of defects in the BaO, such as O vacancy donors, and significantly increase the work function [Shih et al, 1981]. Figure 2.4 depicts the changes in the total work function during reactivation after vacuum ambient exposure.

The evaluation of the base metal activity of the oxide cathode was studied by the Adia and Hitachi research group [1982]. This study evaluated the activity of the various compositional base metals by measuring the reaction products, Ba vapor pressure, thermionic emission current and surface composition of the oxide. Activity evaluation was made using base

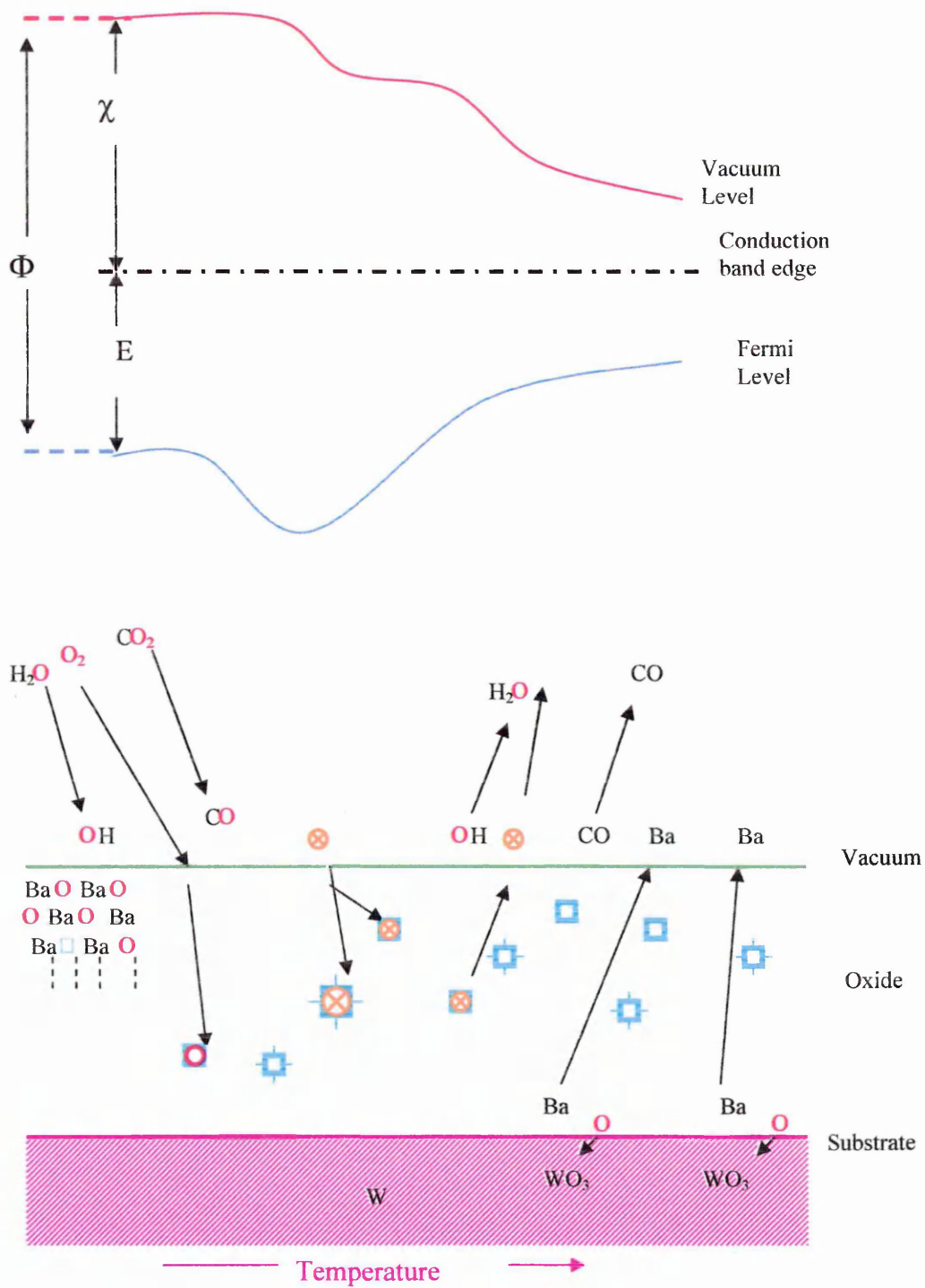


Figure 2.4: \circ -oxygen atom, \square -O vacancy, \square - thermal generation donor and \otimes - additional unidentified adsorbents [Haas et al,1981].

metals of Zr, W and Mo activators which were alloyed to the Ni core metal up to the solubility limits. The results can be illustrated in Figure 2.5 and are as follows:-

1. The vapor species from the oxide coating on the inter base metal is mainly BaO. However, those from oxide coating on the active base metal are Ba and Sr elements.
2. The stronger the reducing capability of the base metal, the higher the saturation emission current and resistivity against O₂ gas introduction [Beyner et al, 1965].
3. Measurement of emission current deterioration caused by O₂ gas introduction can clarify the base metal activity [Adia et al, 1982].
4. The surface of the oxide coating on the active base metal became CaO rich with heating time. This was considered to be due to the preference of reactions between BaO, SrO, CaO and the activator [Adia et al, 1982].
5. To obtain a long life oxide cathode, it is necessary to minimize Ba adsorbate atoms supplied to the CaO rich surface of the (Ba, Sr, Ca)O ternary oxide. This surface was formed naturally while heating the ternary oxide on the active base metal. Thus, selection of activator elements and control of the reaction product are essential in oxide cathode fabrication [Adia, 1982].

The surface extended x-ray absorption fine structure (SEXAFS) was used to study the local geometry around barium atoms on thermionic cathodes [Norman et al, 1987]. On the surface of tungsten and tungsten-osmium

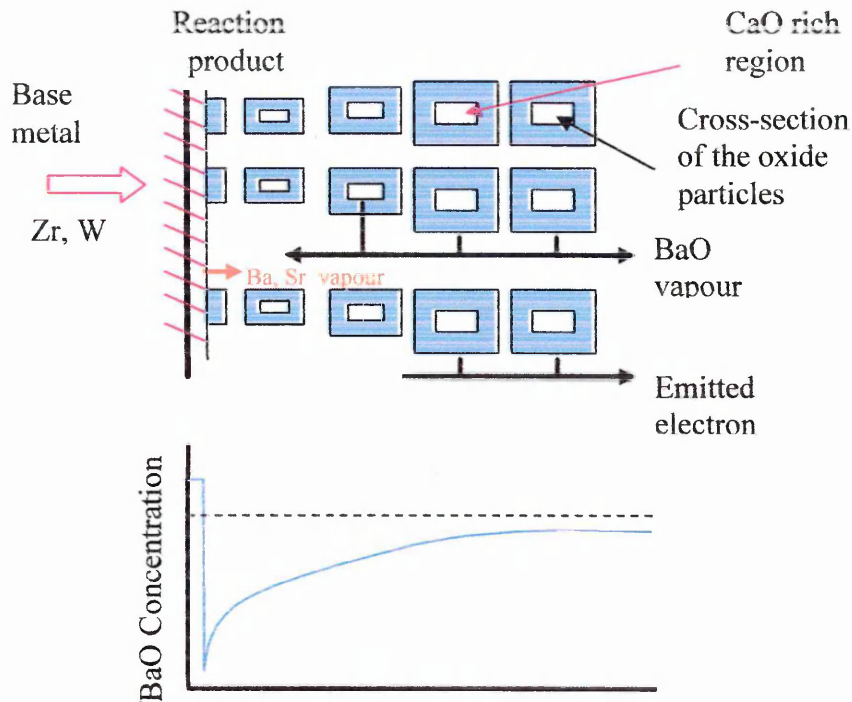


Figure 2.5: Illustration of conceivable situation of the oxide cathode using active base metal [Adia, 1982].

alloy dispenser cathodes, Ba was bonded to oxygen with well defined short-range order. The Ba-O distance was similar $\left(2.62 \pm 0.04 \text{ \AA} \right)$ for the two kinds of cathodes, with oxygen atoms occupying hollow sites of the substrate. However, the alloy cathode had Ba bonded to two oxygen near neighbors (compared to one for the tungsten cathode), which enhanced the surface dipole, thus explaining the observed lower work function.

The electronic structure of the emissive layer of B-type thermionic cathodes (the molar ratio of the BaO, CaO and Al_2O_3 , 5:3:2) was also investigated [Müller Wolfgang, 1988] using SFXATS. It was found that the chemical

structure of the BaO/W emissive layer can be characterized as a barium salt of the O/W substrate. The O/W electronic structure provides for an effective charge transfer from Ba into the metal.

The resulting large surface dipole is responsible for the low work function giving excellent emission properties of the cathode, as shown in Figure 2.6.

The strong ionic bond in the Ba-O/W complex explained the high thermal stability of the surface. Barium was found to be strongly oxidized, while oxygen and the metal substrate were in a reduced chemical state [Müller Wolfgang, 1989].

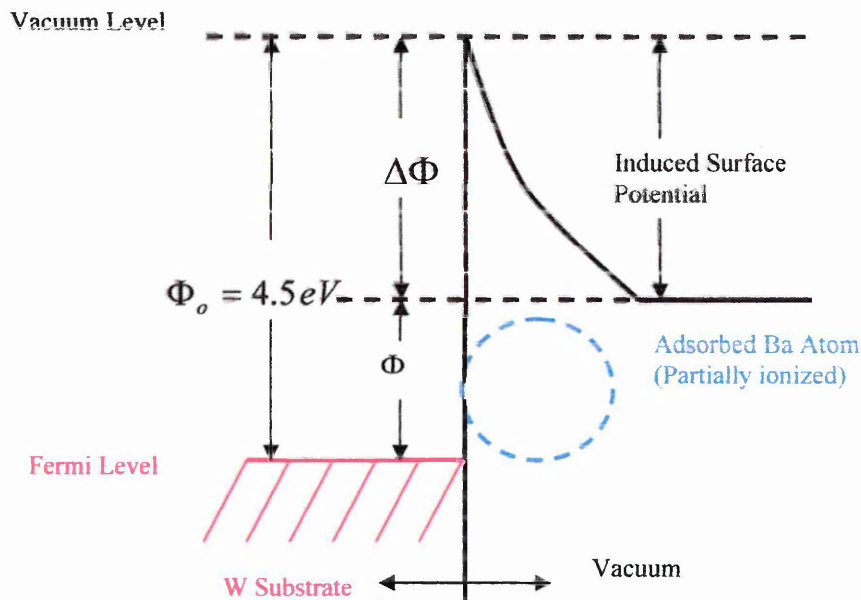


Figure 2.6: Potential energy diagram showing the work function of W adsorption of Ba atoms [Müller Wolfgang, 1988].

A comparison between non-activated and activated W-I cathodes, measured at identical positions, showed a strong reduction in the number of the initially observed BaO_x particles, which was due to evaporation during the activation procedure [Makovicka, 1997].

2.6 Emission lifetime studies

The decay of emission during cathode life might be explained by a slow sintering of the coating and a consequent closing of the pores. The deactivation of the filament by over heating might be attributed to the same cause. The non-saturation on the emission current might be due to a pseudo-space charge formed by occlusion of electrons on the surface of the coating particles [Becker et al,1931].

There is a linear relationship between the logarithm of the lifetime and the reciprocal of the cathode temperature, as show in Figure 2.7. The emission life formula is based on the assumption that the rate determining step is Ba diffusion inside the pellet. Emission life τ is given by [Aida et al,1993]:

$$\tau = Ad^2 \exp\left(\frac{E}{kT}\right) \quad (2.2)$$

Experimental results confirmed the strong dependence of τ on d (the oxide pellet thickness) and T . In this case, the activation energy of lifetime E was about $3.2eV$ to $3.5eV$.

Life test measurements of M-type cathodes (impregnated) carried out in diodes have been used to establish life models or predict the potential life of

cathodes. Diode life tests involve space charge current densities of 1.5 and $2 A/cm^2$, giving confidence for its use at lower current

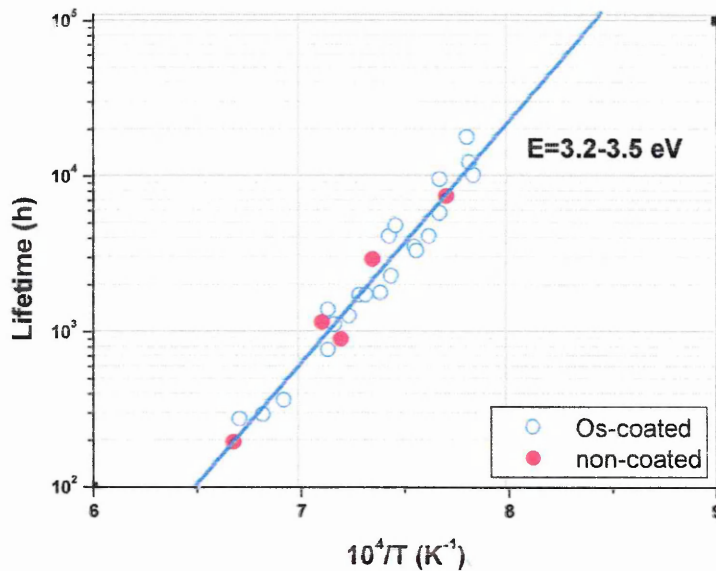


Figure 2.7: Lifetime when emission current drops, as function of cathode temperature [Aida et al,1993].

densities for comparison with TWT (traveling wave tube) data [Aida et al,1993].

Nevertheless, a comparison of both sets of data indicates that results obtained with diodes can give a good estimation of the current in TWT's. From the results, the lifetime (10% of current loss) in TWT's was estimated at 200,000 hrs, 170,000 hrs and 150,000 hrs for a load of 0.5, 1.5 and $2 A/cm^2$, respectively at a temperature of $985^\circ C_b$ (the cathode brightness temperature) [Dieumegard et al, 1997].

Two types of Ir-coated dispenser cathode ray tubes (CRT's) have been developed and their particles application has been realized by Higuchi from Toshiba [1999]. The heater powers of these cathodes are $1.31W$ and $0.79W$. Due to this heater power, life tests up to $42,000h$ were conducted at two levels of cathode temperature. Based on the residual emission ratio, stability of the Ir layer and the size of ion-bombardment nickel, it was found that the minimum life expectancy was more than $70,000h$.

Gärtner and his co-worker from Philips [2003], reported that accelerated life tests are needed in order to quantify oxide cathode improvements and predict life under standard operating conditions. In the case of lifetime acceleration by elevated temperature, a reliable life prediction backed by theory can be made. An increase of temperature by about $100^{\circ}C$ gives a life acceleration factor of about 10. Additional continuous dc load can be used for judging the dc load-ability of the cathode, but a complete model description is still missing in this case and more investigations are needed to develop a model.

During the life of a cathode, an interface layer grows between the nickel alloy and the oxide, which is comprised of reaction products. The interfacial layer sets limits on the cathode performance and useful operational lifetime by inhibiting the barium reduction reaction. Jenkins and others from L.G. Philips [2003], discussed sample preparation procedures for exposure of the interface. They used several surface and bulk analytical techniques to study interface formation. SEM, AES and SIMS data were presented, which provided a preliminary insight into the operating mechanisms during the cathode's lifetime. There was evidence that the activator elements in the

nickel alloy base, Al and Mg, are able to diffuse to the surface of the oxide during activation and ageing. These elements were enriched at the interface after an accelerated life.

2.7 Element analysis and technique

Recently, it has been demonstrated that a programmed temperature desorption study is a very useful tool. For studying surface chemistry involving Ba and BaO, this technique is particularly necessary since multiple adsorption states were found. Studies such as measuring AES (Auger Electron Spectroscopy) peak height changes, as a function of heating would have difficulty in distinguishing various adsorption states. In combination with QMA (Quadruple Mass Analyzer), they were able to identify the desorbing species from tungsten and to differentiate multiple adsorption states on tungsten. For some of the states, they were able to identify the nature of the adsorption site and determine the binding energy, the kinetics of desorption and the population at each state. For Ba adsorption on tungsten, they have identified at least three distinct adsorption sites. The lowest desorption temperature state given rise by the multilayer desorption sites. The higher temperature sites are from first layer type sites. Of the two states, the lower binding energy state consists of Ba atoms bound directly on tungsten, and the higher binding energy state consists of Ba atoms bound to tungsten as well as oxygen. At low temperatures ($<1400K$), the adsorption Ba atoms are desorbed as atomic Ba, but at high temperature ($>1300K$) BaO desorption commences [Shih et al, 1999].

An UHV LEIS (low-energy ion scattering) setup has been converted into a dedicated apparatus to study the surface composition, structure and dynamics of real dispenser cathodes and cathode model systems based on W crystals. LEIS, AES and LEED (low-energy electron diffraction) are used to investigate the surface characteristics, and the cathode emission properties are derived in situ from a close-space diode configuration. The focus was on the quantitative surface composition of B-type and M-type dispenser cathodes by LEIS. A straightforward quantification was hampered by the influence of the cathode work function on the neutralization of the ions. It is shown that the ion fraction decreases as the work function of the cathode decreases. The Ba surface density was observed to increase with decreasing work function. [Cortenraad et al 1999].

The chemical transportation of the Mg and Al doping impurities takes place during an annealing under a controlled atmosphere of a nickel alloy thin foil. Different analytical techniques were used for this study: SEM, coupled with electron probe microanalysis (EPMA), transmission electron microscopy (TEM), AES, secondary ion mass spectrometry (SIMS), glow discharge optical emission spectrometry (GDOES) and X-ray diffraction. It was shown that chemical transport occurred mainly by a grain boundary mechanism with significant pile-up of compounds. The resulting precipitates were identified. Moreover, it was shown that their chemical composition clearly depends on their location relative to the grain boundary pattern. [Poret et al 2000].

The decomposition and corresponding changes in electrical properties of carbonate materials used in oxide cathode manufacture have been studied by

a range of techniques [TGA (thermo-gravimetric analysis) and SEM], both during initial decomposition and for the activation and initial stages of operation of the cathode. The results have shown that the decomposition and activation processes both occur by multi-step reactions, with the rate of these, and the corresponding effect on the electrical properties, being dependent on the temperature. The microstructural changes occurring during these processes have been shown to be completed significantly prior to these ongoing electrical changes, indicating the chemical rather than physical changes dominate the conduction behavior during this period [Al-Ajili et al 2000].

Three years ago, Roquais and his group [2002], used complementary analytical techniques to characterize the mechanical transport of Mg and Al in the cathode nickel base as a result of annealing under H_2/H_2O atmosphere. A better knowledge of the diffusion phenomena of Mg and Al could be obtained as well as better understanding of mechanisms involved in the formation of these compounds. Those two elements diffuse to the nickel surface, where they react with oxygen and accumulate in the form of compounds identified as being a mixture of $MgAl_2O_4$ either with MgO or Al_2O_3 . The enrichment of the Ni surface with Mg and Al caused by annealing is very remarkable, their concentration at the surface being a few atoms % compared to 0.01% to a few 0.01 atom % in the bulk. Moreover, not only the Ni surface but also a near surface region of the nickel of about $5 \mu m$ is affected by the creation of Mg and Al based compounds. Because Mg and Al diffuse mainly through grain boundaries, the compounds form preferentially in the latter. Their

distribution over the surface builds two surface patterns: the first one showing the network of grain boundaries existing at the beginning of the annealing step, and the second one the final network of grain boundaries. Those compounds have to be considered as an initial interface between the nickel and the (Ba,Sr,Ca)O coating.

Surface analysis of thermionic dispenser cathodes with a W matrix and Re, Ir and Os/Ru surface coatings was performed by means of low-energy ion scattering and Auger electron spectroscopy. It was found that the Ba-O complex responsible for the low work functions of the cathodes has similar properties for the different coatings, the atomic Ba/O ratio is close to unity on all cathodes, with the O atoms positioned in a plane below the Ba atoms. The bonding between the Ba and O atoms as observed in low-energy Auger spectra is also almost identical on all cathodes. However, a significant difference in the absolute Ba-O coverage was observed for the various cathodes. This density is determined by the strength of the bonding of the O atoms in the Ba-O complex with the substrate atoms. [Cortenraad et al 2003].

Poret from Thomson multimedia/SBU Displays & Components [Poret et al 2003], studied the phenomena of the evolution of compounds considered as constituents of the initial interface between the triple oxide coating of (Ba, Sr, Ca) O and the nickel alloy base of a one piece oxide cathode. This work focused on the characterization of the cathode nickel without its triple oxide coating, so as to bring a first step in the basic understanding of compound transformations. Different nickel melts with variable Mg and Al contents were

examined. It was observed by in-situ optical microscopy that the quantity of crystallite compounds drops dramatically along all heating steps of the cathode activation under vacuum. For some melts, depending on their composition, the surface appears almost free of compounds, which is associated with best cathode performance. By examination of a wide range of nickel compositions, they were able to establish a relation between the Mg and Al content and the amount of compounds on the nickel surface.

2.8 Ba effect on the conductivity and emission of the oxide cathode

Becker [1929], experimentally showed that metallic barium deposited on the surface of the oxide either by electrolysis or by evaporation from an outside source, produced changes in the cathode activity (current density). Conduction was mostly due to electron transport but partially ionic in nature; the ratio of electron to ion transport depended upon the temperature and the composition of the oxide and the plate potential. The conductivity of the oxide was not entirely Ohmic and diffusion current might flow against the opposing field contributing to the conductivity.

Becker illustrated that the active layer of the oxide coating was at the outer surface [Becker et al,1931]. The activity depended on the concentration of the barium and oxygen on this surface and also upon the amount of metallic barium dispersed through the oxide. The core material did not directly affect the emission, but did greatly affect the ease with which free barium was produced by heat treatment of electrolysis.

The thermionic electrons originate in the oxide just underneath the

adsorbed barium mono or multi-layers. However, most of the current through the oxide is conducted by electrons, a small portion being carried by barium and oxygen ions.

It was assumed that the source of emission was the composite layer formed by occlusion of alkaline earth metal on the surface of the coating and that the electrons emitted, diffused through the interstices in the oxide coating into the vacuous space [Lowry, 1930].

The oxidation and thermal adsorption of the evaporated Ba films on different substrates indicated that the active state for B-type impregnated cathodes (calcium carbonate was added to reduce the barium evaporation rate) can be reproduced by a near monolayer of the stoichiometric BaO on the W surface [Hass et al, 1983]. The density of Ba atoms (or O atoms) in this monolayer should be one half that of W atoms based on size considerations of the Ba compared to the W, which was confirmed by LEED (low-energy electron diffraction). Measurements of the diffusion of Ba compounds from pores, the substrate interaction and the thermal evaporation indicated that on the W substrate, the monolayer BaO stoichiometric ratio was not a stable configuration and had a work function of $\approx 2eV$. The substrate work function was lowered because of the dipole formed by the adsorbed BaO. Studies of the electron interactions between the Ba and O indicated that a more complete electron transfer exists between the Ba and O for the BaO layer on the Ir substrate than on the W substrate. These results are based on the observation that O 2P states on

the W substrate appear to be filled not only by Ba 6s but also by W valence electrons.

The effect of barium supply into a (W-Sc₂W₃O₁₂)-coating film on the emission distribution of a scandate cathode (cathode contains scandium element) was investigated by [Sasaki et al 1999]. Scandate concentration on the oxide cathode surface was increased by activation heating. This increase was coincident with the rise in emission current by heating. However, when the film was coated on the unimpregnated tungsten pellet, the scandium concentration did not increase. These results indicated that the barium supplied into the film was necessary for liberating scandium atoms from the scandium tungsten in the film and for forming a monolayer of Ba-Sc-O on the surface. Sasaki measured the heating-induced change in the scandium content of the film. The result showed that the scandium content decreased only in the part of the film that covered the impregnated areas. No decrease was observed in the film that covered the tungsten metal. The liberation of scandium was considered to take place only in the film to which barium atoms were mainly supplied. This non uniform scandium liberation in the film caused a non uniformity in the Ba-Sc-O monolayer on the cathode surface, which in turn caused emission non uniformity.

2.9 The addition of Ni powder

A new type of cathode that consists of an oxide-impregnated Nickel matrix of controlled porosity was examined by Balas and his co-workers [1955].

This type of cathode, prepared by controlled sintering methods, has a porosity of approximately 50%. The calculated work function was about $1-1.25\text{ eV}$ using Richardson's equation plots. A high current density value of $J = 10\text{ A cm}^{-2}$ was achieved, when the cathode was operated at temperatures around 1145 K .

The effect of this nickel impurity on the reaction of an oxide cathode with carbon monoxide in the oxide coating was studied by Pikus et al [1964]. It was shown that this reaction depends strongly on the activation state of the cathode; its temperature and the CO pressure can lead to cathode activation as well as cathode poisoning. The reaction results were the oxidation of CO to CO_2 .

A nickel impurity exerted a significant influence on the reaction of the cathode with CO, similar to that produced by preliminary electrolytic activation of the oxide cathode. The effect of the nickel impurity was independent of the method employed to interpret the catalytic reaction that oxidizes CO to CO_2 , with the coating used as the catalyst. Both the oxide coating, and the nickel impurity, to a somewhat greater extent, played the role of catalyst.

To increase the emission properties of an oxide-coated cathode, Aleksandrov et al [1968], studied the effect of the concentration of highly dispersed Nickel (up to 15%). The Ni concentration in the range (1–5)% resulted in much improved emission properties. This observation was in complete agreement with the generally accepted viewpoint that an

increased metallic Nickel content of more than 5% in the oxide coating leads to a deterioration in the emission properties of the oxide-coated cathode.

Addition of filamentary Ni particles represented a convenient and effective way to increase the conductivity of the oxide [Al-Ajili et al, 2001]. This increase formed on conversion and activation of oxide cathode, with less than 10 *mass%* addition of Ni. However, a large increase in conductivity was obtained at low temperature. This effect diminished with increasing temperature to less than one order of magnitude difference at 1000 *K*. The conductivity of nickel-containing samples decreased in the first few hours of operation due to ongoing microstructural changes. Nevertheless, the long-term emission behavior of such nickel-containing coatings was enhanced by these additions. This enhancement is believed to stem from increased dimensional stability of the oxide coating imparted by the presence of a skeletal/percolating Ni framework within the oxide coating.

The composite cathode coating could be modelled as two parallel conduction pathways; one component being the continuous metallic pathway formed above the percolation threshold which comprised the dominant conduction mechanism, particularly at low temperatures, whilst the second element comprised the semiconducting oxide, which made an appreciable contribution to the overall conductivity only at elevated temperatures. The standard formula for parallel resistance and conductivity in the d.c. system and the contribution of the percolation path through the metallic phase addition can be determined as [AL-Ajili, 2001]:

$$\sigma_{metal} = \sigma_{total} - \sigma_{oxide} \quad (2.3)$$

This equation determines the contribution of the metallic component to the conduction behavior of the system. The calculated values for this metallic contribution to the conductivity should show a linear behavior with temperature. The slope of the best fit determines the activation energy values at various temperatures. The temperature coefficient of resistance is determined using the following equation [Bennet, 1974 and Ohring, 1995]:

$$\rho_T = \rho_o (1 + \alpha \Delta T) \quad (2.4)$$

Where ρ_T, ρ_o are the resistivities at two temperatures separated by the range ΔT . The calculated value of α was determined as approximately 0.002, which is in the anticipated range for a pure metal [AL.Aliji, 2001, Bennet, 1974 and Ohring, 1995].

A preliminary investigation was carried out into the development of a novel cathode material with enhanced conductivity using low volume fraction additions of an acicular conductive phase. The manufacturing process was compatible with current commercial manufacturing processes and was anticipated to result in small additional costs. The results indicated that this form of conductive phase solve many of the problems previously identified in attempts to enhance conductivity by conductive phase addition, and encouraging results were obtained in emission trials [Hodgson et al, 1999].

2.10 Phenomena of Basic emission

According to Nergaad [1952], the oxide cathode consists of four principal regions, representing the sample model, to explain the operation of the cathode. These regions are the base metal, interface layer, oxide layer and surface, as shown in Figure 2.8, which are created because of the conversion and activation of the cathode and lifetime.

The interface layer is formed by reaction of reducing agents like Si, Ti, Mn, Mg, Al, C or even W, with the oxide coating, leading to the formation of e.g., MgO, Al₂O₃ or to binary oxides like Ba₂SiO₄. The thickness of the interface layer increases with increased time of operation.

2.11 The effect of the interface layer

Several interface phases have been identified in a layer. These include, BaZrO₃, MgO, BaAl₂O₄, Ba₂SiO₄, Ba₂TiO₄, Ba₃WO₆, Ba₃MoO₆, Ba₂SrWO₆ and (Ba,Sr)SiO₄. These oxide metals have high resistivity which may vary depending on the cathode temperature. The resistivity of Ba₂SiO₄ for example decreases from 10⁶ Ω.m at 1000 K to 1.66×10⁵ Ω.m at 1250 K.

Ba₃WO₆ has a resistivity of 2.5×10⁵ Ω.m at 1000 K [Gärtner, 1999].

The thickness of the interface layer increases with increasing time of operation.

The thickness of Ba₂SiO₄ is found to increase from 1–2 μm after 4000 h of operation.

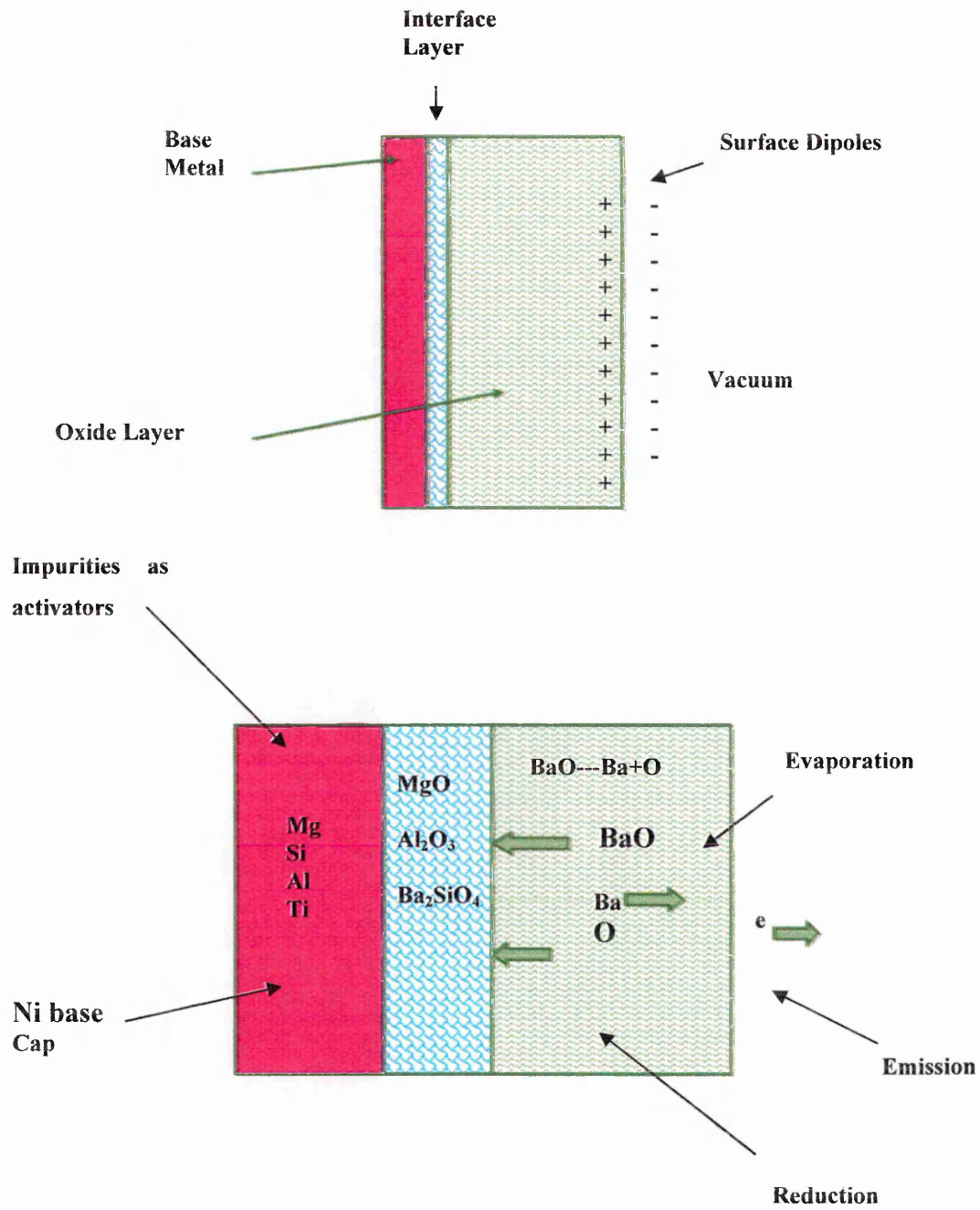


Figure 2.8: The four principal regions of the oxide cathode

2.12 Thermionic mechanism models

2.12.1 Ba mono-atomic layer model

The electron emission work function in this model is calculated by using the Richardson-Dushman equation:

$$J = AT^2 \exp(-e\Phi / kT) \quad (2.5)$$

This work function is given by [Kasap, 1997 and Yamamoto, 1997]:

$$\Phi = \Phi_o + \alpha T \quad (2.6)$$

Beyer and Nikonov [1964] give the work function for triple-oxide cathodes, as:

$$\Phi = (1.1 \pm 0.05) + (5 \pm 1)10^{-4} T \quad (2.7)$$

For (Ba,Sr)O the work function is:

$$\Phi = (1.2 \pm 0.05) + (5 \pm 1)10^{-4} T \quad (2.8)$$

While for BaO the work function is:-

$$\Phi = (1.6 \pm 0.08) + (5 \pm 1)10^{-4} T \quad (2.9)$$

It has been noticed that on addition of other alkali earth elements to the Ba the work function decreases.

2.12.2 Donor model

Oxygen vacancies are created in the BaO by traces of impurities in the metal substrate, which reduce the BaO to Ba. These vacancies serve as donors from which electron emission takes place into the vacuum when the cathode is heated.

The free Ba atoms thus produced also gradually migrate to the surface and

then evaporate. The other oxides in the cathode play such roles as reducing the Ba evaporation rate and reducing the work function. The current density J (A cm^{-2}) according to this model is given by Wilson [1931]:

$$J = 1.73 * 10^{-6} * N_d^{1/2} T^{5/4} * \exp\left[-\frac{(E_d / 2 + \chi)}{kT}\right] \quad (2.10)$$

The work function (activation energy) for the electron emission is given by the relation $\Phi = (E_d/2) + \chi$.

2.13 Conduction theories of the oxide-coated cathode

There has been extensive work on oxide coated cathodes concerning various aspects of the operating properties. Most of the early efforts were directed toward these cathodes coated with the crystalline powders. Later investigations on single crystals of barium oxide provided much of the understanding of the semiconducting properties of this compound. A summary of some of the experimental progression theories are given in this chapter. Most of these studies pursued the subject from the point of view of defect chemistry. While experiments were performed to examine the chemical properties of these oxides, the correlation with the operation of a real oxide coated cathode is yet to be completely determined. The lack of a widely accepted physical model indicates the complexities involved in the cathode operation.

For many years oxide-coated cathodes have been almost universally used in the cathode-ray and other electron-beam vacuum tubes. At present, the oxide cathode is still of considerable practical importance as an electron emitter. In

this chapter, simple models are proposed to explain the electronic processes in an oxide cathode.

2.14 Conduction mechanism in oxide cathodes according to Loosjes and Vink

The device used by Loosjes and Vink [1949], was made of cathodes with a flat surface of 8 mm^2 consisting of a nickel cylinder with a wall thickness of 0.15 mm and external diameter of 3.2 mm , closed at one end and covered with a $50\text{ }\mu\text{m}$ thick coating of $\text{BaSr}(\text{CO}_3)_2$.

The cathodes were specially selected with a flat surface. Two of them were mounted in a tube in such a way that the carbonate coatings were pressed against each other by means of springs. This ensured that the layers were always pressed against each other by the same force, regardless of any change in the thickness of the separate layers caused by decomposition of the carbonates during the process of formation, as shown in Figure 2.9.

In Figure 2.10, the logarithms of the conductivity, $\log \sigma$, are plotted against $1/T$ for the two layers at different stages of activation. From this figure it can be seen that the $\log \sigma - 1/T$ curves consist of two or three parts.

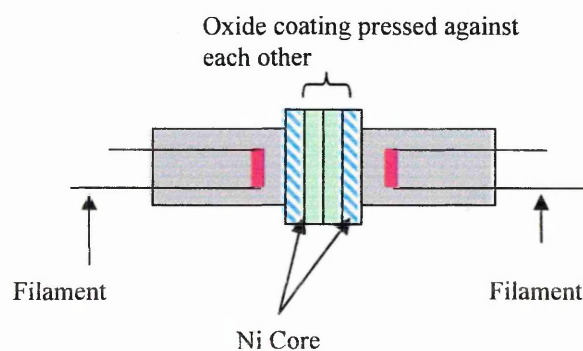


Figure 2.9: Mounting of two cathodes pressed against each other.

There was the low-activation temperature part (part I), which in each case extends to about 700–800 K, followed by part II where the temperature dependency of the conductivity is in two different mechanisms, whilst often for temperature above 1000 K (part III) the temperature dependence of the conductivity begins to become less pronounced.

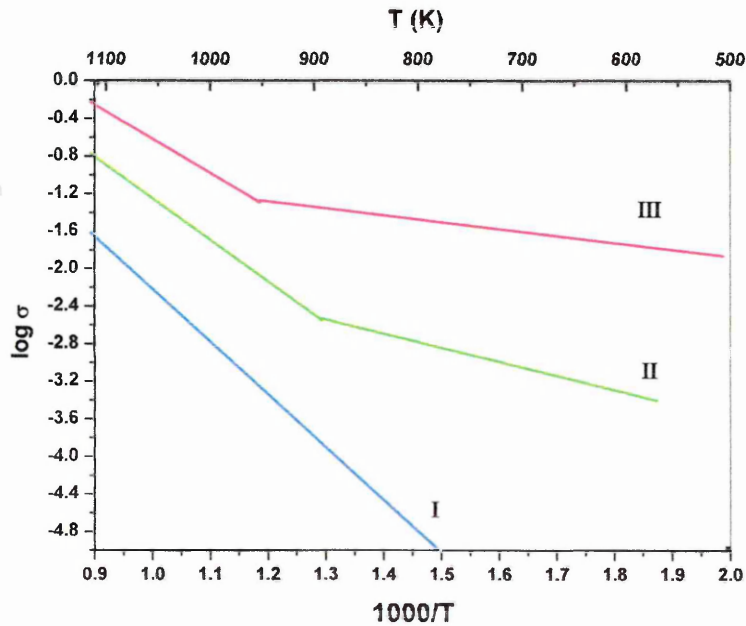


Figure 2.10: $\text{Log } \sigma - 1/T$ curves for succeeding stages of activation (I-III)

[Loosjes and Vink, 1949].

2.14.1 Interpretation of I/V measurements (The model)

Loosjes and Vink [1949] considered two conduction mechanisms (b and c) which depend exponentially on temperature and are given by the following relation:

$$\sigma = \sigma_o e^{-e\phi/kT} \quad (2.11)$$

For the two mechanisms the σ_o 's and the work functions ϕ are different. For

each of these two mechanisms (1 and 2) when $\log \sigma$ was plotted against $1/T$ they found the straight lines b and c of Figure 2.11. If b and c are connected in series, the resultant conductivity will be determined at every temperature mainly by the mechanism with the lowest conductivity. If one now plots the logarithm of the resultant conductivity against $1/T$, one finds curve 1 of Figure 2.11.

If, however, these mechanisms are connected in parallel to each other the resultant conductivity will be determined at every temperature mainly by the mechanism with the highest conductivity. In that case if one plots the logarithm of the resultant conductivity against $1/T$ one finds curve 2 of Figure 2.11.

To represent the temperature dependence of the conductivity σ that is observed experimentally by:-

$$\sigma = \sigma_1 + \sigma_2 = \sigma_{o1} e^{-e\phi_1/kT} + \sigma_{o2} e^{-e\phi_2/kT} \quad (2.12)$$

It appears that this is possible only for temperatures up to about $1000K$. For higher temperatures the temperature dependence of the observed conductivity is less than that calculated from equation 2.10, By using the values of $\sigma_{o1}, \sigma_{o2}, \phi_1$ and ϕ_2 computed from the results at temperatures below $1000K$.

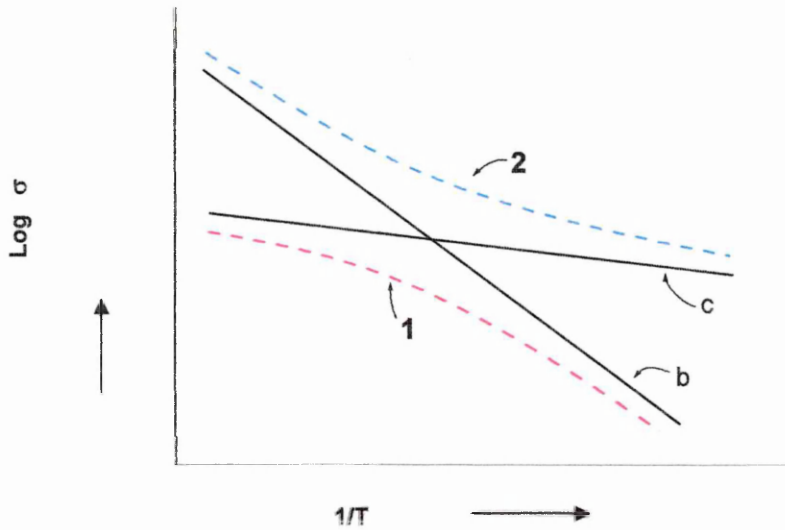


Figure 2.11: $\text{Log } \sigma - 1/T$ curves of two conduction mechanisms (b and c) and the resultant conductivity when c and b are connected in (1) series (2) parallel to each other [Loosjes and Vink, 1949].

2.14.2 Interpretation of the I/V measurements

On examining the I/V curves for the same stage of activation, one sees that the I/V characteristics can be linear or sub-linear.

Figure 2.12 shows plots of a few such cases. There are three temperature regions to be distinguished. For temperatures below 800 K , the I/V characteristics are always linear. The characteristics are tending to be sub-linear for temperatures between $(800-1000)\text{ K}$, and at sufficiently high temperatures ($T > 1000\text{ K}$) the $I-V$ curves become linear again.

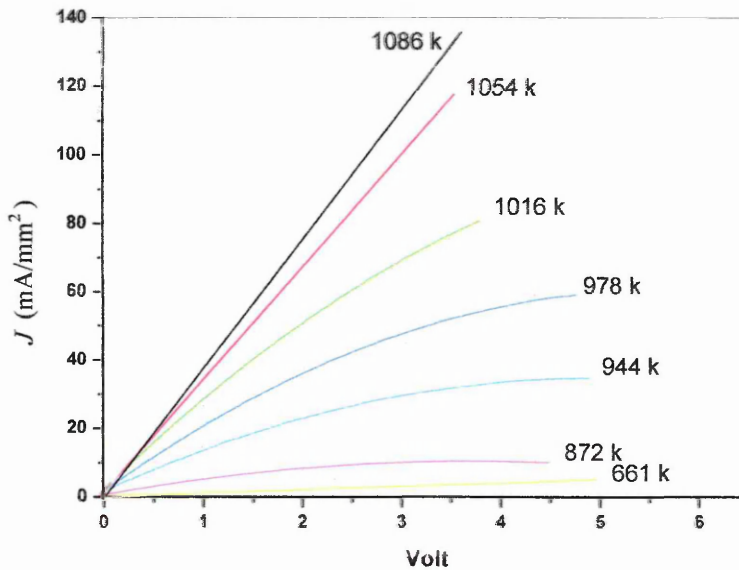


Figure 2.12: the I/V characteristics of one of the Loosjes and Vink samples [Loosjes and Vink, 1949].

With such a picture it is difficult to explain that the activation energy calculated for the high temperature mechanism has the same value as is usually found for the energy corresponding to the work function of the oxide coated cathodes [Becker, 1931].

One can explain this sub-linear curved characteristics by assuming that the electrons have to pass through a barrier layer situated at the interface between the Ni electrode and the oxide coating [Wright, 1947].

Applying Wright's explanation to Loosjes data, it may be concluded that the electron transport during the high temperature regime would be subjected to a barrier-layer effect at the interface, whereas the electron transport during the low-temperature regime mechanism does not experience such an effect. Another mechanism of electronic conduction is therefore proposed. In Loosjes opinion it is the conduction by means of electrons present in the pores

between the electron-emitting grains of the porous oxide coating that play an important part in accounting for the properties of the conduction mechanism observed in the oxide coating. In just the same manner as the outer grains of an oxide-coated cathode keep up an electron cloud in a layer immediately adjacent to the surface of the cathode. It is certain that the pores in the layer will be filled by an electron gas formed by the electron clouds of the surrounding grains.

This new conduction mechanism is sufficient to account for the conduction properties of the oxide cathode.

The oxide coating layer becomes charged negatively because of the electrons coming from the Ni electrode and diffusing through the coating [Lowry 1930]. According to this theory, the electrons in the pores come from the surrounding grains. These grains will therefore have a positive charge, and therefore the layer as a whole will be electrically neutral [Loosjes et al, 1949].

Accepting for a moment the idea of electronic conduction through the electron gas in the pores, it is obvious that the temperature dependence of the conductivity will be closely related to the temperature dependence of the density of the electron gas present in the pores. It immediately becomes clear that this temperature dependence of the density of the electron gas, in the layer covering the surface of the emitting grains, will be the same as that of the emission [Loosjes et al, 1949 and Becker 1931]

The sub-linear I/V characteristics of this high temperature mechanism can also be easily explained by the model of the conduction through the electron

gas in the pores. In an electron gas, in the absence of a field and in thermal equilibrium, the electrons have a mean velocity \bar{v} in all directions, irrespective of whether the medium in which they move is a metal, a semiconductor or vacuum.

When a field F is applied the electrons (having a charge e and a mass m), they are subjected to an acceleration a in the direction of the field applied during the time t which the electrons take to cover their mean free path l

$$a = \frac{eF}{m} \quad (2.13)$$

For the mean increase of the velocity, $\overline{\Delta v}$, in the direction of the field during the time t :

$$\overline{\Delta v} = \frac{eF}{2m} t \quad (2.14)$$

For the calculation of this time t , two cases are to be distinguished:-

The mean velocity \bar{v} in any direction in the absence of a field is high with respect to the mean increase of the velocity in the direction of the field. In this case the mean velocity \bar{v} remains practically constant during the acceleration and we have:-

$$t = \frac{l}{\bar{v}} \quad (2.15)$$

and

$$\overline{\Delta v} = \frac{eF l}{2m \bar{v}} \quad (2.16)$$

At the end of the mean free path this increase in velocity will be destroyed through collision. Therefore $\overline{\Delta v}$ represents the mean drift of the electrons in

the direction of the field and the current density (in A/m^2) will be:-

$$J = \xi \overline{\Delta v} = \xi \frac{eF}{2m} \frac{l}{v} \quad (2.17)$$

Obviously, in this case Ohm's law is valid, as is experimentally found for metals and semiconductors. It is clear that Ohm's law is valid only if the time t (as in this first case) is independent of the field applied.

The mean velocity \bar{v} in any direction in the absence of a field is small with respect to the mean increase of the velocity in the direction of the field. Due to this case, $\overline{\Delta v}$ can be calculated as follow:-

$$t = \frac{l}{\Delta v} \quad (2.18)$$

and

$$\overline{\Delta v} = \frac{eF}{2m} \frac{l}{\Delta v} \quad (2.19)$$

Hence

$$\overline{\Delta v} = \sqrt{\frac{eF}{2m}} l \quad (2.20)$$

In this case, the current density can be calculated by the following expression:-

$$J = \xi \sqrt{\frac{eF}{2m}} l \quad (2.21)$$

Ohm's law is now no longer valid because, as is seen from (2.18) and (2.20), t is no longer independent of F . In this extreme case a parabolic I/V characteristic would be expected.

For the conduction through the electron gas in pores, the current density is

calculated using equation (2.21). The reason for this is that the mean free path of the electrons in the electron gas in the pores is much larger than that for the conduction electrons in metals and semiconductors. The mean free path in metals and semiconductors is of the order of 10^{-9} , but for the electrons in the electron gas present in pores, the mean free path is given by the size of the pores. The porosity being about 50%, it may be said that the mean free path is half the mean grain size, i.e. $1-3 \mu\text{m}$. This is larger by a factor of about 10^3 .

2.15 Relationship between thermionic emission and electrical conductivity of oxide-coated cathodes

It has been a well known fact that the thermionic emission of the oxide-coated cathode depends much upon the condition of the decomposition process of carbonate and the activation process [Narita, 1953].

2.15.1 The characteristics of "N" type and "S" type cathodes

Narita [1953] suggested two structural types due to the cathode decomposition and activation processes. These types are:-

- **Sintered cathode ("S" type):**

These cathodes are decomposed under high gas pressure and at very high temperatures during evacuation and they always found to have low emission and the oxide particles are considered to sinter and have no distinct grain-to-grain boundaries, as schematically shown in Figure 2.13. The grain-grain potential barrier is very low. These cathodes will be designated as "S" type

cathodes which were prepared in Narita's [1953] experiments by using barium carbonate, which is more convenient for sintering than barium-strontium carbonate.

Narita supposed that semiconductor-type conduction through the grains will be predominant in "S" type cathodes.

The variation of electron affinity χ with the activity of "S" cathode and the existence of a metastable state in the emission may give the possibility of the formation of a monolayer of barium on the surface of the activated oxide which reduces the work function.

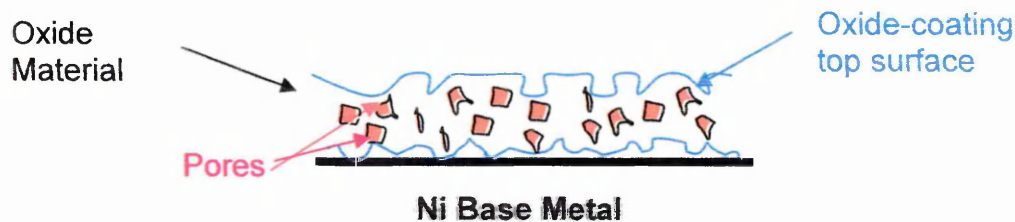


Figure 2.13: The schematic diagram of the sintered type cathode [Narita 1953].

- *Normal cathode ("N" type)*

The normal cathode ("N" type) is of superior activity, it should be allowed to decompose carefully (under low gas pressure and high temperature) where less sintering should take place. In this case, the oxide particles have a certain distance between grain boundaries resulting in a rough contact between grains. The grain-grain potential barrier is thus higher and is involved

in the electron transportation. Narita [1953] supposed that "N" type cathode usually has such a structure, as shown in Figure 2.14.

In "N" type cathode, the height of the contact potential barrier between grains will be so large that the electron conduction through pores among oxide-particles may appear at high temperatures (above 800 K) as Loosjes - Vink advocated [1949].

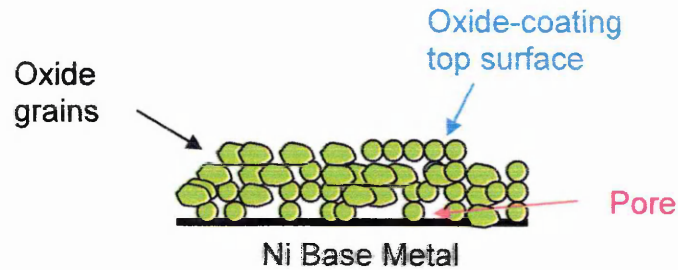


Figure 2.14: The schematic diagram of the normal type cathode [Narita 1953].

Thus the whole resistance of the oxide layer is assumed to be made of three kinds of resistances, the resistance through the grains R_1 , the resistance due to pore between two grains R_2 and the resistance of the "M" type conduction R_3 , as shown in Figure 2.15.

The total resistance R may be given by:

$$\frac{1}{R} = \sum_n \frac{1}{a_n R_1 + b_n R_2} + \frac{1}{c R_3} \quad (2.22)$$

The numerous types of measurable conduction are probably due to the difference in values of the multiplied parameters a_n, b_n and c . These parameters are the number of resistance in one grain group.

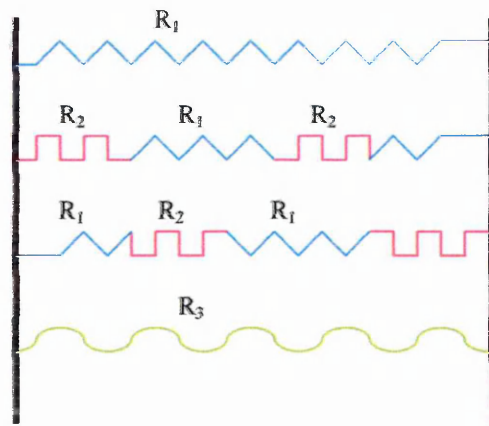


Figure 2.15: A schematical diagram of the resistance in the oxide coating [Narita 1953].

2.15.2 M-type conduction

Narita [1953] observed a new conduction mechanism due to the barium contamination (metallic conduction called the "M" type conduction). It has been reported that this type has a small activation energy (less than $0.1eV$) of conduction in the oxide cathodes. Such type of conduction is realized easily (denoted M-type conduction) by the method of changing the cathode activation by sputtering barium onto the surface of the oxide cathode.

However this conduction is so unstable due to the activation energy being less than $0.1eV$ and is impossible to observe beyond $550K$. When the cathode was heated to high temperatures, its conductivity at the low temperature decreased suddenly. This instability of the conduction was believed to be due to the evaporation of barium from the oxide-coating at high temperature.

Narita [1953] supposed that M-type conduction may be occurring through a thin barium layer covering the oxide particles.

Both the emission and the conductivity were varied by the evaporation of

barium to the cathodes [Narita, 1953]. The conductivity increased as the amount of deposited barium evaporated from batalum getter, as shown in Figure 2.16. The conduction became measurable beyond two atomic layers of barium and was approximately of the same order as M-type conduction in oxide-coated cathodes.

This conduction is scarcely temperature dependent (metallic conduction), suggesting that M-type conduction may be a surface conduction through the multi-atomic thin film of barium on the surface of the oxide particles.

• Narita's work can be summarised as follows:-

1. The relationship between emission and conduction for both sintered and normal cathodes was obtained at every stage of activation change by evaporation of barium atoms onto the cathode.

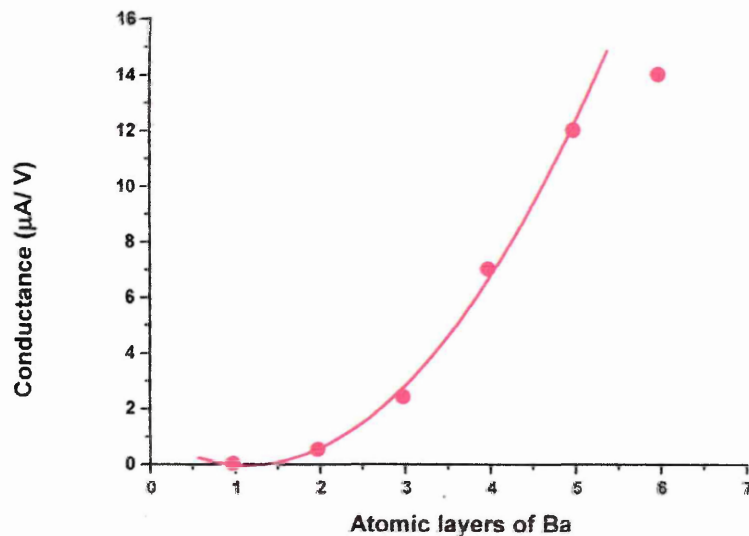


Figure 2.16: The increase of the oxide cathode conductance by deposition of barium atomic layers [Narita 1953].

2. The emission of the "N" cathode is proportional to the conduction above $800K$ and the semiconductor theory seems, at a glance, to be well applicable.
3. The width of the conduction band χ for "S" cathode known from $\phi - E$, was very high compared with that of "N" cathode and it varied with the change of cathode activity.
4. The difference between the "S" and "N" cathodes can be explained from the assumption of the existence of electron gas conduction through pores in "N" cathode coating and the effect of a monatomic layer on the cathode surface.
5. Conduction with a lower activation energy than $0.1eV$, appeared in the process of evaporating barium onto the cathode at very low temperatures. This conductivity was interpreted as the surface conduction of the electron through multi-atomic layers of barium on the oxide particles.
6. In low temperature range both "S" and "N" cathodes had M-type conduction. It was confirmed that the "S" cathode was more conductive than the "N" cathode [Narita, 1953]. The M-type conduction of both cathodes decreased owing to the evaporation of barium from the cathodes through heating, while the thermionic emission increased, accompanied by the slight decrease of the work function [Narita, 1953]. This may be interpreted as the transition from multilayer to monolayer of the surface barium coverage.

2.16 Theory of the oxide-coated cathode

2.16.1 The characteristics of the oxide coated cathode

Early investigations [Herrmann and Wagener, 1951] proved that the emission is directly associated with the presence of excess metal in the oxide. It was shown that it was either wholly a surface phenomenon, or due entirely to processes at the oxide-metal interface. In fact there is a direct relation between the conductivity through the oxide coating and the electron emission from it [Hannay et al, 1949], as shown on Figure 2.17. The electron emission and oxide conductivity increased together during activation and both are destroyed simultaneously when the cathode is poisoned. The temperature resistivity coefficient in the oxide falls considerably during activation, as shown in Figure 2.18. The curves marked as I, II, III and IV are taken during the activation stage.

The oxide conduction current occurs at the same current density saturation as thermionic emission takes place [Wright, 1947]. Wright also demonstrated the behavior of an interface compound which exists between the metal and the oxide. This may be a silicate, aluminates or other complex elements, depending upon the constitution of the core metal, and he showed that it gives rise to a rectifying junction at the metal surface.

More results were involved in the development of Dearnaley's [1969] model to which a principle background is those of Heinze and Wagener [1939].

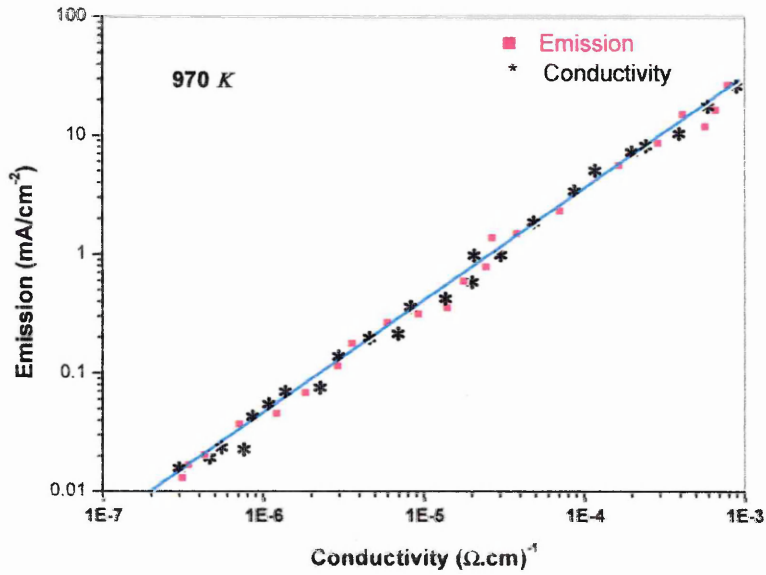


Figure 2.17: The direct relation between the conductivity through the oxide coating and the electron emission [Hannay et al, 1949].

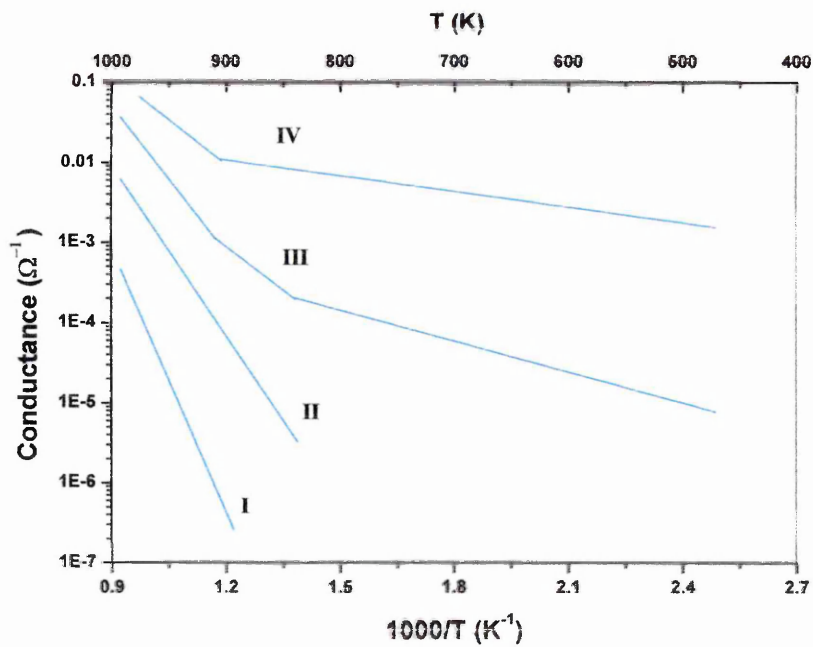


Figure 2.18: Dependence of conductance on temperature for the BaO, SrO and CaO cathode [Hannay et al, 1949].

They made an interesting observation of the distribution of emission from an oxide cathode at successive stages of activation. They formed electron images of the cathode surface and thereby observed that emission takes place from small bright centers.

Initially the saturation emitted current was less than $10^{-9} A$ and only a few centers were present. As activation proceeded the number of sites increased but their size and distribution pattern varied little, but the range of saturation current increased by a factor of 10^7 .

Projection-tube microphotography has been used by Mecklenburg [1942] to demonstrate that emission centers are less than 400 \AA in size and show a pattern related to the grain size and distribution in the oxide.

2.16.2 The theory of the conduction filament

Dearnaley [1969] put forward a model for activation, conduction and emission of an oxide-coated cathode in order to explain the behavior of certain other oxide layer structures.

In oxide-coated cathodes, he proposed that the presence of reducing agents at the activation temperature which results in the removal of some oxygen from the coating. At certain favorable points on the metal-oxide interface the oxygen may locally become conducting, perhaps due to an aggregation of oxygen vacancies, which may occur particularly at grain boundaries in the polycrystalline structure. An electric field was applied during activation, and the filament tended to grow through the oxide coating.

A high oxygen concentration evolves from the structure of the oxide material

at high temperature. Due to the fact that the Debye temperature of the alkaline earth oxides is quite low, despite their refractory nature: thus θ_D for barium oxide is about 250°C . Owing to their low mass the oxygen atoms will undergo violent thermal agitation at $T \sim 5\theta_D$ and may be ejected from the structure. The heavier barium atoms remain relatively undisturbed.

Dearnaley [1969] estimated the mean square displacement of oxygen atoms in BaO at 1250°C to be 0.8\AA while for barium atoms, displacement being inversely proportional to the mass, is an order of magnitude less. It is therefore understandable that oxygen can evolve at the activation temperature, and for the same reason the oxygen vacancies will possess a relatively high mobility. In this case, the conducting chain is created by a high concentration of oxygen vacancies and terminating at the metal base. The applied field will cause a very large electric stress at the other end, extending as it does into the insulating oxide. Under such a stress, and at the activation temperature, he proposed that further oxygen vacancies migrate to this tip and cause it to grow until the chain penetrates the oxide layer. The increased conductivity of the layer will eventually reduce the electric field and filament growth will come to an end.

Under the applied electric field, emission will already have begun, initially perhaps by field emission, but the current flowing through the chain will rapidly cause local heating and enhance the thermionic emission from the surface. In this case the exponential factor $\left[\exp\left(-\frac{\phi}{KT}\right) \right]$ which dominates the emission equations of Richardson (equation 2.3) is enhanced both because the local work function is reduced [Becker, 1935] and the local temperature is

increased [Koller, 1925 and Rothe, 1926]. However, it is difficult to draw definite conclusions from experiments in which the electron energy spectrum is measured by variation of retarding potential. The actual temperature of the emitting centers will be a function of the current drawn and the slope of the current- potential plot cannot as yet be usefully interpreted. Such plots would be expected to indicate a temperature lower than that of the emitting sites, since at maximum retarding potentials there would appear to be fewer energetic electrons.

The oxide in this model is clearly not a semiconductor which made Dearnaley [1969] expect to apply the emission equation of the saturation current density J_s :-

$$J_s = J_o T^2 \exp \left[\frac{- \left(\phi - Y e^{\frac{3}{2}} E^{\frac{1}{2}} \right)}{kT} \right] \quad (2.23)$$

But now T , E and ϕ must be allowed to vary over the cathode surface.

The close relation that exists between the oxide conductivity and the emission current may now be understood (Figure 2.17) since both arise from the same mechanism. During activation the number of conducting chains grow but the effective work function of each emitting site remains almost constant [Heinze and Wagener, 1939]. As the current through the conducting filaments rises, the oxide temperature (if the electrons are drawn away by dc accelerating field) becomes higher and so emits yet more electrons. The failure of oxide

cathodes to show true current saturation was therefore understandable. The electrons may be considered to be traveling as plasma through the narrow conducting region: the electron temperature may for a transient period exceed the lattice temperature. The lattice temperature will rise until thermal agitation ruptures the chains and the conductivity will be affected due to the particular atomic spacing and inter-band angles. The Debye temperature of the alkaline earth oxides is, as we have seen, quite small. Their maximum temperature will lie between the cathode operating temperature ($\sim 800^\circ\text{C}$) and the melting point ($\sim 1900^\circ\text{C}$). The filaments will break due to thermal vibration and under the influence of the low-frequency pulsed applied electric field then re-form again after cooling with a thermal relaxation time. The saturation of emission corresponds to the establishment of dynamic equilibrium with conducting filaments emitting, heating up, rupturing, cooling down and re-forming under the applied field. It is understandable that, as Wright [1947] observed, saturation of oxide conductivity occurs under just these conditions.

Dearnaly's [1969] picture of the composite cathode must take account of this and is illustrated schematically in Figure 2.19, which shows the conducting filaments extending between the interface material and the oxide surface.

Owing to the well-known tendency for crystal defects to accumulate at grain boundaries it is likely that chains of oxygen vacancies will tend to form along the edges of crystallites in the cathode surface. This is confirmed by some of the experiments on the distribution of emitting sites [Mecklenburg 1942].

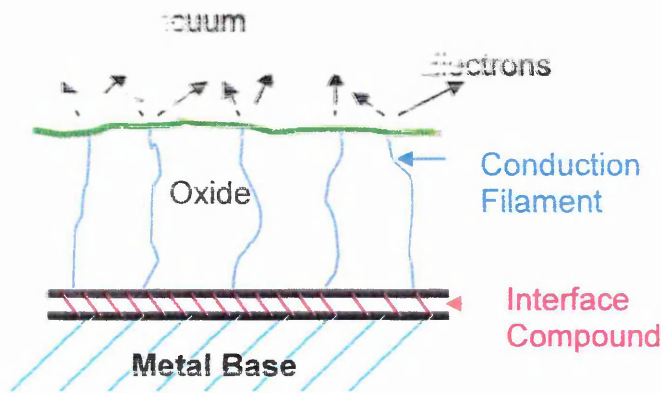


Figure 2.19: The schematic diagram of the conducting filaments [Dearnaly, 1969].

2.17 Electronic processes in the oxide cathode

For this discussion, it is not necessary to include the pore conduction process, which becomes significant at very high temperatures. Considerable work on photoemission was reported, but far fewer investigations were carried out on the thermionic emission properties of BaO crystals [Chin et al, 1974]. A similar relationship between the thermionic electron emission and the electrical conductivity was sought in the experimental study of BaO crystals. However, little correlation could be established between the electron emission and electrical conductivity for BaO crystals. This may be additional experimental evidence that the electrical conductivity measured from the oxide coating can not be interpreted as a bulk property of these oxides.

2.17.1 Ion adsorption effects

Because of the complexity involved in an actual oxide cathode, the adsorption of barium has been identified as an essential factor in thermionic cathodes

[Zalm, 1968]. Since the evaporation of BaO takes place at a much faster rate than that of SrO and CaO, the adsorption of barium ions on the strontium-calcium oxide is believed to be the activation process in a triple-oxide cathode. It is observed that barium adsorption can also take place on interfaces between oxide crystallites. The porosity in the oxide coating allows the formation of such adsorbed interfaces in the same manner as that of the emitting surface. Consequently, electron accumulations will occur at these ion-adsorbed interfaces as well as in the emitting area of the oxide crystallites. As a result, the barium adsorption serves not only to increase the electron emission at the cathode surface but also to enhance the electron conductivity between the oxide crystallites. With the above assumption it is conceivable that the rate of barium-ion adsorption at the interfaces is equal to that at the emitting surfaces. This would explain the linear relation of electron emission and conduction found in these experiments [Hannay et al, 1949]. Since the electron conductivity of BaO crystals cannot be increased through this adsorption process, the relationship of the thermionic emission with the electron conductivity is not expected to be linear. Hence, it is not surprising that the conductivity of the activated-oxide layer is two orders of magnitude higher than that of BaO crystals at high temperatures [Chin, 1974].

2.17.2 Simplified analysis of an idealized model

The adsorbed ions throughout the interfaces and the conducting paths along the crystallites are illustrated schematically in Figure 2.20. The conductivity is the sum of these paths along the interfaces of the oxide crystallites. In order to facilitate the estimation of the conductivity of the oxide crystallites they are

depicted in Figure 2.21 as simple cubes with an edge width D . For simplicity, these identical cubes are stacked in a regular array with some separation between them in each layer. The separations, as indicated in this model, simulate the porosity of a real oxide coating on the cathode. Also, separations are shown only between grains in each layer and not between layers.

This is really a simplification rather than an indication of any anisotropy in the formation of the coating.

From this idealized model, it is obvious that the length of the conducting paths is not greatly increased from the apparent thickness of the oxide coating. The conductance G of the coating is the sum of the contributions of all the paths

i :-

$$G = \sum \frac{\sigma a_i}{L_i} \cong \frac{\sigma}{L} \sum a_i \quad (2.24)$$

Where the conductivity σ along the path is considered the same for all paths, L is the thickness of the coating, and a_i is the cross-sectional area of the conducting part of the grains.

Although this estimate is valid only for cubes, the same reasoning can be employed to find the approximate conductivity of the grains of other shapes.

If the surface layer of cubes is the major conductive part, the cross-sectional area of the conductive path is actually $4L(D-L)$ instead of D^2 , the geometric cross section of the cube [Hutson, 1959]. Here, L is the approximate depth of the surface layer where the conductivity is greatly enhanced due to the ion adsorption. It will be shown later that for an inactivated grain the effective length L may reach $\frac{D}{2}$, so that electron conduction can be nearly uniform

throughout the grain.

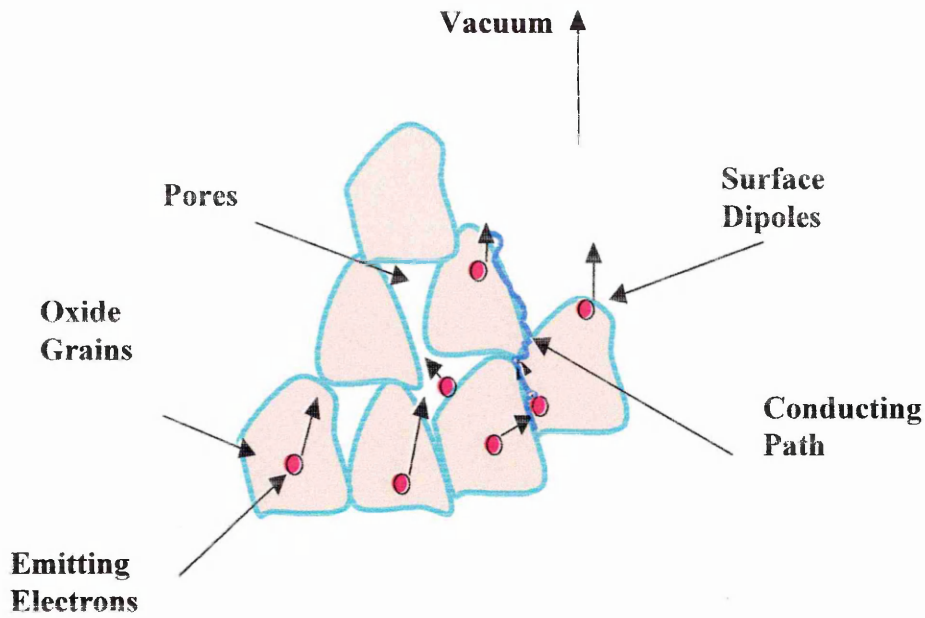


Figure 2.20: The structure of the oxide grains in a real oxide cathode

[Chin et al, 1974].

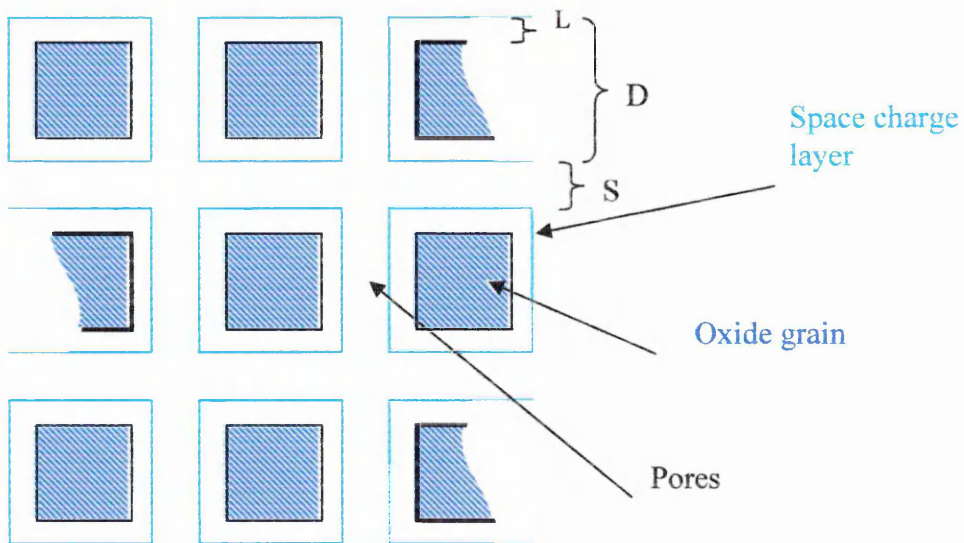


Figure 2.21: A cross-section view of the oxide grains in a well activated

cathode [Chin et al, 1974].

The thickness L of the surface layer will decrease as the barium adsorption progresses. In a well-activated cathode coating, the value of L is expected to be only a small fraction of the grain size D [Chin, 1974].

At the operating temperature of 1100 K , the electron density evaluated from the measured conductivity of inactivated oxides is not greatly increased from the intrinsic value of the material at that temperature as indicated in table 2.1 [Zalm, 1968, Saum et al, 1959 and Whited et al, 1969].

Before the oxides are activated, the electron conduction is assumed to be nearly uniform throughout the grain. The apparent electron density n_a will be equal to the effective density n_e in the grain. In the case of (BaSr)O crystallites, it may be considered that there is an intermediate case between that of BaO and SrO [Doloff, 1956].

The space-charge density ξ in *coulombs/cm³* may be obtained from the formula:

$$\xi = \frac{qn_e}{\cos^2\left(\frac{X}{\sqrt{2}\lambda}\right)} \quad (2.25)$$

λ is the usual Debye length which can be calculated using the formula:

$$\lambda = \sqrt{\frac{\epsilon kT}{4\pi e^2 n_e}} \quad (2.26)$$

After integrating the charge density ξ up to the surface with the coordinate

X , the total space charge Q (coulomb/cm²) can be expressed as:

$$Q = \sqrt{2\lambda} e n_e \tan\left(\frac{X}{\sqrt{2\lambda}}\right) \quad (2.27)$$

For well-activated crystallites, the conductivity as shown in table 2.2 is about $2 \times 10^{-3} (\text{ohm.cm})^{-1}$ at a temperature of 1100K. Consequently, the apparent electron density n_a in the well activated coating becomes:

$$n_a = \frac{\sigma}{\mu e} = 2.5 \times 10^{15} \text{ cm}^{-3} \quad (2.28)$$

The electron mobility μ was assumed to be $3 \text{ cm}^2/\text{volt.sec}$ for BaO single crystals [Chin, 1974]. As a result of the space charge accumulation on the oxide crystallites, the electron density n_b at the beginning of the surface layer may be estimated from:-

$$n_b = \frac{n_a D^2}{4L(D-L)} \quad (2.29)$$

Table 2.1: Physical constants and parameters for Alkaline Earth Oxide
[Chin et al, 1974].

| | BaO | SrO | CaO |
|-----------------------------------|-----------------------|-----------------------|-------------------|
| Band gap E_g (eV) | $4.4 - 0.001 T$ | $5.9 - 0.001 T$ | $7.6 - 0.001 T$ |
| Dielectric constant (k) | 34 | 13.1 | 11.1 |
| n_i at 1100k (cm^{-3}) | 4.7×10^{12} | 1.69×10^9 | 2.1×10^5 |
| Inactivated | 10^{-5} | 3×10^{-6} | |
| σ_o (ohm.cm) ⁻¹ | | | |
| n_o (cm^{-3}) | 1.25×10^{13} | 3.75×10^{12} | |
| $E_c - \phi_o$ (eV) | 1.56 | 1.65 | |
| $\phi_o - \phi_i$ (eV) | 0.09 | 0.75 | |
| λ (μm) | 3.78 | 4.28 | |

Table 2.2: Electrical conductivity at 1100K of Alkaline Earth crystals and coatings [Chin et al, 1974].

| | Conductivity (ohm.cm) ⁻¹ |
|------------------------------|-------------------------------------|
| BaO Single crystal | $1-2 \times 10^{-4}$ |
| SrO Single crystal | 10^{-7} |
| CaO Single crystal | 10^{-8} |
| Inactivated BaO Coating | $10^{-5}-10^{-4}$ |
| Activated BaO Coating | $1-5 \times 10^{-2}$ |
| Inactivated (Ba,Sr)O Coating | $3 \times 10^{-6}-10^{-4}$ |
| Activated (Ba,Sr)O Coating | $2 \times 10^{-3}-10^{-2}$ |

2.18 Conduction mechanisms and Narita theory

According to the semi-conductor theory and Fowler's theory [Hanney et al, 1949], the thermionic current emission i and the electrical conductivity σ are given respectively by the following formula:

$$i = \sqrt{N_e} \frac{e(1-r)}{2\pi m^* h^{3/2}} (2\pi m^* kT)^{5/4} \exp[-(\chi + E_a)/kT] \quad (2.30)$$

$$\sigma = \sqrt{N_e} e \mu_e \left[\frac{2\pi m kT}{h} \right]^{3/4} \exp\left(-\frac{E_a}{kT}\right) \quad (2.31)$$

And therefore:

$$\frac{i}{\sigma} = \frac{1-r}{2\mu_e \pi m^*} (2\pi m^* kT) \exp(-\chi/kT) \quad (2.32)$$

Equation 2.32 suggests that the emission must be directly proportional to the conductivity at any fixed temperature and χ electron affinity.

Narita [1952], studied the thermionic emission and electrical conductivity of sintered oxide-coated cathodes. The measurement by means of an embedded probe was compared with that of the normal oxide-coated cathodes. Their emission and conductivities at 785K, work functions Φ , activation energies E , and the apparent values of the electron affinity χ obtained are tabulated in table 2.3.

Such small values of the activation energy for conduction through the grains are difficult to understand, and this conduction was believed to be a surface

Table 2.3: The electrical parameters for initial and fully activated states**[Narita, 1952].**

| Cathode type | i mA/cm^2 | σ Mho | Φ eV | E eV | χ eV |
|---|----------------------|----------------------|-----------|--------|-----------|
| N { <i>Initial</i> <i>Activated</i> | 9×10^{-3} | 1.5×10^{-4} | 1.2 | 1.04 | 0.16 |
| | 8.1×10^{-2} | 1.2×10^{-3} | 1.03 | 0.86 | 0.17 |
| S { <i>Initial</i> <i>Activated</i> | 7×10^{-5} | 1.2×10^{-5} | 1.89 | 0.94 | 0.95 |
| | 2.8×10^{-2} | 1.7×10^{-4} | 1.06 | 0.44 | 0.62 |

conduction through a multi-atomic barium layer on the surface of the oxide particles. This was confirmed by comparing it with the conduction through a very thin barium film deposited on a silica plate.

From these results it was believed that in oxide coating there may be three mechanisms of electron conduction:-

1. Conduction by an electron gas in the pores or conduction through grains limited by contact potential barriers between grains.
2. Pure conduction through grains.
3. Surface conduction through surface barium layers.

All of these are connected in parallel in the general case, and the mono-atomic surface layer of barium serves to reduce the work function.

It was proposed that the conductivity of a porous semiconductor, such as an oxide-coated cathode, was influenced by the presence of an electron gas in

the pores of the aggregate. Hensley [1952] calculated the magnitude of the conductivity component which depended on two simplified models approximating the geometry of a pore. The conditions, under which such components of the conductivity can appreciably modify the total conductivity, were analyzed. It was further shown that such a porous semiconductor would possess two sources of thermoelectric emf. One is in the crystals of the aggregate and the other is in the interstices between the crystals. A simple theory for the thermoelectric power of the electron gas in a pore was developed.

There was evidence from measurements of the conductivity of oxide cathodes in the temperature range $300-600K$ to suggest that at least two processes contribute to the conduction mechanism [Higginson, 1958]. One of these might be identified with the movement of barium ions over the surfaces of the minute crystallites, which constitute the oxide coating. The other process was thought to be electronic conduction, the oxide particles being N-type excess semiconductors, limited by barriers, e.g. electron traps due to oxygen, between the crystallites. Impaired movement of barium ions may be then explained by oxygen poisoning in this temperature range on the crystallite surfaces and increased electron trapping at crystal-crystal interface [Higginson, 1958].

New models for the oxide-coated cathode must be introduced to understand these differences in the evaluation of the activation energy and work function due to the experimental results.

According to Narita, oxide coated cathodes are classified into four different types based on the energy band structure. These types are:

- α -type:-

This type may be observed as the initial state of the "S" cathode before the activation and may be of simple semiconductor type. In this type:-

$$\phi = E_o + \chi \quad (2.33)$$

E_o and E_a are the energy difference from the bottom of the conduction band to the Fermi level and to the donor's respectively, as shown in Figure 2.22.

Where E_o is larger than $\frac{1}{2}E_a$ for inactivated state. The experimental numerical values of E_o and χ are probably $0.8 \sim 1.0 eV$ and $1.0 eV$ respectively, and then $\Phi = 1.8 \sim 2.0 eV$ [Narita et al, 1948].

- β - type:-

The structure of the cathode in this type is considered as a semiconductor possessing a monolayer of barium on the surface and is realized as the activation state of "S" cathode. The work function of this type is lowered due to dipole moment at the surface and the Fermi level is located half way between the bottom of conduction band and the donor levels, for the well activated cathode, as shown in Figure 2.23.

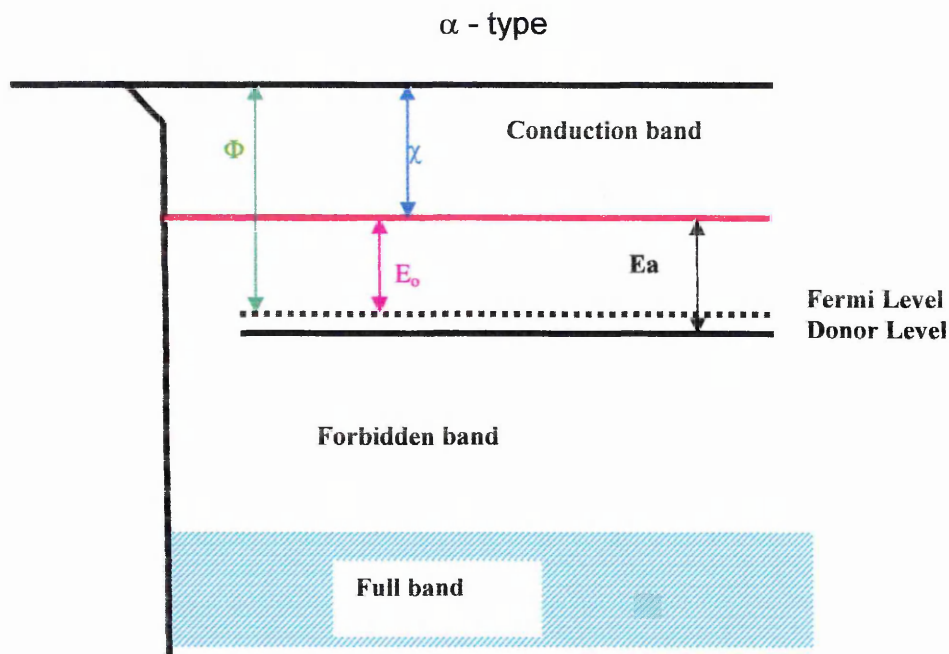


**Figure 2.22: The band structure of the α type oxide cathode
[Narita, 1953].**

As χ is lowered by $U = 0.45\text{eV}$ and the probable value of E_a is 0.9eV , Narita thus obtained:-

$$\phi = E_o + \chi - U = \frac{E_a}{2} + \chi - U = 1\text{eV} \quad (2.34)$$

- γ - type:-

When the base metal contains reducing elements, such as Mg, Si, or when

barium is added to the cathode from an external source, the barium content in the cathode is so large that a multiatomic layer of barium may be formed on

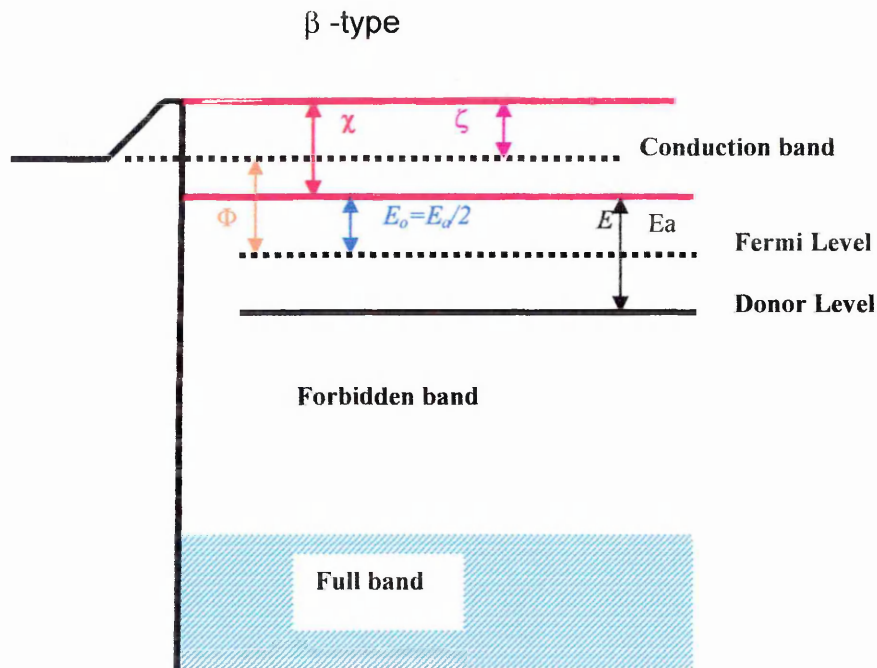


Figure 2.23: The band structure of the β type oxide cathode [Narita, 1953].

the surface of oxide particles through which M-type conduction appears, as shown in Figure 2.24.

In this case the work function is slightly higher than that of a monolayer (less than $0.1eV$), thus the work function is given by:-

$$\phi = (\chi - U) + E_o + 0.1 \approx 1.1eV \quad (3.35)$$

The conduction is of M-conduction and its activation energy is in the range of $E_o = 0 - 0.4eV$.

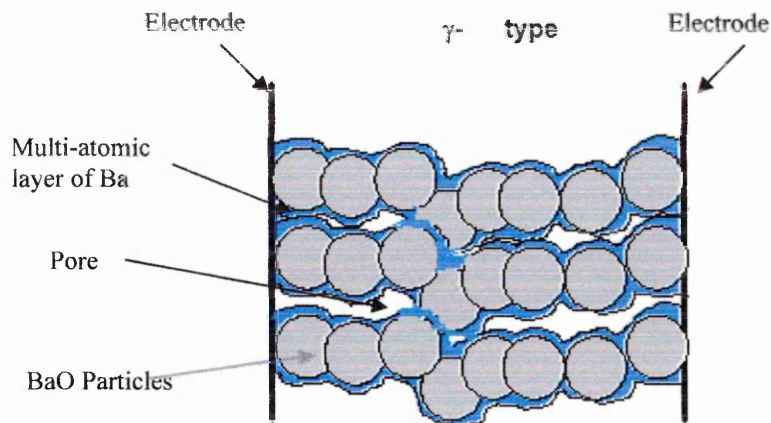


Figure 2.24: The multi-atomic Ba layer covered the grains in the γ type oxide cathode [Narita, 1953].

- δ -type:-

When a contact potential barrier exists between oxide particles, as in the case of a "N" type cathode and as shown in Figure 2.25, the activation energy of the conduction is equal to that of pore conduction which is slightly lower than the work function and it is given by:-

$$E_o = \phi - \nu = 0.8 \sim 1 eV \quad (2.36)$$

The work function is the same as that of β -type since the current density of this type is usually good compared with the other types and ν is the difference between the work function and the activation energy.

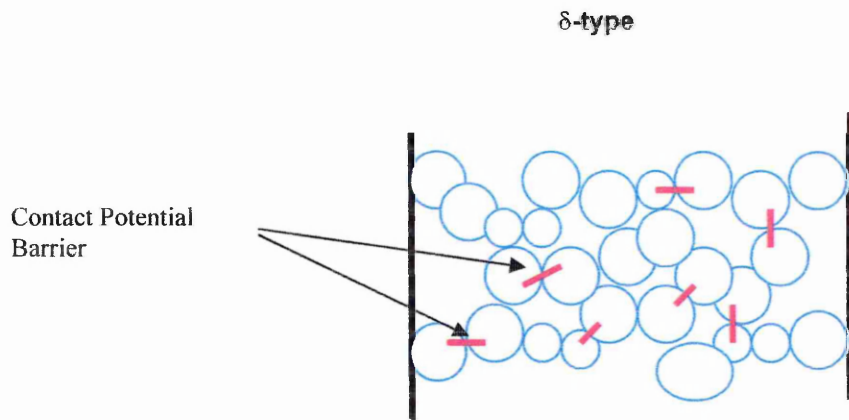


Figure 2.25: The contact potential barriers in the δ type oxide cathode

[Narita, 1953].

Chapter 3

Industrial cathodes preparation and experimental technique

3.1 Introduction

This chapter gives an overview on the current L.G. Philips oxide cathode preparation and recent benchmarking investigations. The procedures of the oxide cathode assembly were studied and were used in this research to investigate the electrical properties and the formation of the interface layer. It is important for the cathode display market, especially the new generation of oxide cathodes, to view the effect of the interface layer activator agents distribution on the electron conduction.

3.2 Cathode assembly

The basic structure of the usual indirectly-heated oxide cathode is shown schematically in Figure 3.1; the cathode comprises the following components: the emitter layer, Nickel cermets cap, Nickel sleeve and the Alumina heater, some of which are described below.

- **Emitter layer**

The typical production-type oxide cathode is a coating of barium and strontium oxides on a base metal such as nickel. The oxide layer is formed by first coating a nickel can or disc with a mixture of barium and strontium carbonates, suspended in a binder material. The mixture is approximately 60% barium carbonate and 40% strontium carbonate. During vacuum

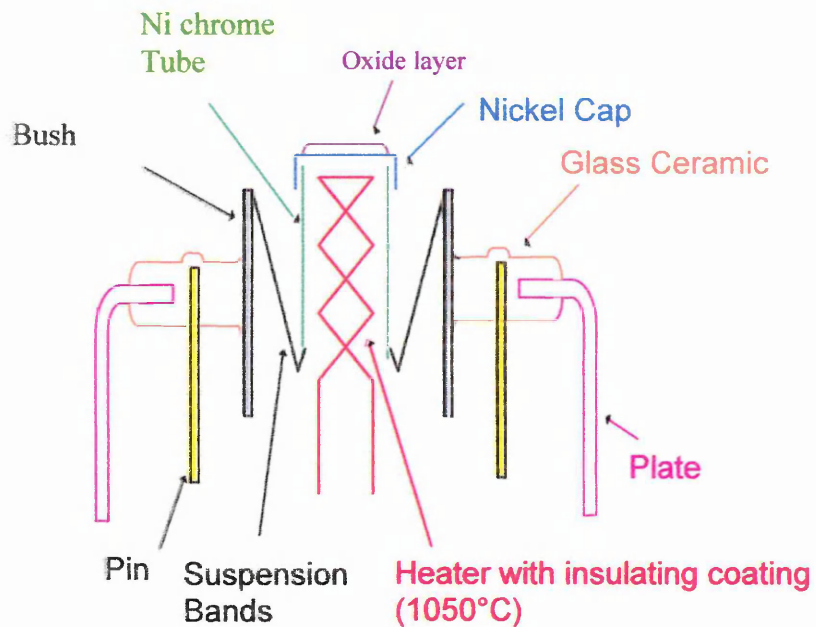
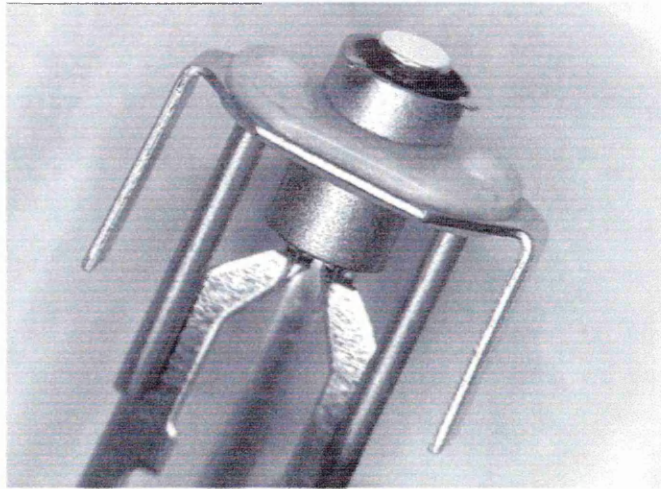


Figure 3.1: Cathode photograph and schematic diagram showing the cross-section of the “oxide cathode plus” assembly [Barratt and Gärtner 2003].

processing of the tubes, they are baked at high temperature. The binder is burnt away, and the carbonates are subsequently reduced to oxides and then the cathodes are now "activated" and will emit electrons.

- **Nickel alloy cap and Nickel sleeve**

Usually the sleeve and cap are made of a base metal such as Ni which contains a small amount of impurities such as Mg, and Al. Other less common base metals include e.g.; Ni-W alloys; Ni-W-Zr alloys, Ni-W-Mg alloys, and Ni-Zr alloys (depend on the oxide cathode generation). In these alloys, the concentration of W and Zr, is much higher than that of Mg and Si in the Ni base. In the case of base metals whose resistivity is relatively high, such as Ni-W or Ni-W-Zr, coating a strip of base metal with the oxides and passing heater current directly through the strip can make a directly heated cathode [Gärtner, 1999].

3.3. Industrial preparation techniques of cathode devices

- **Preparation of the emitter layer composite**

The composite contains carbonates and oxide additions in a suspension fluid (Nitro-cellulose and ethyl alcohol amyl or butyl- acetate). The mixture is ground in a ball mill for about 20 hours.

- **Preparation of the films**

The cathode oxide layer is deposited using the spray technique [Al-Ajili et al, 2001][Hodgson et al, 1999]. The type of nozzle of the spray gun, the air

pressure, the distance between the cathode and the gun and the humidity in the spray chamber are very important parameters that determine the quality of the resulting coating.

- **Removing the nitro-cellulose binder**

Coated cathodes are baked in air at 675 K in order to remove the binder. It should be noted that treatment in the temperature range of $440\text{ K} < T < 675\text{ K}$ is not sufficient to remove the binder and reduces the mechanical strength of the layer.

- **Removing the oxide film**

To remove any oxide film formed during the treatment on the Ni base, a second annealing at $775 - 825\text{ K}$ in Hydrogen is required.

After this treatment the colour of the cathode should be changed from grey via a patchy blackish grey to pure white.

3.4. Cathode Activation

- **Conversion**

The conversion of the carbonates is performed by heating the cathode for a few minutes at temperatures in the range of $1000 - 1200\text{ K}$ and pressures varied from 10^{-3} mbar at the beginning of the conversion process to 10^{-6} mbar after it is completed.

- **Activation**

After completion of the conversion, activation can be achieved by raising both the cathode temperature (up to $1200 - 1400\text{ K}$) and pressure (down to

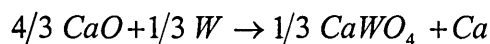
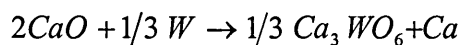
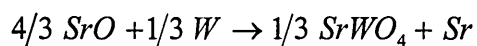
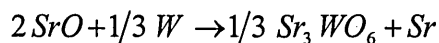
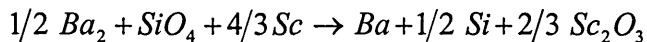
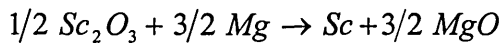
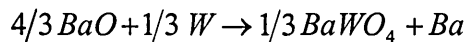
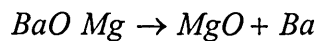
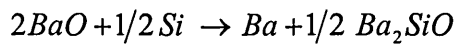
3×10^{-6} mbar) for a few minutes, depending on type of the oxide and metal base.

- **Stabilization**

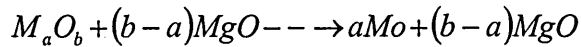
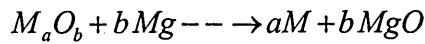
To stabilize the emission, the temperature should be reduced subsequently to the operating range of 1040 – 1100 K .

3.5 Chemical reaction mechanisms during the cathode operation lifetime

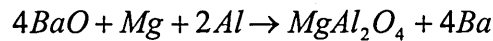
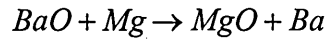
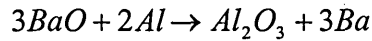
Some of the probable reactions happening inside the cathode depend on the oxide layer compositions and the activators in the Nickel cap, marked as reduction process [Gärtner, 1999]:



The general reactions between the oxide dopant M_aO_b and the reducing agent Mg :-



For oxide cathode plus, the only reactions that can take place are:



3.6 Accelerated life by increased operating temperature

Electrical conductivity and the critical dc density is determined by the density of the shallow mobile donors n_D , which is proportional to the concentration of element Ba [Gärtner et al, 2002]. The generation of free Ba is accomplished by reduction reaction of BaO with activators like Al, Mg, W, diffusing from the cathode Ni base to the interface. Since Ba generation (and loss) increases with operating temperature, cathode life will be shortened. Hence instead of running the cathodes in the UHV chamber at usual operating temperature of $1050K$ (true temperature), accelerated life tests are carried out at $1150K$ (true temperature), which usually will reduce life from 20000 hrs to about 2000 hrs , which is responsible testing time.

By comparing experimental results of accelerated life-test at elevated temperature with theoretical model estimations, life predictions for lower and for operating temperature can be derived. The theoretical model is based on the temperature dependence of the diffusion coefficients of the activators in cathode Ni [Petersen et al, 1957 and Allison et al, 1959]. From the pre-exponential factors and diffusion activation energies, the temperature

dependence of the diffusion coefficients was calculated and is depicted in Figure 3.2. Essentially it can be seen, that the increase of diffusion coefficients is comparable for different activators for a temperature increase of about 100 K, which can be seen from the list of the ratio in table 3.1.

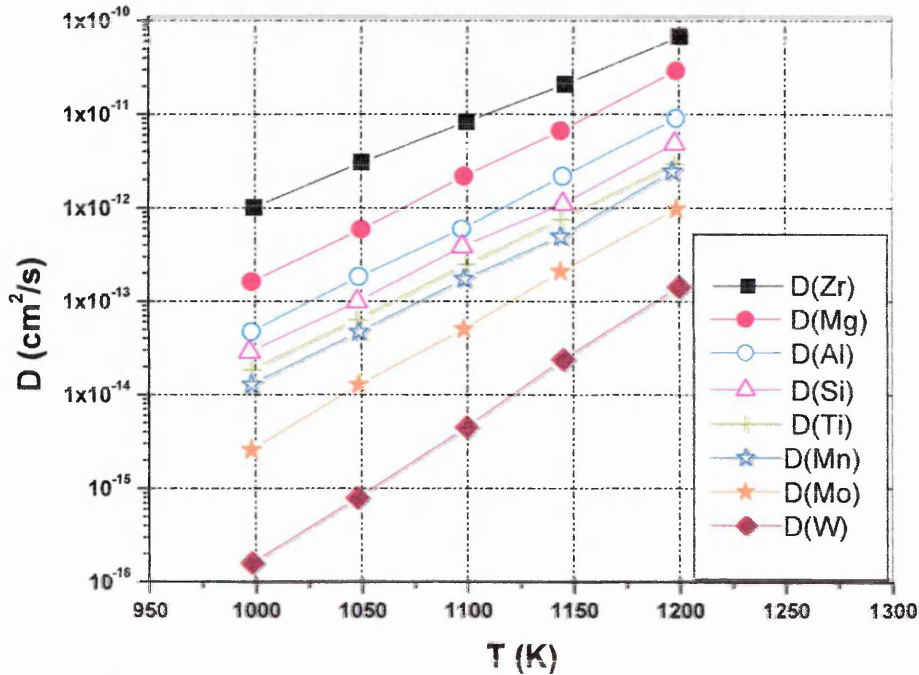


Figure 3.2: Temperature dependence of diffusion coefficients in oxide cathode [Peterson et al, 1957 and Allison et al, 1959]

Table 3.1: List of the ratios of the diffusion coefficients $D(1050\text{ K})$ to $D(1143\text{ K})$ for the most important activators.

| Activators | Zr | Mg | Al | Si | Ti | Mn | Mo | W |
|--|-------|------|-------|-------|-------|-------|-------|-------|
| $D(1050\text{ K})[10^{14}\text{ cm}^2/\text{s}]$ | 300 | 71.5 | 8.74 | 21.6 | 14.0 | 7.9 | 1.34 | 0.112 |
| $D(1050\text{ K})/D(1143\text{ K})$ | 0.154 | 0.11 | 0.082 | 0.092 | 0.091 | 0.073 | 0.068 | 0.05 |

This would correspond to a cathode life reduction when increasing the temperature from $1050 K_{true}$ to $1150 K_{true}$, to a range between 15% and 5% for all activators of table 3.1, or between 11% to 5% for Mg, Al, W as activators. The average lifetime of Ba/Sr oxide cathodes with these activators at $1150 K_{true}$ is about $1600 hrs$ compared to $\geq 20000 hrs$ in UHV at standard operating temperature [Gärtner et al, 2002].

3.7 Experimental technique and the measurement method

Two experimental techniques were used to activate and operate the cathodes due to the objectives of the investigation and the time of the treatment, and are detailed below.

3.7.1 Cathode to cathode in a vacuum chamber

The cathodes (shown in Figure 3.1) were mounted, face to face in pairs in a specially designed holder and test assembly, as shown in Figure 3.3. The test assembly allowed the oxide surfaces of the two cathodes to be positioned using a commercial UHV linear drive micrometer to give physical contact between them, to enable direct measurements of conductivity to be made. The pressure between the specimens was controlled by stainless steel springs to overcome the expansion from the suspension bands created during the heat treatment. The cathode heater filaments were connected in parallel with an external DC power supply (HP 6034A) to allow the cathodes to be heated in situ during the measurements, with the temperature being determined from a series of prior calibration measurements of heater filament

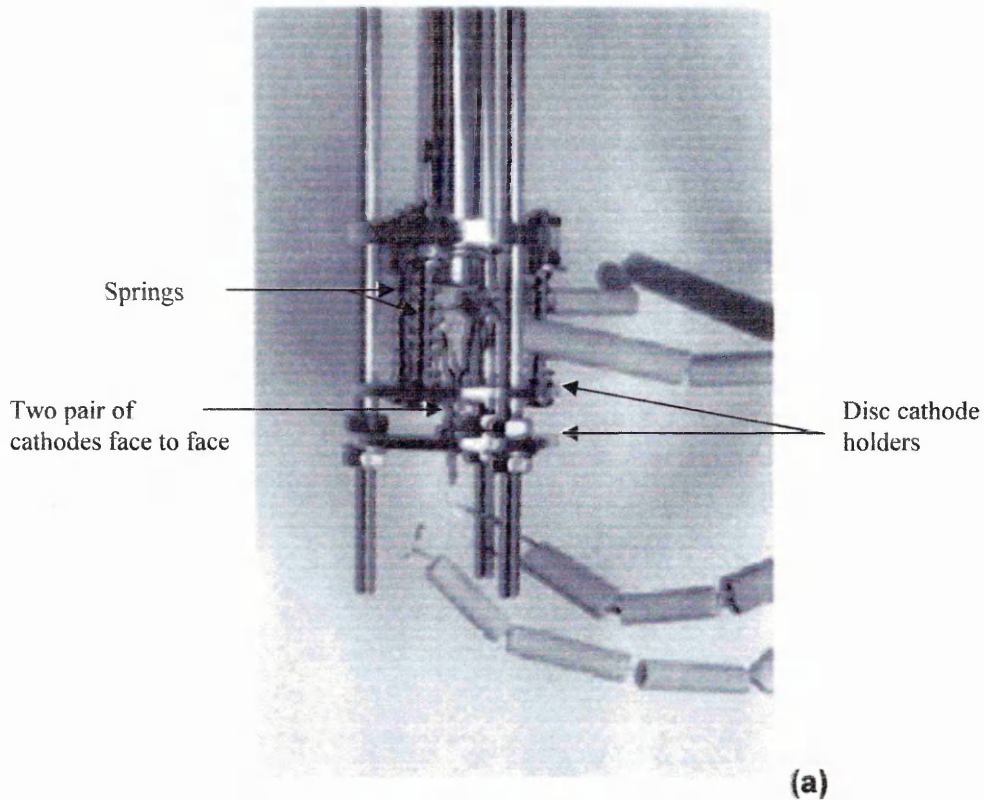


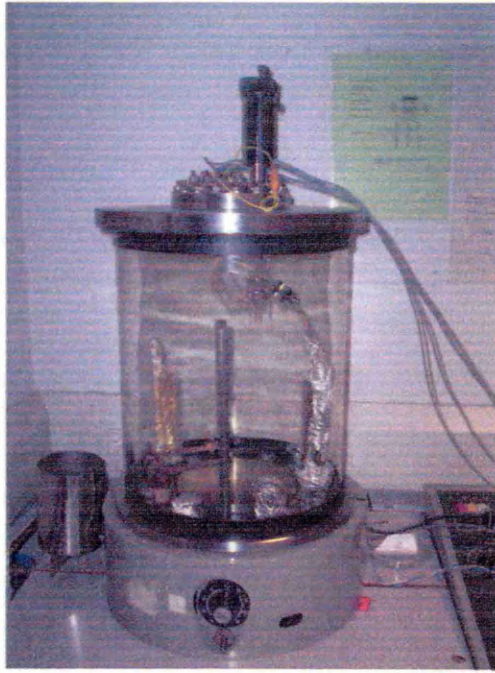
Figure 3.3: (a) The specially designed holder for electrical measurements (b) UHV linear drive micrometer.

voltage versus temperature carried out using a thin wire thermocouple placed in contact with the cathode sleeve. The bright temperature measurement was confirmed using an optical pyrometer. This arrangement was undertaken following the procedure due to Loosjes and Vink [1949].

The assembly was mounted inside a glass chamber which was evacuated to about 3×10^{-7} mbar, as shown in Figure 3.4. This pressure was maintained during all measurements. Using the integral heater filaments, the cathodes were activated and operated at different temperatures and for different periods of time. DC and AC electrical measurements at various temperatures in the range $300K$ to $1425K$ were performed perpendicular to the oxide layer via connections made to the nickel cathode substrates to a programmable Keithley 6517A electrometer and HP-4284 precision LRC electrometer. The circuit diagram is shown in Figure 3.5. The measurements were made immediately after activation stab of the cathodes [Al-Ajili et al, 2000].

All the cathodes were converted and activated according to the steps of the LG Philips activation procedure, as shown in table 3.2 (X was changed from 1–12 hrs and Z was varied in the range 1125–1425 K).

To reduce the real lifetime of the oxide cathode by a factor of 10, the cathode was operated using the L.G.Philips procedure called “acceleration lifetime test”. To achieve this acceleration, the normal operation temperature, $1025K$, was increased to $(1085–1125)K$ [Gärtner,1999].



(a)



(b)

Figure 3.4: (a) The special cathode holder in a vacuum chamber. (b) The vacuum system and measurement set up.

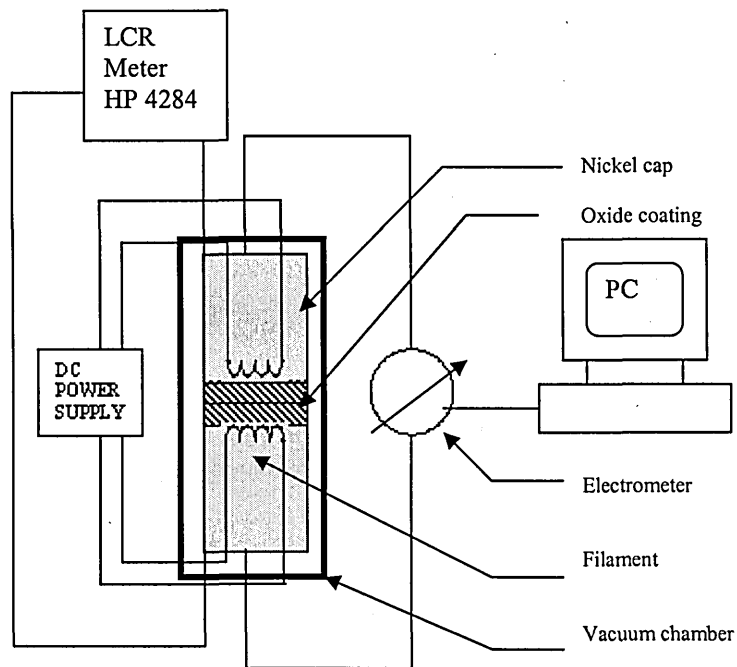


Figure 3.5: Schematic diagram of DC and AC measurements circuit.

Table 3.2: UHV activation and ageing scheme [LG Philips]

| Duration : | Heater current LG / Philips: | Heater voltage (Philips): | Temperature (Ni-Br.) | Diode voltage : |
|-----------------------------|---------------------------------|------------------------------|-------------------------|-----------------|
| Preheating and conversion : | | | | |
| 2 min | 78 mA / 70 mA | 3.0 V | ca. 725 K | 0 |
| 2 min | 91 mA / 83 mA | 4.0 V | ca. 775 K | 0 |
| 3 min | 114 / 103 mA | 6.0 V | ca. 1000 K | 0 |
| Activation: | | | | |
| 3 min | 128 / 115 mA | 7.3 V | 1075 K | 0 |
| X- min | 148 / 133 mA | 9.5 V | Z | 0 |

The first set of the electrical measurements comprised conductivity measurements carried out on a Ni 5% powder cermet oxide cathode activated to $Z = 1200 K$ for $X = 1 hr$ and accelerated up to $600 hrs$ in order to investigate the on-going thermal changes under acceleration conditions on the characteristics of the coating material.

The second set of electrical measurements comprised conductivity measurements carried out on a Ni 2.5% powder cermet oxide cathode (which is oxide cathode plus) activated for different temperatures; $Z = 1125 K$, $1200 K$ and $1425 K$ and a time period of $X = 1 - 12 hrs$, in which the changes in the electrical properties were determined as a function of activation time. These experiments aimed to identify the effect of the activation process on the conductivity of oxide cathode.

3.7.2 Spectroscopy analysis

The characterisation of the activated cathode surfaces was performed using a Philips SEM XL40 equipped with a tungsten filament. The scanning beam voltage was fixed at $20 KV$. The best lateral resolution obtained for cathode investigations was about $100 nm$. An EDX (energy dispersion x-ray spectroscopy) also from Philips is mounted on the SEM XL40 and is used for determination of elemental constituents of the cathode surfaces at the same beam voltage. The detector resolution of X-ray energy is of the order of $138 eV$.

3.7.3 Coated-non coated cathode assembly in an evacuated dummy tube

In the present work, the formation of the interface layer associated with the diffusion of reducing elements (Mg, Al and W) to the Ni cap surface of the oxide cathode and the effect of the diffusion of these elements on the conductivity of oxide cathode were studied by a new method. This method used one pair of oxide cathodes plus in every dummy tube. One of these cathodes is a oxide coated cathode and the other is an uncoated oxide cathode. The test assembly of two aluminum cathode holder discs allowed the oxide surface and Ni cap surface of the two cathodes to be positioned to give a physical contact between them. Figure 3.6, shows the design of the aluminum cathode holder disc. The holder assembly was connected to the dummy tube base (Figure 3.7b) using steel wires which was also used to improve the alignment of the holder assembly with the dummy base, which is shown in Figure 3.7a. This alignment is very important in the next stage of the automatic sealing process. The entire assembly, as shown in Figure 3.8, was mounted inside a dummy tube and then both the dummy and the base were sealed automatically in a special design machine belong to the L.G. Philips industrial workshop.

The dummy tube was evacuated prior to and during the decomposition and activation process to about 10^{-6} mbar . The decomposition process was achieved by backing the whole set of dummy tubes to about $725-775 K$. However, the activation was achieved by employing a D.C. voltage on the uncoated cathode filament to elevate the cathode temperature to about $1200 K$. After the decomposition and activation process was finished, the neck of the dummy tube was sealed off under this condition.

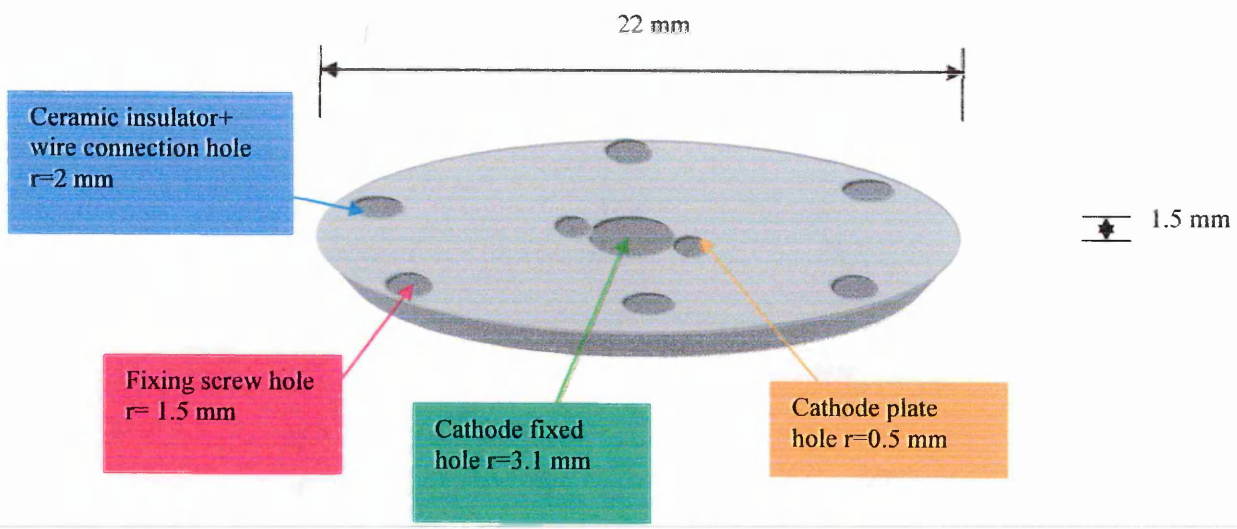


Figure 3.6: Cathode disc holder.

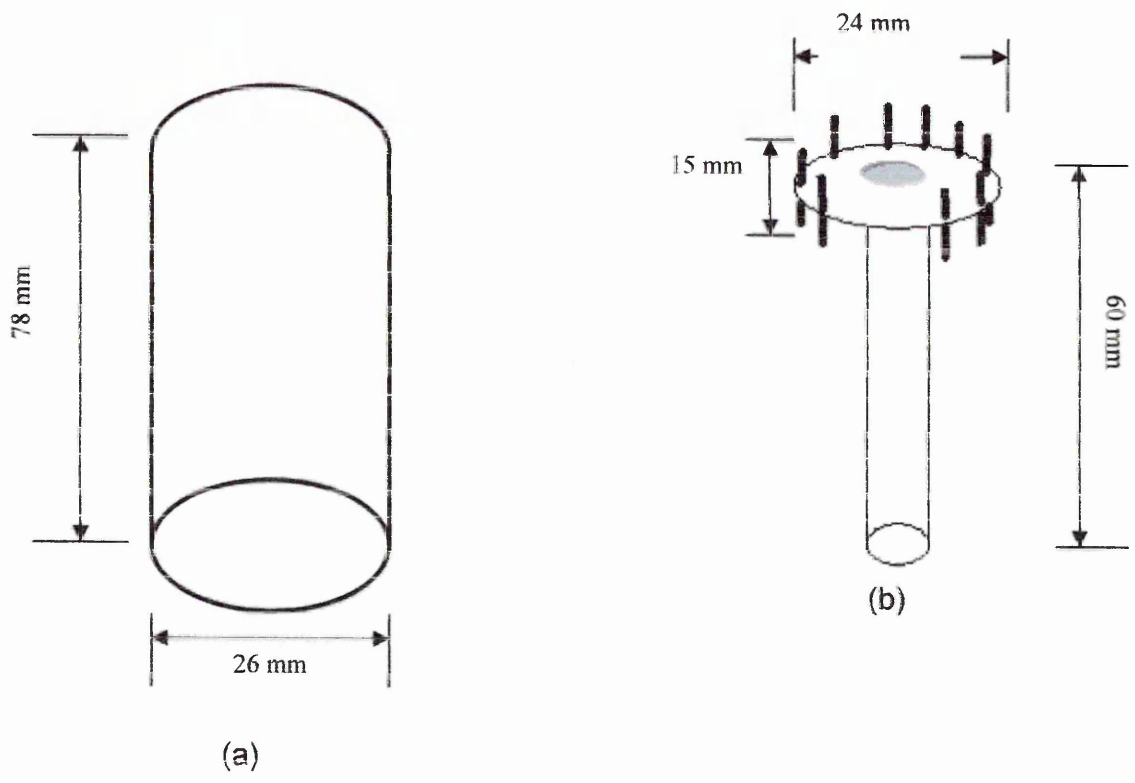


Figure 3.7: Pyrex glass dummy tube (a) the cylinder part (b) the neck, vacuum tube part.

The dummies were then ready to be operated for the lifetime test. The filament temperature of the uncoated cathode was elevated to the accelerating temperature 1085K for lifetime measurements using a control board set to 999min on and one minute off.

The equipments used for this study were L.G.Philips industrial machines in Blackburn.

After oxide cathode plus decomposition and activation, Al and Mg doping takes place during heating to 1085K through an acceleration life test.

Number of dummy tubes was left to be operated for different lifetime and then was electrically tested to get the I/V characteristics of the cathode assembly.

When the I/V measurements were checked finally, the dummy tube was brake down to remove the cathodes from inside the dummies and were sent to SEM and EDX test.

Figure 3.9 shows the circuit diagram for the electrical measurements.

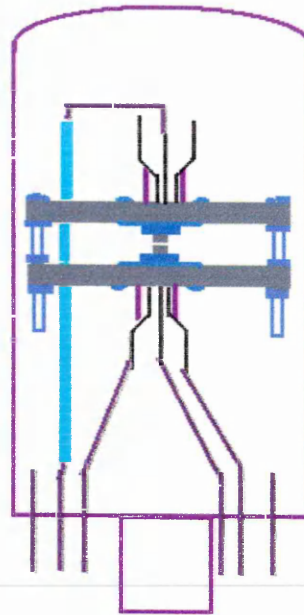
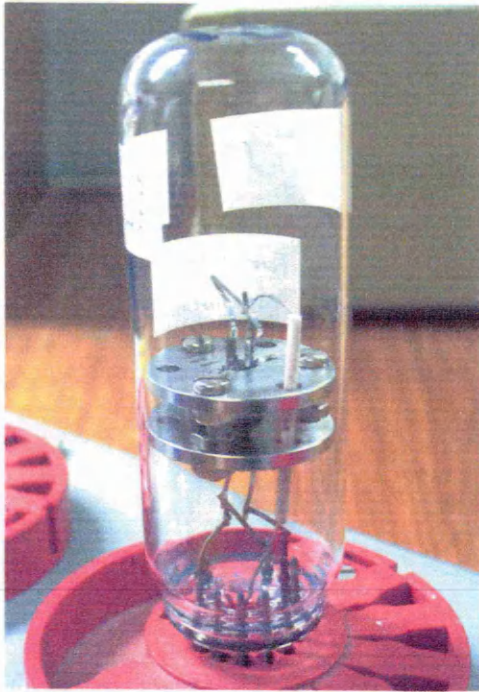


Figure 3.8: A set of two cathodes assembled face to face in a dummy tube ready for electrical measurement.

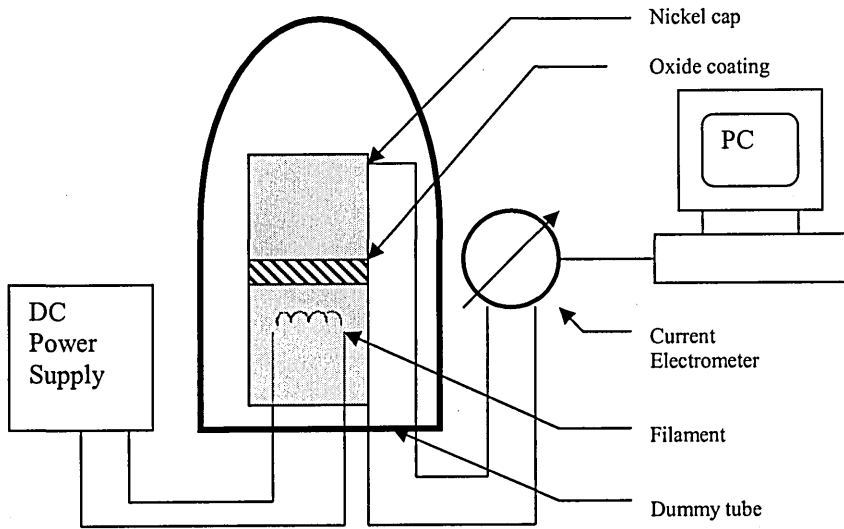


Figure 3.9: Schematic diagram of test and measurement circuit.

CHAPTER 4

Accelerated lifetime test

4.1 Introduction:

One approach to enhance the emission current density is to reduce the cathode coating resistivity by dopant elements of group III, IV or V (e.g. Y_2O_3 , ZrO_2 , V_2O_5), which leads to a decrease in the surface work function. Provision of a low work function is generally considered the mechanism responsible to create a high current density to change the equilibrium rates of Ba formation and deposition [Hayashida et al, 1999 and Gärtner et al, 1997].

The most recent approaches to improving the performance of the oxide cathodes has been the incorporation of conductive metallic phases; this has been studied by a number of workers [Uda et al, 1999, Hodgson et al, 1999, Gärtner, 1992 and Narita, 1995]. Another approach to determine the electrical conductivity of the oxide layer directly is to use a close- space planar diode configured in an UHV chamber, to gather thermionic emission data [Gärtner et al, 2002].

The aim of this chapter is to study the effect of metallic conduction on the conductivity of BaO/SrO through the lifetime of the oxide cathode. There are two possible metallic conduction paths percolated through the oxide material; these are the adsorbed Ba layers and the additional Ni powder.

For this study, a novel type of BaO/SrO oxide cathode was chosen. The cathodes were supplied by LG.Philips Displays and comprised a top layer of Ni5% (by weight) powder cermet with a surface area of 0.0165 cm^2 and a layer thickness of approximately $65(\pm 10)\ \mu\text{m}$ deposited onto a Nickel alloy cap [AL-Ajili et al, 2000]. This Ni cap contains low levels of Mg (0.125%) and Al (0.1%) as activators.

4.2 Experimental measurements

In this section we describe the D.C. and A.C. characteristics including the electron activation energy and the confirmation of the electron conduction mechanism.

The electron activation energy was monitored over the first several hundreds hours of cathode operation lifetime.

In particular we were concerned with the influence of the oxide reduction process and the performance of the Ba coverage layer on the current density and the conduction mechanism behaviour.

The cathode decomposed and activated under these conditions as explained in section 3.6.1 (enough compressing pressure between the two attached cathodes and a very high temperature) and then accelerated through the heating temperature 1125K is most likely to be an "S" type cathode. The oxide particles considered to sinter have a small distance in the grain-to-grain boundaries as shown in Figure 4.1. These cathodes were prepared by using

barium-strontium carbonate which is thought to be sintering less than barium carbonate cathode [Narita, 1953].

The current density measurements were performed at various temperatures in the range $300\text{--}1200\text{ K}$ at 100 hr intervals up to a total of 600 hr . Baseline measurements were made immediately after activation of the cathodes.

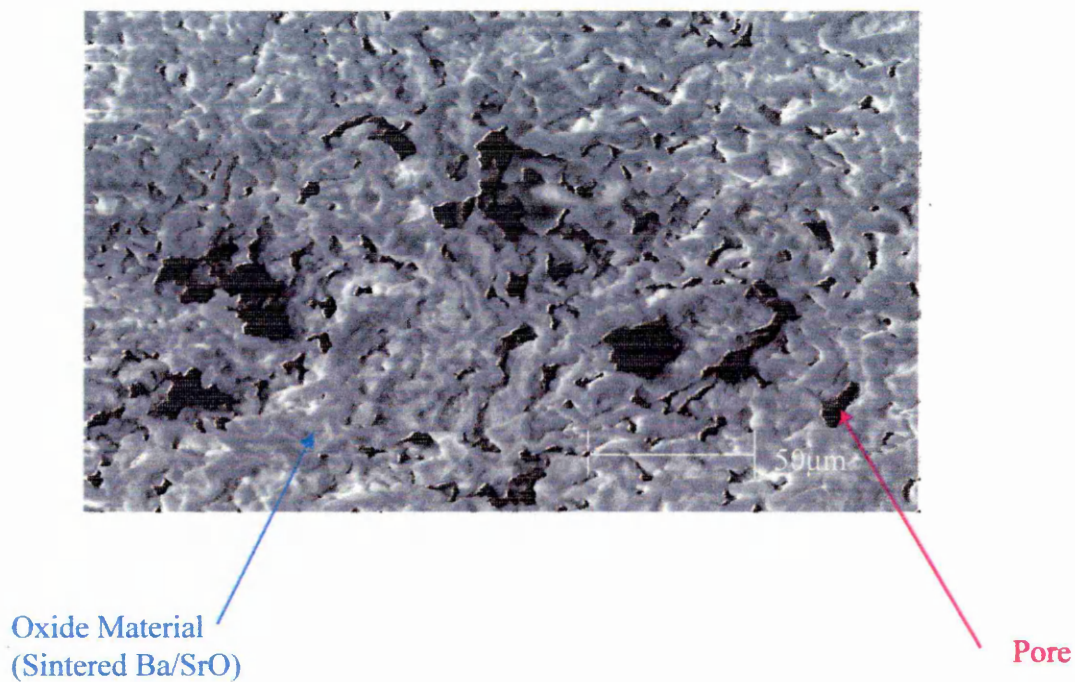


Figure 4.1: SEM image of the top surface of activated "S" type cathode.

4.4.1 DC measurements during the accelerated lifetime

The D.C. current-temperature dependence for the (Ba/Sr) oxide immediately after activation (0 hour run), in the form of $\log \sigma$ versus $1/T$ is shown in Figure 4.2. From these plots it is possible to determine two activation energies for

Chapter 4

this material. "S" type oxide cathodes show energy levels of 1.49eV and 3.8eV respectively, marked by E_{a1} , E_{a2} and E_{a3} in Figure 4.2, which are very close to the first donor and the energy gap of BaO [Nergaard, 1952]. The basic structure of "S" type oxide cathode is midway between a pores oxide material and bulk BaO. This makes the evaluation of the activation energy close to, a BaO crystal. The small shift from the BaO band (shown in Figure 3.1) structure may be as a result of distortion of the BaO structure by the other (mixed) oxides and also because of the metallic phase addition (Ni powder). In the case of the metallic addition phase, it was assumed that the composite cathode coating could be modelled as two parallel conduction paths, one component being the continuous metallic pathway and the other a semiconductor oxide.

The metallic component is formed above the percolation threshold and comprises the dominant conduction mechanism. The semiconductor component is thought to make an appreciable contribution at elevated temperatures [Yamamoto, 1997].

A similar temperature dependent conductivity measurement was performed on samples that had been maintained at 1100K for a period of 100 hours after activation. Lower activation energies in the range $E_{a2} = 0.87\text{--}1.05\text{eV}$ were observed (Figure 4.2b) that may be associated with the formation of a Ba monolayer structure as a result of BaO reacting with Al and Mg and the interference of these activators in the oxide layer as described by the Dearnaley theory of the oxygen vacancy [Dearnaley, 1967].

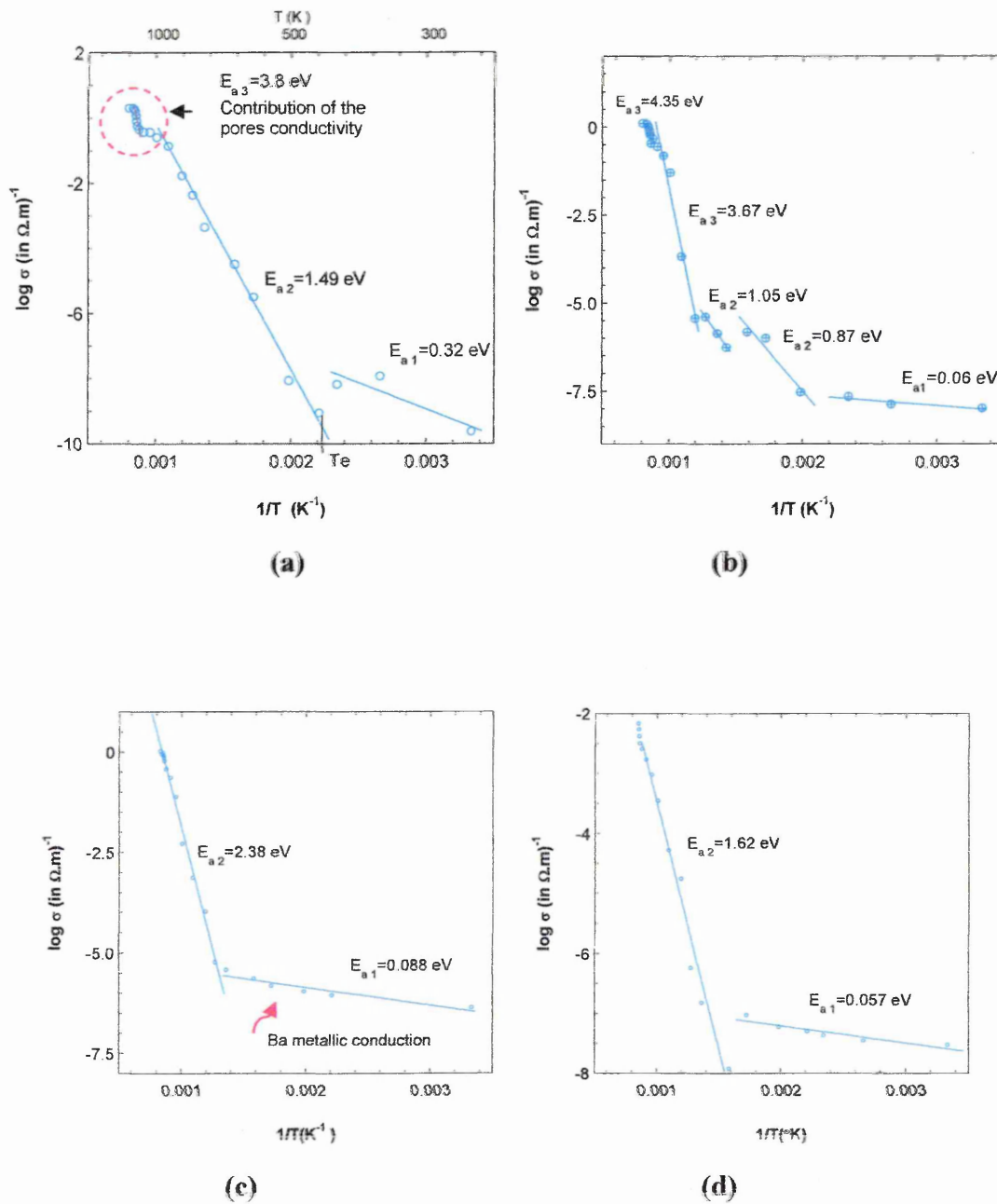


Figure 4.2: The conductivity-temperature dependence after activated the oxide cathode to 1200K, (a) at 0hr accelerated lifetime, (b) after 100hrs accelerated lifetime, (c) after 200hrs accelerated lifetime, (d) after 300hr accelerated lifetime.

The addition of the Ni powder is significant both in terms of mechanical integrity and the provision of electrical connection between the two components. The addition of Ni powder plays a dominant role in contributing electron energy levels, when the temperature is below the normal thermionic emission temperature (T_e) $E_{a1} \approx 0.32 - 0.04 eV$.

The variation in conduction properties of the BrO/SrO coating was monitored every hundred hours and the results are given in Table (4.1). At temperatures above T_e ($T > 700K$), the first or second BaO donor levels appear to be the dominant conduction process over the major part of the measured temperature range (700–1100)K. The domination of one donor level or another may be explained in terms of a structural re-arrangement and to a possible reduction in the number of continuous electrical pathways, due to Ni coarsening [AL-Ajili, 2001].

During the cathode operation time, up to 400 hrs after activation, the current density within the emission temperature range as mentioned above (700–1100)K, is dominated by one of the donor levels given in Table (4.1). The production of free Ba atoms by reduction of the BaO is thought to be a continuous process, due to a cyclic oxidation-reduction reaction [Aida et al, 1982 and Gärtner et al, 1999]. This enables the formation and disappearance of the donor levels during the accelerated operation time.

The threshold temperature for enhancement of the electronic current is thus found to depend on the dominant activation energy and on the performance of Ba metallic pathways (mono or multi layer) [Gärtner et al, 2002].

Table 4.1: The activation energy of 5% Ni cermet oxide cathode

| Acceleration Lifetime <i>hr</i> | Activation Energy E_{a1} (eV) | Activation Energy E_{a2} (eV) | Activation Energy E_{a3} (eV) | T_e (K) Temperature |
|------------------------------------|------------------------------------|------------------------------------|------------------------------------|--------------------------|
| 0 | 0.32 | 1.49 | 3.8 | 434 |
| 100 | 0.06 | 0.87, 1.05 | 3.67 | 500 |
| 200 | 0.088 | 2.38 | ----- | 724 |
| 300 | 0.057 | 1.61 | ----- | 632 |
| 400 | 0.048 | 0.26 | 3.27 | 910 |
| 500 | 0.039 | 1.23 | 0.43 | 910 |
| 600 | 0.056 | 0.15 | 0.15 | 910 |

After 500 *hrs* of continuous operation, the conduction behaviour is found to change dramatically. The conductivity becomes dominated by the high pore density that has a very limited effect on the conduction properties of the oxide cathode immediately after its activation. An explanation for these changes can be found in the micro-structural changes occurring due to the Ba multi-atomic layer which covers the oxide grains and increased the conduction electrons probability through the pathways as shown in Figure 2-20 [Chin, 1974]. It is believed that the cathode heat acceleration continuously excites more activators to reduce the oxide components.

Over the first several hundred hours of operation, the interface layer grows in the regions of contact between the oxide and the cap. It has been shown that after activation of the cathode, the Mg and Al activators diffuse along the cap Ni grain boundaries and distribute over the surface as $MgAl_2O_4$, $\gamma-Al_2O_3$ and MgO at the grain boundaries [Porat et al., 2000 and Roquais et al., 2002].

The measurement method as explained above was to contact the two cathodes face to face to create a semi-closed system. The Ba lost by this system is much less than the open system (a single standard cathode in a dummy tube or in a close-spaced planar diode configuration in a UHV chamber) and contaminated inside the pores and between the grains. Ba atoms coverage the grains surface as an adsorbed mono layer in some where and as a multi-layer on other place is responsible on the decreasing and increasing in activation energy through the operation time. After 400 *hrs* there are many multi-atomic layers covering the surfaces. The conduction through this layer is dominant. The result is enhancement in the current density above the threshold temperature and a lower conduction mechanism lower than T_e , as shown in Figure 4.2 and table 4.1.

It can be seen from Figure 4.3 that the conduction mechanism changes from one being mainly due to thermionic emission to a mechanism involving electron conduction influenced by high space charge on the grain surface. This may explain the increased value of the oxide activation energy E_{a2} .

On the other hand, the threshold temperature (T_e) of operation is generally found to increase with each subsequent 100 *hr* measurement interval, as shown in Figure 4.4. The increasing Ba coverage layers enhance the probability for space charge conduction, which makes (T_e) increase with the operation time [Chin, 1974].

The value of α (equation 2.4) result at zero run hours is ~ 0.0002 . The calculated value of α after operation of the cathode for 200 hrs is determined as approximately 0.02, which is must be due to the metallic behaviour.

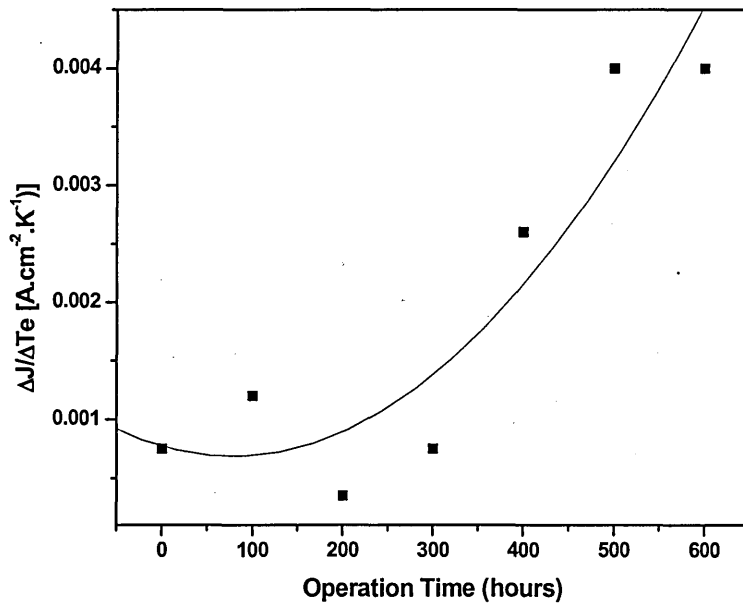


Figure 4.3: The output to the input ratio of the oxide cathode through operation lifetime.

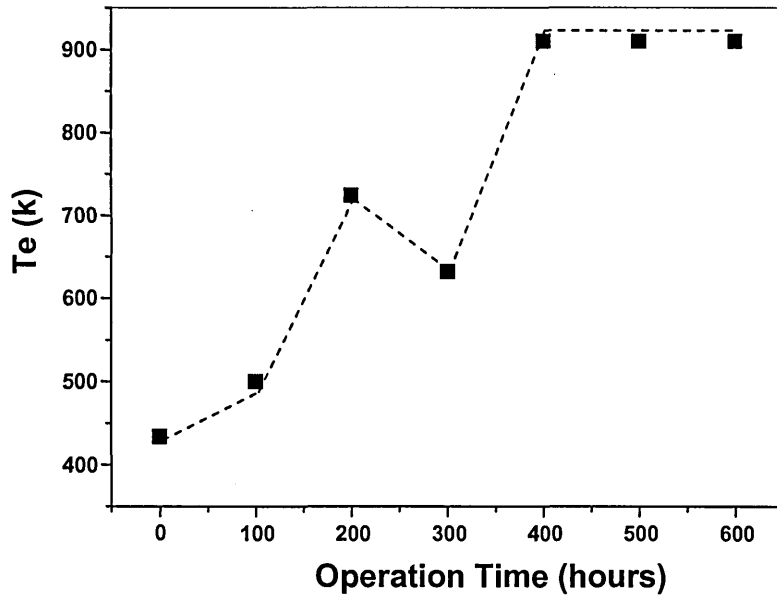


Figure 4.4: Variation of threshold temperature with cathode operating time.

4.4.2 A.C. measurement after accelerated lifetime

The dielectric properties were investigated in terms of frequency depended measurements of AC conductance G at temperatures ranging from $(300-1200)K$. As shown in Figure 4.5, the AC conductance is dependent upon temperature with two different activation energies for the temperature ranges $T \leq 870K$ and $T \geq 870K$. At the temperature $T \geq 870K$, the conductivity becomes independent of frequency. For the temperature range $870 \geq T \geq 670K$, the temperature dependence of the conductivity becomes weaker as the frequency is increased and the conductivity is virtually independent of temperature at $1MHz$ [Al-Ajili, 2002].

At low temperatures, in the range of room temperature, the conductivity is frequency dependent. As we can observe from Figure 4.5, the conductivity

increases by 4 to 5 orders of magnitude. This behaviour related to the case of $\sigma_{DC}(T)$ which was described in Figure (4.2b), when the sample had operated for 100 hours. The large increase in the AC conductivity with frequency at room temperature may due to some kind of conduction mechanism which is most likely to be the hopping mechanism.

When the conductivity is measured with an AC technique of frequency $\omega = 2\pi\nu$, the characteristics of a great variety of materials with diverse chemical compositions, either crystalline or amorphous, can be written as [Jonscher, 1983 and Ortiz-López, 2003]:

$$\sigma(\omega, T) = \sigma_{DC}(T) + a(T)\omega^s \quad (4.3)$$

Where $\sigma_{DC}(T)$ is the direct current (or the static, $\omega = 0$) conductivity, $a(T)$ is the factor that depends on temperature but not on ω , and s is an exponent in the range $0.6 \leq s \leq 1$.

Equation (4.3) predicts that if (at a certain temperature) σ_{DC} is much less than the second term, then $\sigma(\omega, T) \propto \omega^s$, so that a log- log plot of σ against ω describes a straight line with slope s .

On the other hand, if σ_{DC} becomes larger than the second term (by increasing temperature, for example), then $\sigma(\omega, T) \propto \sigma_{DC}(T)$, in which case the AC technique renders a measurement of σ_{DC} , and a plot of σ against ω in log- log scale should give a horizontal straight line.

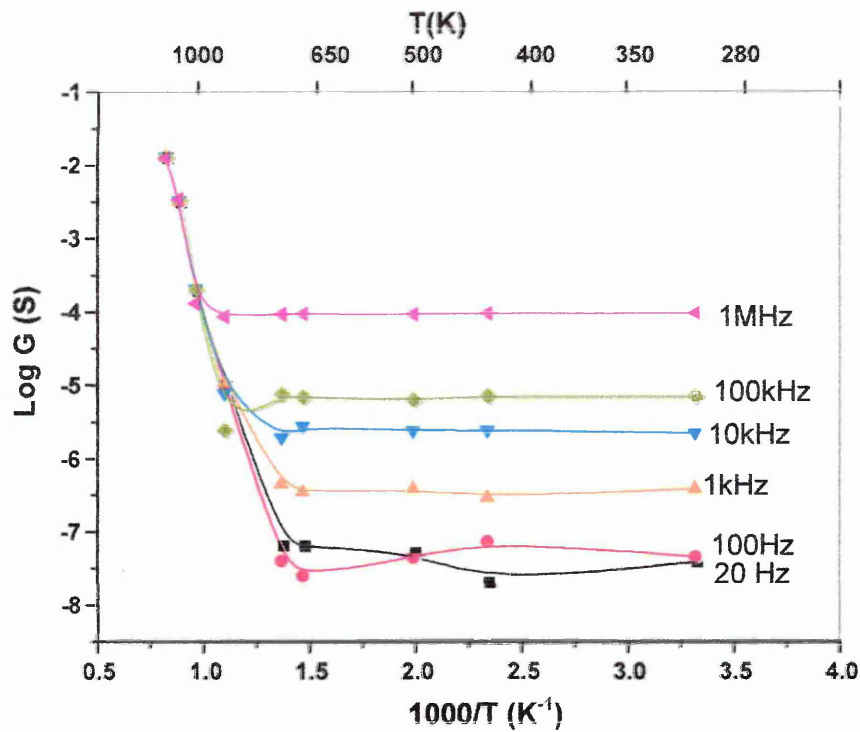


Figure 4.5: Conductance as a function of temperature at different frequencies for the 100 hours run.

When plotting in Figure 4.6 , the data of σ against $\nu = \omega/2\pi$ on a log-log scale for this sample, clearly observe a linear behaviour implying a negligible contribution of σ_{DC} according to Eq. (4.3).

The best fit to the data gives $s = 0.7 - 0.9$ for the temperature range (300–500)K. Such behaviour appears to indicate that hopping is the predominant conduction process via the traps of nickel additional powder and the Ba adsorbance layers [Dakhel, 2004 and Ondo-Ndong et al, 2003] .

From careful examination of this figure we can deduce that $\sigma_{DC} \leq 10^{-9} (\Omega.cm)^{-1}$, because σ_{DC} should be close to the value of σ measured at the lowest frequency (20Hz). In this case σ_{DC} value matches very well with the conductivity value of the DC measurement as shown in Figure 4.2.

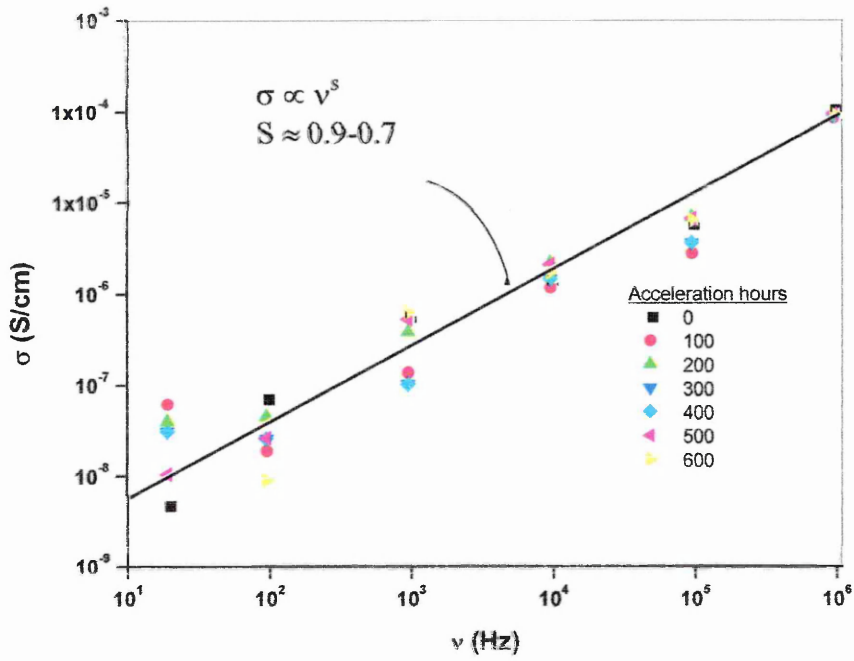


Figure 4.6: Log-Log plots of conductivity $\sigma(\nu, T)$ against frequency ν , for the temperature range 300-670 K

Chapter 5

Formation of an interface layer in thermionic oxide cathodes

5.1 Introduction

The efficient operation of the cathode depends upon the activation of the emissive oxide layer of the cathode. This involves the reaction of the converted alkaline earth oxides of the emissive layer with activator elements present in the Ni cap substrate. The activation proceeds over a period of hours, the activators (in this study, trace levels of W, Mg and Al) initially dispersed through the Ni grains diffusing along the Ni grain boundaries and then reacting with the BaO to form an oxide layer containing mostly activator oxides. This leads to the formation of a high activation surface field [Poret et al, 2000, Saito et al, 1990 and Ohira et al, 1999]. As the activation continues, the reaction continues to grow by further reduction of BaO to form metal oxides such MgAl_2O_4 , $\gamma\text{-Al}_2\text{O}_3$ and MgO [Roquais et al, 2002].

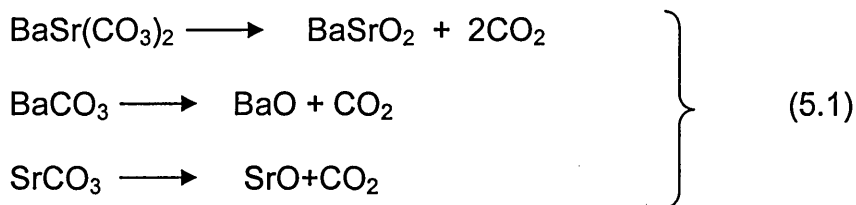
This chapter describes the results of activation dependent changes in the surface morphology and the composition of cermet oxide cathodes. Similar studies were also performed on the nickel cap surface. Results of these studies were then used to obtain a physical understanding of the formation of interfacial layer and its influence on the effective conductivity of activated cathodes.

5.2 The activation of the cathode at the optimized temperature

For this study a novel type of BaO/SrO oxide cathode plus was chosen. The cathodes were supplied by LG.Philips Displays and comprised of a top layer of a *Ni*2.5% (by weight) powder. The measurement method is same as described in section 3.7.1.

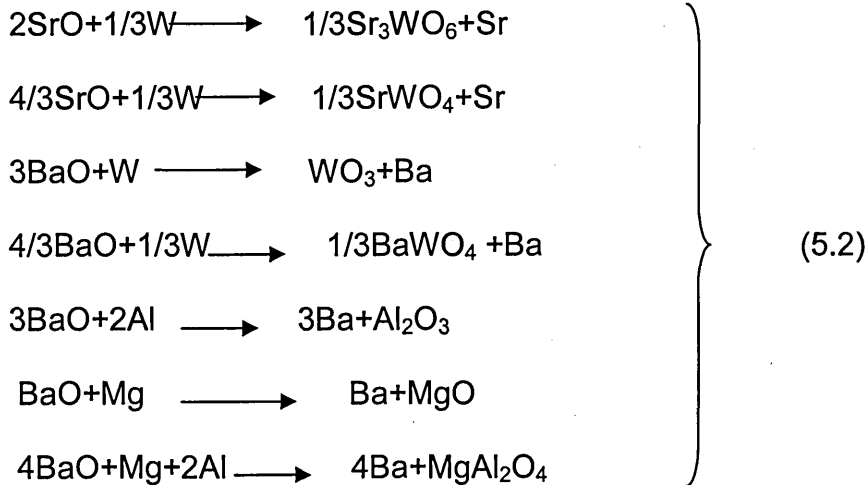
Due to the LG Philips activation procedure and the consequent processing steps, all the cathodes were converted and activated as shown in table 3.1. Using the integral heater filaments, the cathodes were activated at 1200K (Standard activation temperature) for different periods of time between one hour and twelve hours [Aida, 1982]. The measurements were made immediately after activation of the cathodes.

The activation of an oxide cathode is essentially a two-stage process as we mentioned in chapter two, involving firstly the thermal decomposition of the barium-strontium carbonate precursor to respective oxides according to the following equations:



In the second stage (which is the focus of this study), the BaO/BaSrO₂ reacts further with the so-called activators in the Ni cap material (elements such as W, Mg and Al). This reaction is highly dependant upon the nature and

percentage of the impurities in the Ni cap and their relative reaction capability. The probable reactions that can take at the place interface are [Gärtner, 1999]:



The concentration of WO_3 , Al_2O_3 , MgO and MgAl_2O_4 in the interface region between the cap surface and the emissive layer will increase with increasing activation time [Roquais et al, 2002]. Most likely the first four chemical reduction processes (see Equations (5.2)) took place after a few hours of activation.

5.3 Experimental analysis for the optimized temperature

5.3.1 Morphological and elemental analysis

These studies were undertaken to follow the evolution of the various oxides during the activation process which subsequently influence the total resistance of the oxide cathode. Figure 5.1 presents three electron micrographs, the first two of which show the grain structure on the top layer of the oxide material. The first diagram was obtained after the activation of one

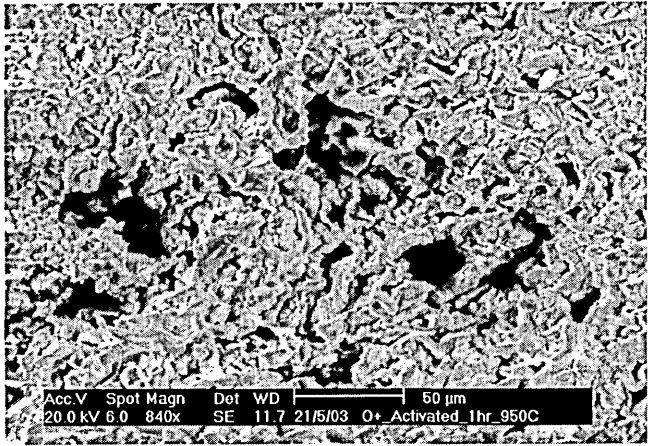
hour while the second sample was activated after twelve hours. The 12hrs activation at this temperature is considered to be equivalent to a cathode operation for more than one hundred hours at the operation temperature of 1050K [Gärtner, 2003]. These cathodes became more sintered with the rise in activation time and the sintered oxide particles were found to have small grain-to-grain boundary distances. This observation agrees well with earlier work on oxide cathodes [Narita, 1953 and Jenkins, 2003]. As it became more sintered, the grain size has increased from approximately $6\mu m$ to $10\mu m$ after twelve hours of activation. It is also apparent that the porosity decreased with the increasing activation time. The contact area between the oxide layer and the Ni cap was about 20% for an inactivated cathode. Also when the two cathodes were separated after activation, some oxide layer was found to be peeled off from the cap, leaving the interfacial layer intact. These factors offered access for spot analysis of the Ni cap.

The SEM image of the Ni cap surface in the interface area gives a qualitative indication of the interface oxide layer thickness, as shown in Figure 5.1c.

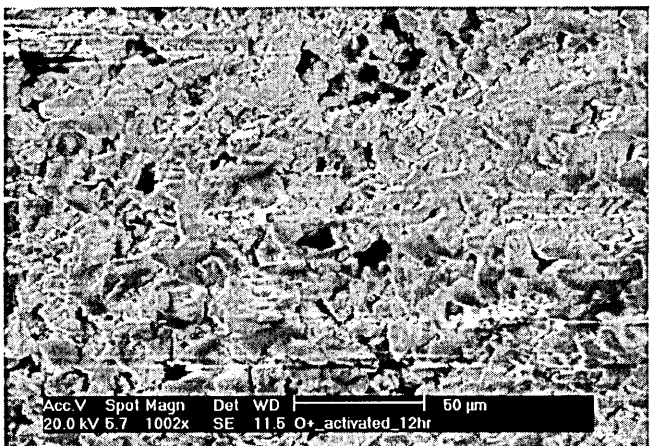
Figure 5.2 shows the EDX based compositional analysis of the top surface of the oxide layer. An abrupt increase in the count is observed to have occurred after 3hrs of activation.

The top surface of the oxide layer became Ba-rich possibly due to the presence of free Ba. The observation of Ba content higher than that of Sr may be attributed to probable loss of Ba from the cathode surface.

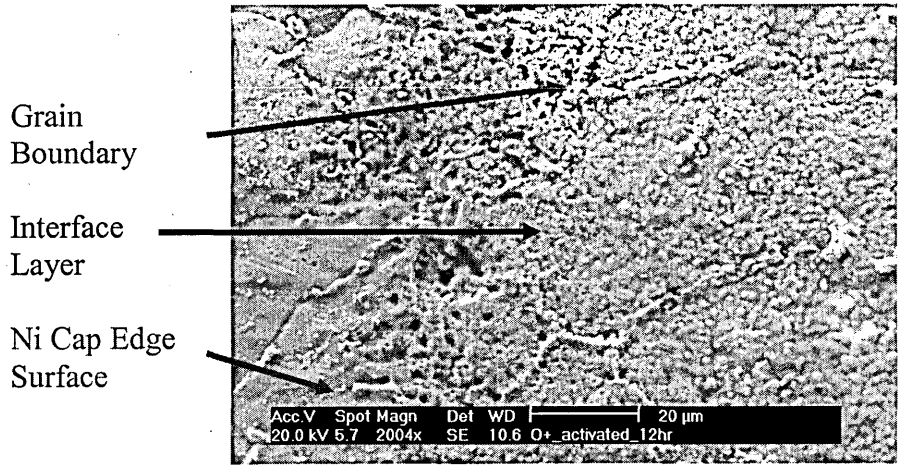
As shown in Figure 5.3, the EDX elementary mapping analysis of the interface layer on the Ni cap shows that tungsten was the first element to diffuse



(a)



(b)



(c)

Figure 5.1: Two scanning electron micrographs of the top surface of oxide cathode activated to (a) one hour and (b) twelve hours. (c) Scanning electron micrograph of the Ni cap surface after twelve hours activation.

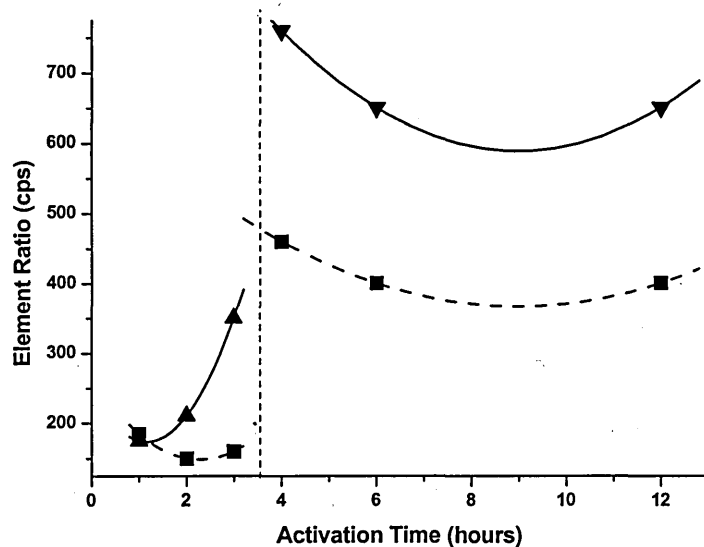
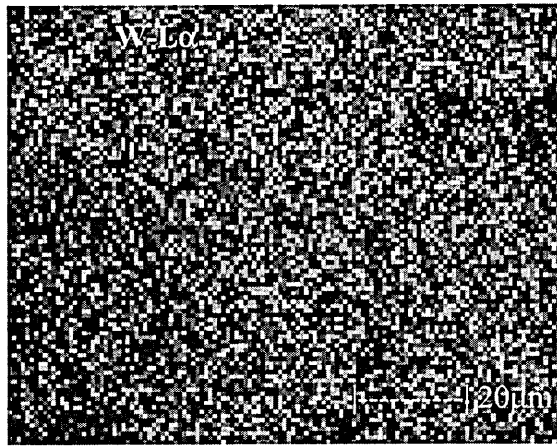


Figure 5.2: Results of X-ray elementary analysis for Ba-L α (\blacktriangle solid line) and Sr-L α (\blacksquare broken line) as a function of the activation time.

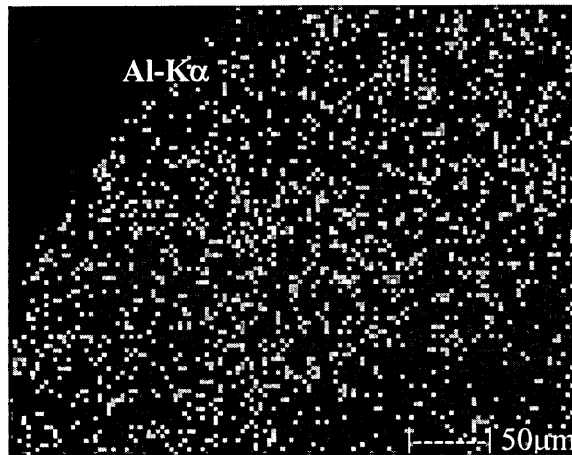
through the Ni boundary grains to the Ni surface, forming one of the tungsten oxide compositions as shown in Equations (5.2).

The thickness of tungsten oxide layer is expected to increase with increasing activation time. The activation for a longer period promoted the diffusion of additional activator elements to the cap surface. The presence of Al in the oxide form (e.g. Al_2O_3) was observed in an appreciable quantity after 3 hrs of activation [Pore et al, 2000 and Roquais et al, 2002].

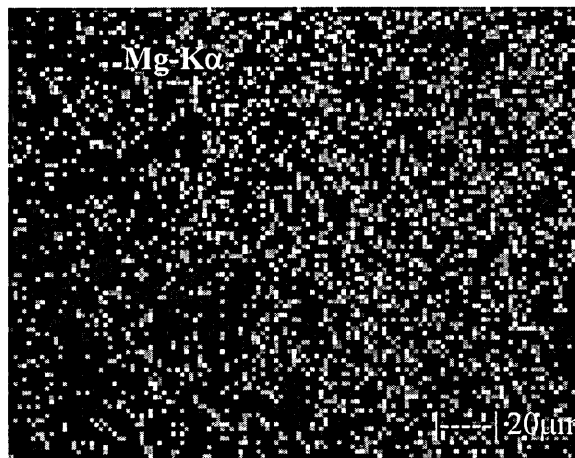
Magnesium in oxide (e.g. MgO) form was found in small proportions only after a long time of activation for about 12 hrs at 1200K and these particles are believed to be distributed on the surface of the cap concentrated in the Ni grain boundaries. Mg may also be present in the MgAl_2O_4 form according to



(a)



(b)



(c)

Figure 5.3: SEM images of the Ni cap surface for (a) W-K α after one hour activation, (b) Al-K α after three hours activation and (c) Mg-K α in oxide forms after twelve hours activation.

Roquais [2002]. Further analysis of X-ray data was performed to determine the ratios of W and Al which diffuse through the Ni cap surface.

Figure 5.4 illustrates the variation of the percentage proportion of tungsten oxide and aluminium oxide as a function of activation time of the oxide cathode. It is shown that during the first three hours (region marked I) the aluminium oxide diffuses to the surface on top of the tungsten oxide, indicating that the growth of the aluminium oxide dominates over tungsten oxide as shown in region marked II. This observation was limited to the penetration depth of X-ray beam; in practice W impurities in the Ni cap may be of higher proportion than detected. Figure 5.5 describes the results of X-ray studies on the identification of the Ni content in the oxide coating.

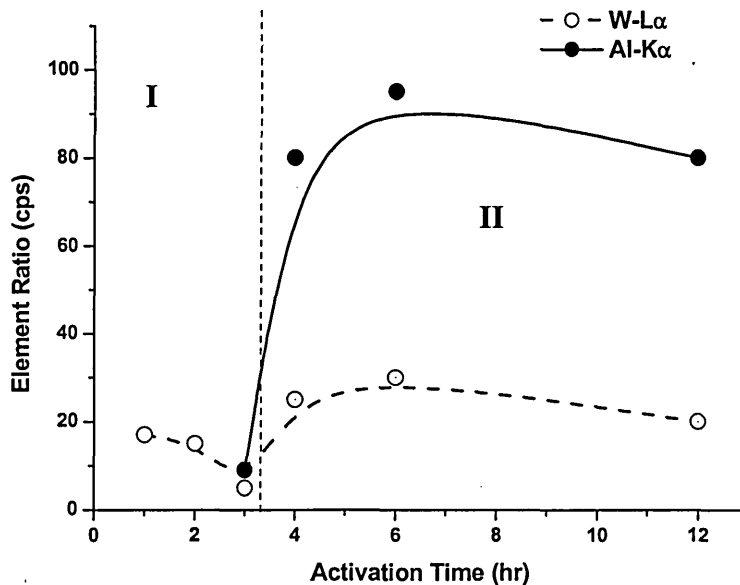


Figure 5.4: Diffusion of Al-Kα (● solid line) and W-Lα (○ broken line) on the cap surface versus the activation time.

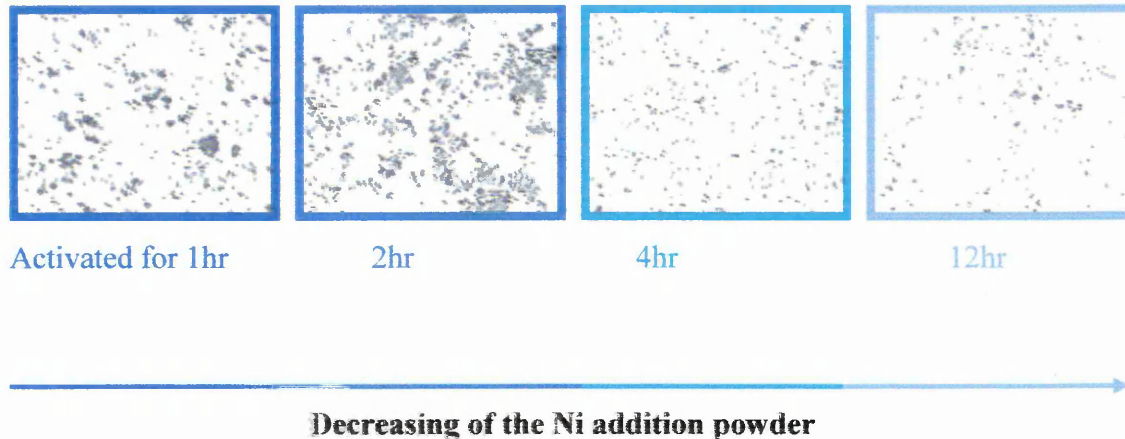
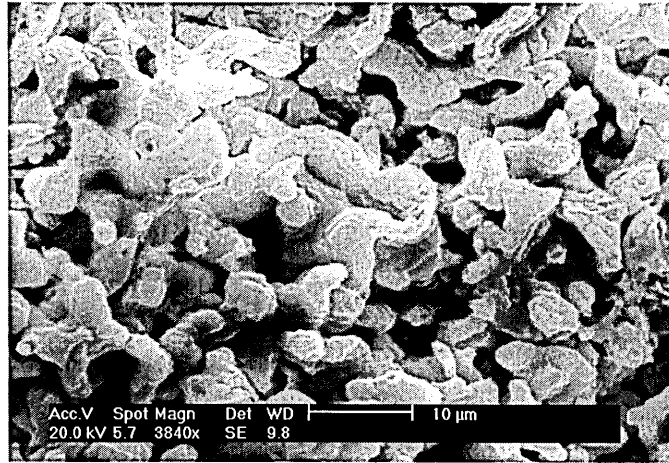


Figure 5.5: EDAX studies for distribution of the Ni powder addition (2.5%) in the top surface of the oxide coating

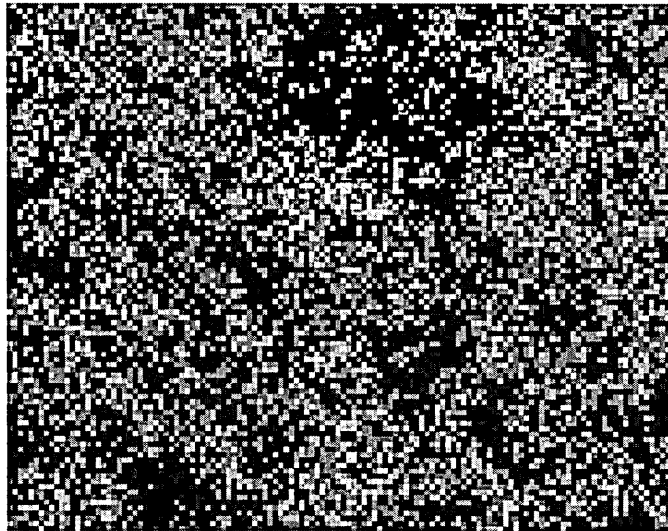
It became apparent that the Ni disappeared gradually with longer activation from the top oxide surface. EDX analysis for the oxide top layer shows some appearance of Al element distributed on the grain surface. This could be evidence for the Dearnaley theory of the oxygen filament which is percolated and influences the oxide grain structure through the activation of the cathode. These oxygen filaments correlate with the high reduction reaction of the aluminium which may encourage the Al to move to the surface. The percolation of the aluminium oxide through the Ba/SrO structure will change the system resistivity to join the activators oxide resistance. The conductivity of the oxide cathode depends on the kind and the value of this resistance.

Figure 5.6 shows the SEM image of the top surface of the oxide coating activated for *3hrs* and the Al elementary mapping on the same location. The

image indicates that the Al distributed on the oxide coating grain surfaces more than pore areas. These surfaces are oxygen-rich or the existing of the oxygen vacancies is high.



(a)



(b)

Figure 5.6: SEM images of the oxide layer (a) SEM image for the top of the oxide coating cathode activated for three hours (b) Al- K α mapping in the same location.

5.3.2 D.C. Electrical characterisation

Figure 5.7 shows a typical Arrhenius plot in terms of the variation of effective conductivity σ with temperature T for the cathode assemblies activated for twelve hours. It appears that a transition in behaviour occurred at a temperature of $500K$.

For the temperature regime $T \leq 500K$, conduction is almost independent of temperature while a steep rise in conductivity was observed for temperatures above $500K$. Two parallel processes are found to be responsible for the conduction for the 12 hour long activated cathode assembly according to the relation 2.12 [Loosjes and Vink, 1949]:

A value for E_{a1} is estimated to be $17meV$ for the temperature independent regime at $T \leq 500K$. This energy E_{a1} is believed to represent the average intergranular potential barrier and the principal conduction mechanism is identified as electron tunnelling through the barrier between the grains. The high temperature conduction through this polycrystalline cermet layer is related to the trapping and detrapping mechanisms at the grain boundaries. A value of $E_{a2} = 0.9eV$ is estimated for the high temperature regime of $T \geq 500K$. This is regarded as being the average depth of trap levels relative to the conduction band edge. In this case, the cathode may be considered as a β -type (section 2.18).

The concentration N_e of the excess barium is found to be in order of $10^{20} m^{-3}$ from the Fowler's Equation 2.31 [Narita, 1953]. Using $\mu_e = 1000 cm^2/V.s$ and

$e = 1.6 \times 10^{-19} C$ for the mobility and charge, respectively of the conduction electron.

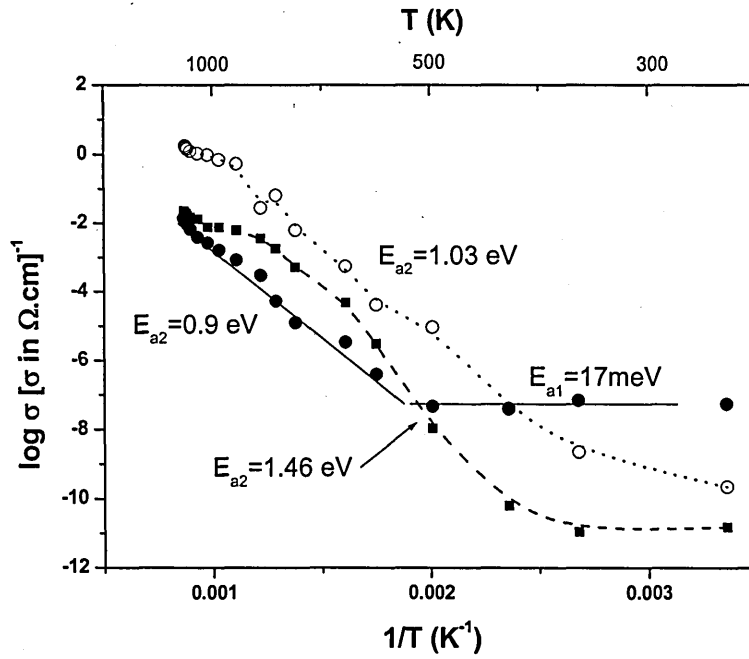


Figure 5.7: Dependence of conductivity on temperature for the cathode assemblies activated for one hour (■ broken line), four hours (○ dot line) and twelve hours (● solid line).

The effective mass m was taken to be equal to the rest mass of electrons for this calculation.

For the sake of comparison, the second Arrhenius plot was included in Figure 5.8 for the cathode assemblies activated for one hour. Two mechanisms are found to have existed but the transition from one process to another is gradual. A value of 1.46 eV was obtained for E_{a2} for the temperature between 400 K and 600 K and this value is close to the energy band gap of BaO [Nergaard, 1952]. For the temperature regime $T \leq 500 \text{ K}$, the one hour long activated cathode assembly exhibited much smaller conduction than one

activated for twelve hours. On the other hand, the conductivity was found to be large within the temperature regime of $T \geq 500K$ for the cathode activated for one hour than that for twelve hours. This low temperature behaviour of differently activated cathode may be attributed to the presence of a high density of grains having large sizes. The formation of free Ba monolayer after twelve hours of activation is also believed to cover the grain surface reducing the work function of the surface [Chin et al, 1974]. Cathodes activated for one hour are more porous than these activated for twelve hours and the contribution of pores becomes significant at high temperatures [Loosjes and Vink, 1949]. Electron mean free paths are comparable to the pore sizes, giving an enhanced to the conductivity in the temperature range of $T > 500K$. The effect of the interfacial layer growth may be understood by employing the two resistors model in which a barrier resistance R_i due to an interface layer is in series with the resistance R_o due to the activated oxide layer (see Figure 5.8). The effective conductivity σ for this two resistor network can be written in the form:

$$\sigma = \frac{\sigma_i \sigma_o}{\eta \sigma_o + \sigma_i} \quad (5.3)$$

Only a small amount of activators are expected to diffuse to the cap surface during a one hour long activation, making η very small and the conductivity of the cathode assembly is primarily due to the oxide layer. It is probable that all the chemical reactions listed in Equation (5.3) were not complete.

As illustrated in Figure 5.8, both the oxide and interfacial layers underwent compositional formation dependent upon the duration of activation.

Activated Oxide Cathode

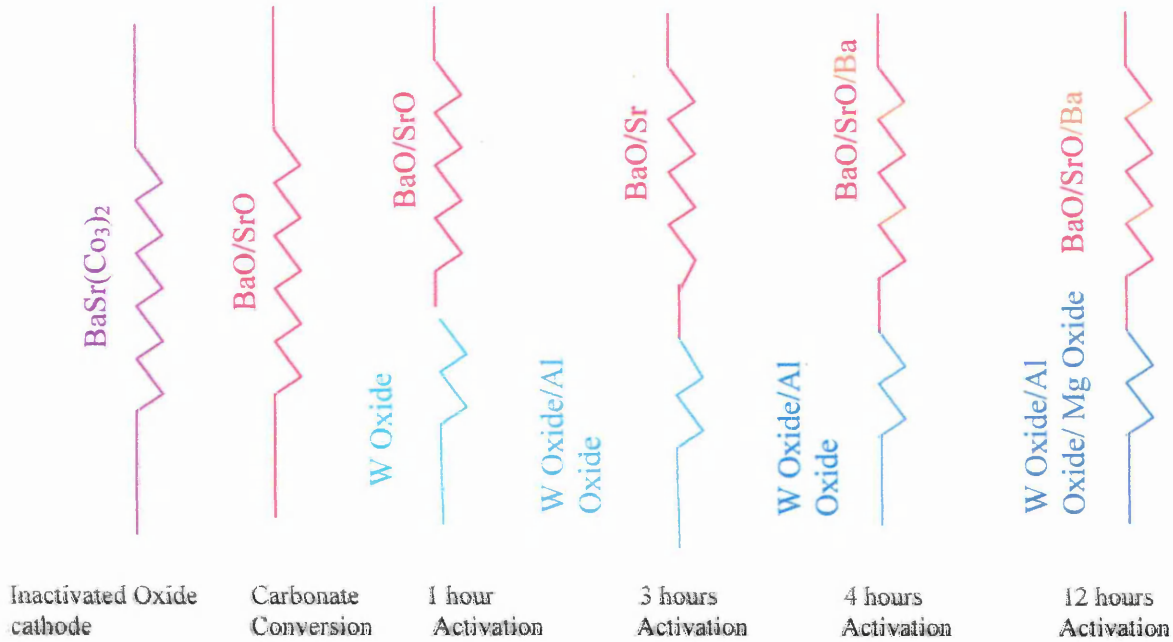


Figure 5.8: Two resistor model for formation of the interfacial layer and activation oxide coating.

Longer activations produced an interfacial layer which is a heterogeneous system consisting primarily of aluminium and tungsten oxides.

The specific resistivity of WO_3 increases normally with increasing oxide thickness, and also increases by two orders of magnitude ($10^4 - 10^6$), when the oxygen concentration is increased from 5% to 30% [Aki et al, 2003 and Gillet et al, 2003]. Also the resistivity of Al_2O_3 decreases from $(10^{12} - 10^9) \Omega.cm$ when the temperature is increased from 670 – 825 K [Nakai et al, 1997]. This seems to have happened at the interface layer of hot cathodes, particularly at the operation temperature. Values of $10^6 \Omega.cm$ and $10^{12} \Omega.cm$ are reported for

the resistivity of WO_3 and Al_2O_3 layers at room temperature [Gillet et al., 2003 and Nakai et al., 1997], respectively and the interface layer thickness is expected to be approximately $1-2\ \mu\text{m}$ deep [Gärtner, 1999]. Using the data for the aluminium and tungsten counts, the value of σ_i is estimated to be $10^{-8} - 10^{-9}\ (\Omega.\text{cm})^{-1}$ and σ_0 is therefore found from Equation (5.3) to be $10^{-8}\ (\Omega.\text{cm})^{-1}$ at room temperature. Similar calculations yield the values of $10^{-3}\ (\Omega.\text{cm})^{-1}$ and $10^{-2}\ (\Omega.\text{cm})^{-1}$ for σ_i and σ_0 , respectively at the operation temperature of 1025K .

Further analysis was carried out for a cathode activated for different lengths of time and Figure 5.9 shows a tendency of monotonic increase of $\frac{\sigma_0}{\sigma_i}$ corresponding to the operating temperature of 1050K with the rise in activation time. It can be seen that the interfacial layer conductivity at 1050K becomes appreciable for the cathode assemblies which have been activated for relatively small length of time although the contribution from the pore conductivity to σ_0 may be significant.

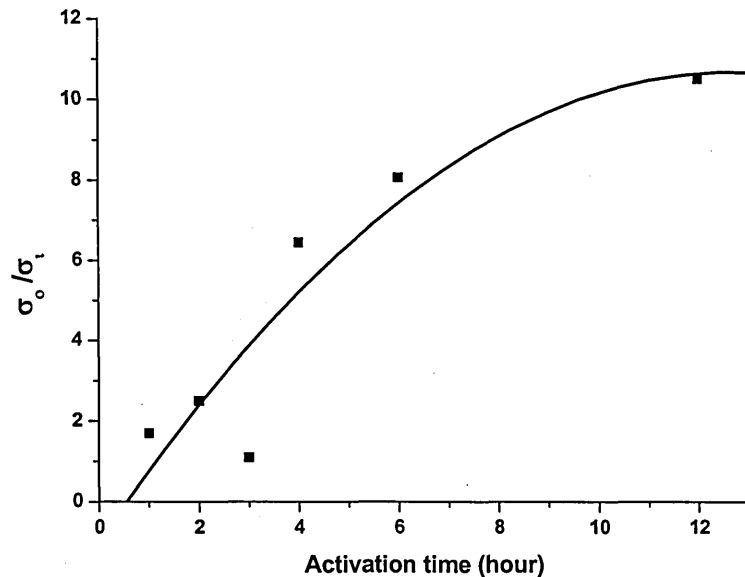


Figure 5.9: Influence of the interfacial layer conductivity as a function of activation time.

5.4 Optimisation of parameters for activation of oxide cathodes

For the oxide material, the conduction mechanism as noted, primarily depends exponentially on temperature due to the Loosjes conductance formula. One of the two terms may describe pores conductivity which contributes to the total conductivity.

From early studies on the emission characteristics from monatomic layers, such as Cs, Th, and Ba on tungsten emitters, it was deduced that any damage to the surface film, either by evaporation or by oxidation, destroys the emission. Because of the complexity involved in an actual oxide cathode, the adsorption of the barium was identified as an essential factor in thermionic cathodes [Zalm, 1968]. Since the evaporation of BaO takes place at a much faster rate than that of SrO and CaO, the adsorption of barium ions on the

strontium-calcium oxide is believed to be the activation process in a triple-oxide cathode.

From the texture and activation of the triple oxides, it is evident that barium adsorption can also take place at the interfaces between oxide crystallites (pores). The porosity in the oxide coating allows the formation of such an adsorbed interface in the same manner as that of the emitting surface. Consequently, electron accumulation will occur at this ion-adsorbed interface as well as in the emitting area of the oxide crystallites.

Using the integral heater filaments as before, the oxide cathodes plus were activated at $1425K$ and $1125K$ for different periods of time 1–12hrs. DC electrical measurements at various temperatures in the range between $300K$ and $1200K$ were performed.

5.4.1 Structural and elemental analysis

SEM images in Figure 5.10 show significant changes in the pore density and grain size of Ba/SrO oxide layers of activated cathodes, depending upon the activation temperature and time. The pore density was found to have decreased with the period of activation at $1125K$. The mean grain size of BaO/SrO was estimated to be $\sim 3\mu m$ for cathodes activated for two hours and it was found to increase to $5 - 6 \mu m$ when the activation time was increased to four hours. This is mainly due to a structural phase transformation from the normal oxide type (N-type) to the sintered type (S-type).

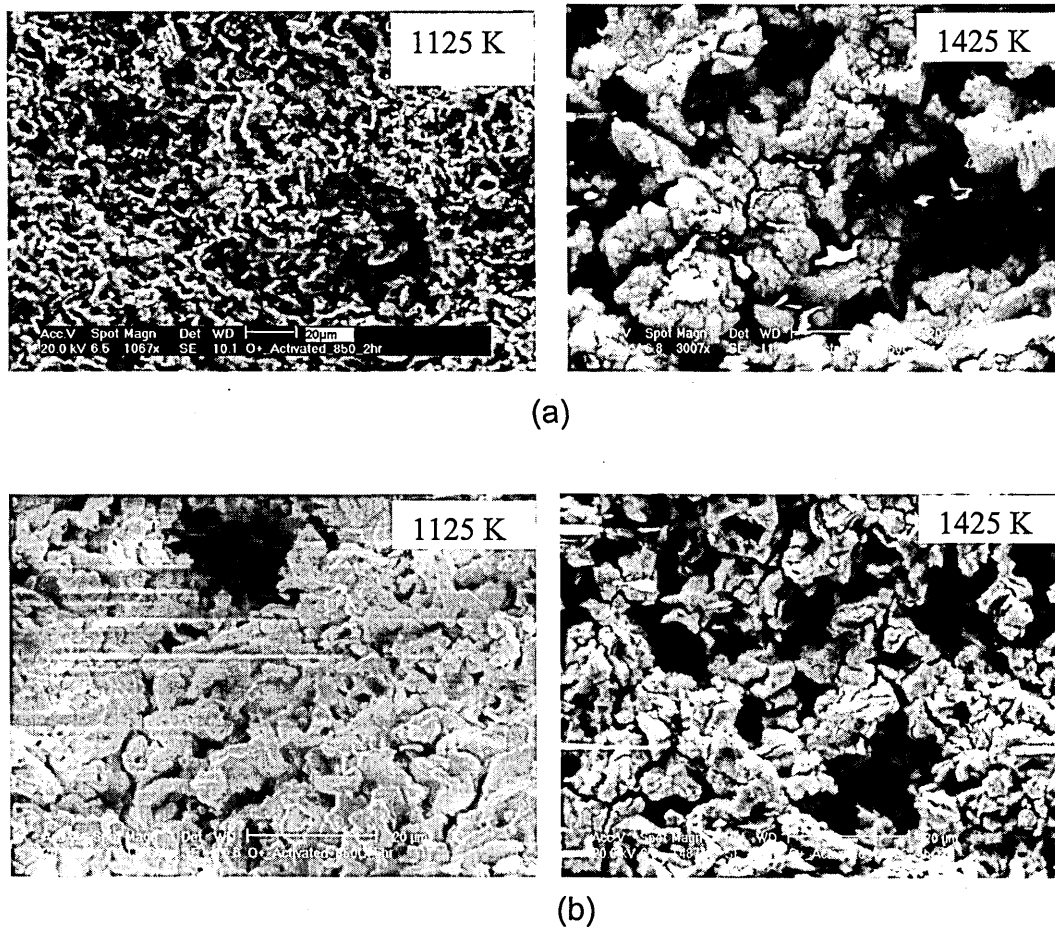


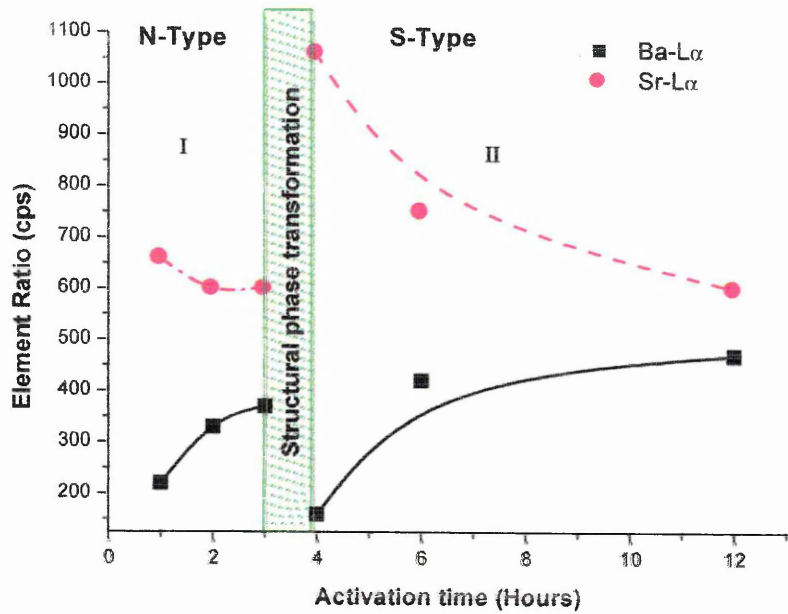
Figure 5.10: SEM images for the top surface of oxide cathode after activation at 1125 K and 1425 K for (a) for two hours (b) for four hours.

The pressing of the two mounted cathodes supported by the high activation temperature and high vacuum is thought to change the oxide structure from N-type to S-type. This phase transformation will give rise to changes in the various properties of the oxide coating including the electron conduction mechanism.

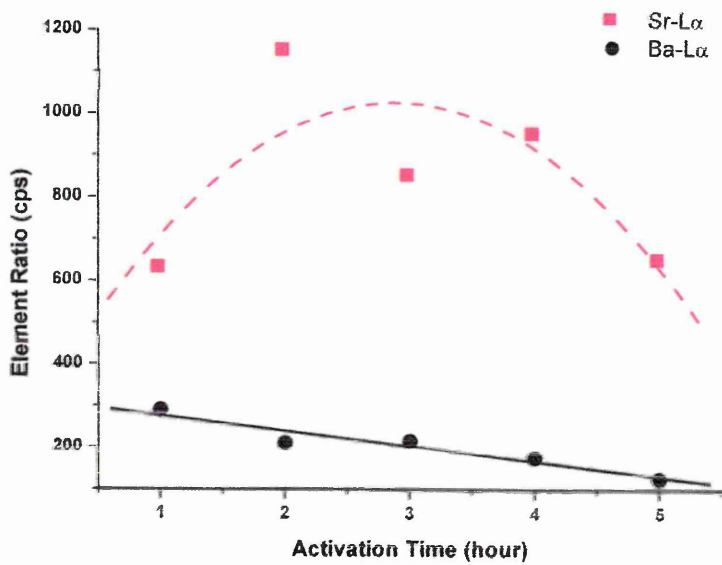
Similar changes in the pore density were not observed when the cathode was activated at 1425 K for the time periods of 2 – 4 hrs . The grain size however decreased from $13\mu m$ to $6.5\mu m$ with the increase of activation time from 2 – 4 hrs . This reduction in grain size on activation at higher temperature is thought to be due to the rapid evaporation of Ba out of the oxide cathode.

Results of EDX analysis for the Ba and Sr on the top surface of the oxide layer were presented in Figure 5.11. A rise in the Ba counts from 220CPS to 370CPS was estimated as the activation time was increased from 1hr to 3hrs at a temperature of 1125K. An abrupt change was observed in the surface content of Ba after an activation time of 4 hrs. The Ba proportion was found to have further increased during the cathode activation for periods of time above 4 hrs. The surface content of Sr was found to have decreased with the increase in time of activation at 1125K which can be explained in terms of the limited penetration depth of the x-ray beam. The observation was also possibly masked by the Ba mono or multi-layer covering the grains. When the cathode was activated at 1425K, the Ba contents showed a monotonic decrease during the first five hours of activation. The value of Sr proportion has varied in the range between 630–1150CPS. This behaviour indicates that the Ba atoms were easily evaporated out of the system at this high activation temperature. The decrease in Ba content has in turn influenced the sintering properties of the BaO/SrO grains leading to further shrinking in the grain size. These two processes were however difficult to control at sintering temperatures as high as 1425K.

Figure 5.12 shows SEM images obtained with an improved resolution for the top surface of oxide cathode activated at 1125K and 1425K for two hours. The Ba contamination on the oxide layer was much higher for activation at 1125K than 1425K. For oxides activated at 1125K, free Ba was distributed over the grains and inside the pores while the high temperature activation produced smaller Ba coverage, mostly over the grain surface.

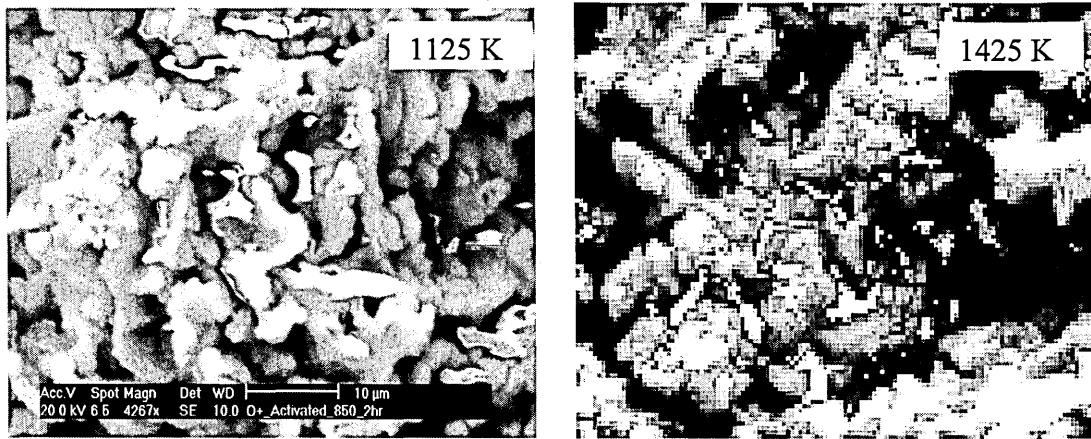


(a)

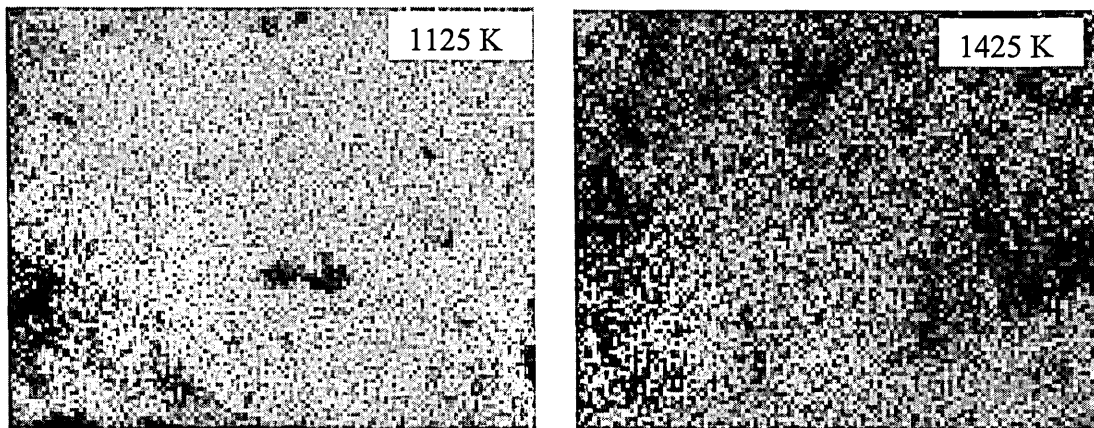


(b)

Figure 5.11: X-ray elementary of the Ba-L α (solid line) and Sr-L α (broken line) as a function of the activation time (a) 1125 K (b) 1425 K .



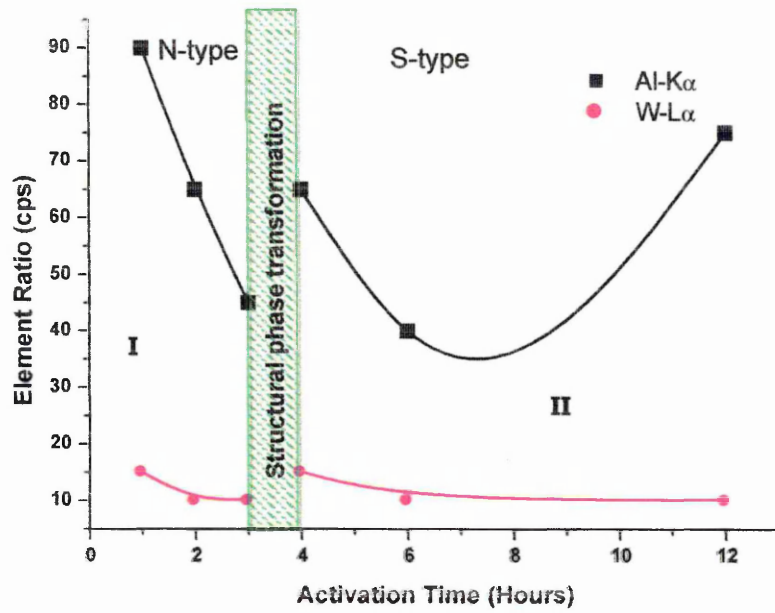
(a)



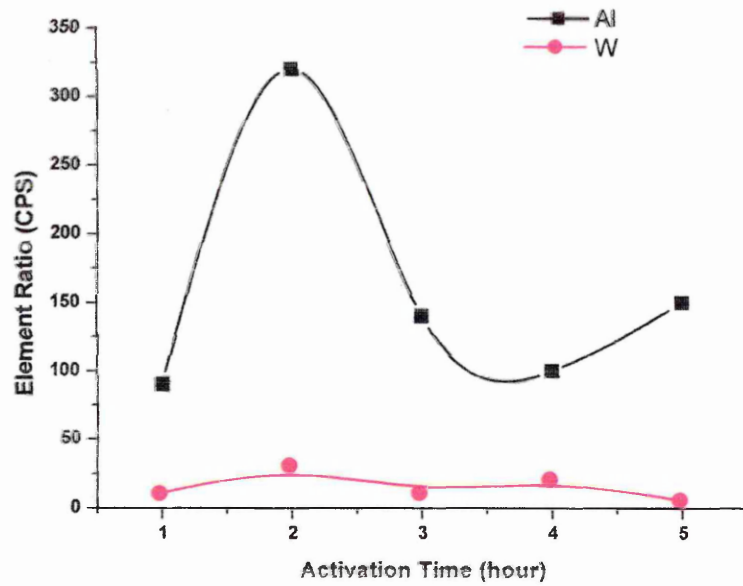
(b)

Figure 5.12: SEM image for (a) the top surface of oxide cathode activated for two hours (b) Ba elementary mapping on the same location.

Figure 5.13 illustrates the variation of the proportion of tungsten oxide and aluminium oxide on Ni cap surface as a function of activation time of the oxide cathode. During the first three hours (region marked I), Al oxide diffused to the surface on top of the tungsten oxide. Although the W activator in the Ni cap is of higher proportion than that of Al, the growth of the aluminium oxide dominated over tungsten oxide as shown in region marked II in Figure 5.13a.



(a)



(b)

Figure 5.13: Diffusion of Al-K α and W-L α on the cap surface versus the activation time (a) 1125 K (b) 1425 K .

The decrease in the Al agents in region I on the Ni cap surface indicated that the Al particles were able to leave the interface and diffuse through the oxide layer. This was further supported by earlier findings, where the Al element was found to be distributed on the surface of the oxide layer [Jenkins et al, 2003].

In general this can be interpreted in terms of activators leaving the Ni cap surface, penetrating the oxide material and causing the reduction of BaO directly from the oxide grains and thus increasing the density of electrons gas. The electron gas density may further increase if there is an increase in the Ba adsorption layer on the oxide grain surface which reduces electron emission work function of the pores [Chan et al, 1974 and Dearnal, 1969].

When the cathode was activated at 1425K for two hours, the reduction reaction by the Al produced an increase in the Al proportion distributed on the Ni cap surface. The increase in the evaporated Ba as well as the low Debye temperature for BaO ($\theta_D = 525\text{K}$) produced a high oxygen concentration at $T > 4\theta_D$ [Dearnal, 1969]. This availability of oxygen encouraged the Al to diffuse inside the oxide material, causing the Al proportion to decrease on the Ni cap when the cathode was activated for more than two hours.

There were no noticeable changes in the W proportion due to the fact that the tungsten oxide diffused inside the oxide material as well.

Figure 5.14 shows SEM images and elementary mapping of a cross-section of an oxide cathode activated for one hour. A comparison of the images shows a homogeneous distribution of Ba and oxygen in the oxide coating when activated at a temperature of 1125K . However, when the cathode was activated at 1425K , a high Ba contamination was observed on the surface and

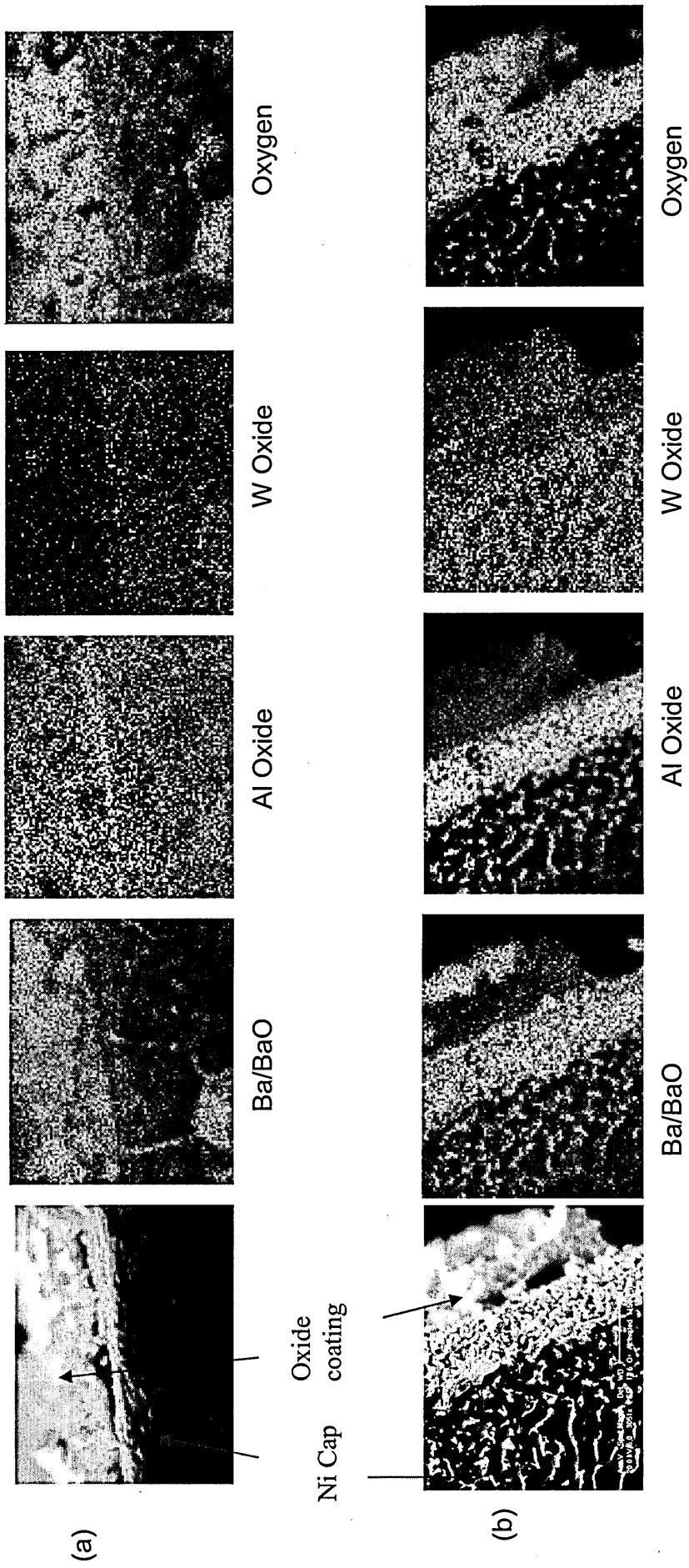


Figure 5.14: Cross-Section SEM images and elementary mapping for oxide cathode activated for one hour (a) at 1125 K (b) at 1425 K.

at the interface of the oxide coating. An activation temperature of 1125K was found to be an optimum condition that gave a broad distribution of Al within the Ni cap and throughout the oxide coating. Oxide cathodes activated for 3 hrs at a temperature of 1200K contained a very small amount of Al on the Ni cap surface and on the oxide coating surface. For cathodes activated at the temperature of 1425K , Al was found to be mostly concentrated at the interface layer.

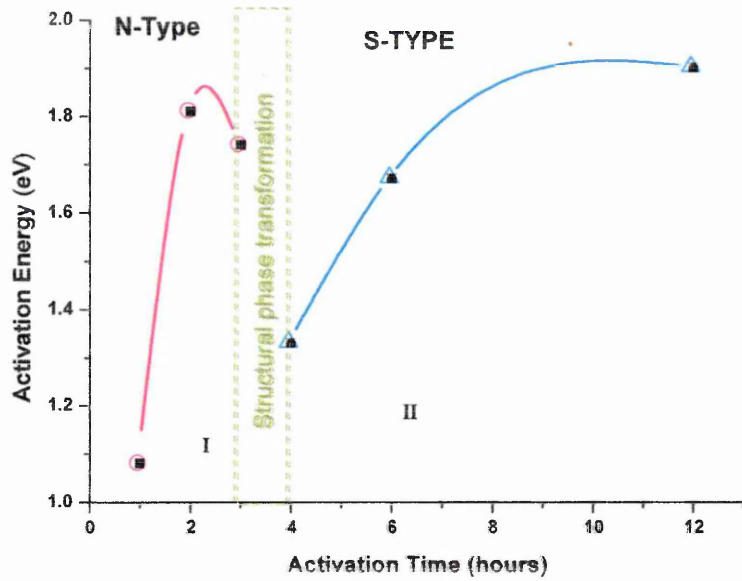
The Al oxide penetration ratio inside the oxide material seems to be a pore density dependent process. It has formed pathways following the pores and grain surfaces. After three hours of high temperature activation the Mg appeared to diffuse with a small amount on the Ni cap surface and thus participated in the reaction process.

5.4.2 Electrical properties

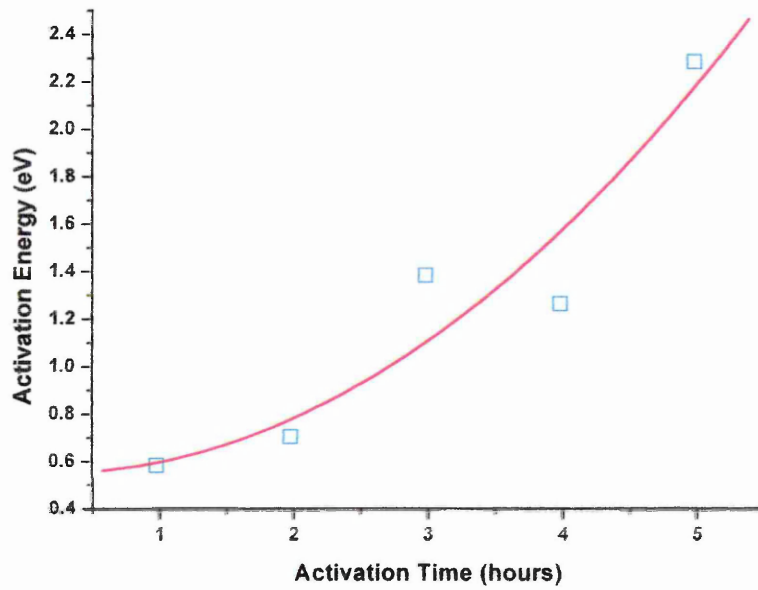
Figure (5.15a) illustrates the variation in the activation energy of the new type cathode (oxide cathode plus) after being activated at 1125K over different time durations. The activation energy for the dc conduction is found to increase with the duration of activation for the two observed structures of the N- and S-type. A decrease in the activation energy was only evident over the period of phase transformation which is shown to occur within the activation period between $3-4\text{ hrs}$.

The activation energy (E_a) has been evaluated using the equation 2.12.

Where $e\phi_1 = E_o$ is the oxide activation energy and $e\phi_2 = E_p$ is the activation



(a)



(b)

Figure 5.15: The variation of the activation energy versus the activation time, activation temperature (a) 1125 K (b) 1425 K .

energy due to conduction through pores, which has significant contribution to the total conductivity at high temperature $T > 800 K$.

The conduction mechanism and the electron transportation is cathode-type dependent. However, approximations have been made in the present calculations by considering that the measured current is mainly due to conduction by electrons within the oxide grains, with a small (negligible) contribution from an electron gas within the pores.

The calculated value of $E_a = 1.08 eV$ for cathode activated for one hour indicates a lowering in the grain boundary energy barrier which may be explained in terms of the free Ba accumulation in this location [Chin et al, 1974]. The value of E_a is increased to $1.8 eV$ when the cathode was activated for 2 hrs and can be classified as a δ -type cathode [Narita, 1953]. This increase is correlated to the increase in the proportion of the Ba (as shown in Figure 5.11) to be adsorbed on the BaO/SrO grain surface and thus initiate a more significant contribution by pores conductivity. As a result, the conductivity has increased, as shown in Figure 5.16. The conductivity of a cathode activated for 3 hrs shows a small decrease due to the decrease in the pore density close to the structural phase transformation region.

The activation energy continued to increase when cathodes were activated over longer time durations due to the decrease in pore density, and thus a decrease in pores contribution to the conductivity. The higher activation energy values can be associated with conduction due to larger oxide grains.

Figure 5.15b shows a monotonic increase in activation energy for cathodes activated at the temperature of $1425 K$. For the first 2 hrs of activation at such

a high temperature E_a is increased in the range $E_a = 0.58 - 0.7 \text{ eV}$ in which can be sort as γ -type cathode (section 2.18). This short duration of activation at high temperature is sufficient to cause a high rate of activation and reduction and thus a significant barium adsorption layer, as shown in Figure 5.12b. The activation energy continued to increase up to 2.28 eV for duration of 5 hrs activation. This is mainly due to the significant loss of Ba as well as the possible higher potential barrier between the shrinking oxide grains.

Figure 5.16 shows variation of cathode conductivity as a function of activation time over different activation temperatures of 1125 K and 1425 K . In general, both types of activation treatments have resulted in a decreasing conductivity as the duration of activation has increased. This can be mainly associated with the weak contribution of pores to the total conductivity due to cathode sintering.

Figure 5.17 shows a plot of $\log \sigma$ against $1/T$ for cathodes activated at 1125 K and 1425 K for a duration of 12 hrs . Electron transport is through the BaO/SrO grains and pores. Curve (a) shows a much smaller increase in the cathode conductivity with increasing temperature above a threshold value of $T = 625 \text{ K}$ for cathode activated at 1125 K . This can be understood as the result of increased cathode resistance which is the sum of σ_{oxide} and σ_{pore} connected in series.

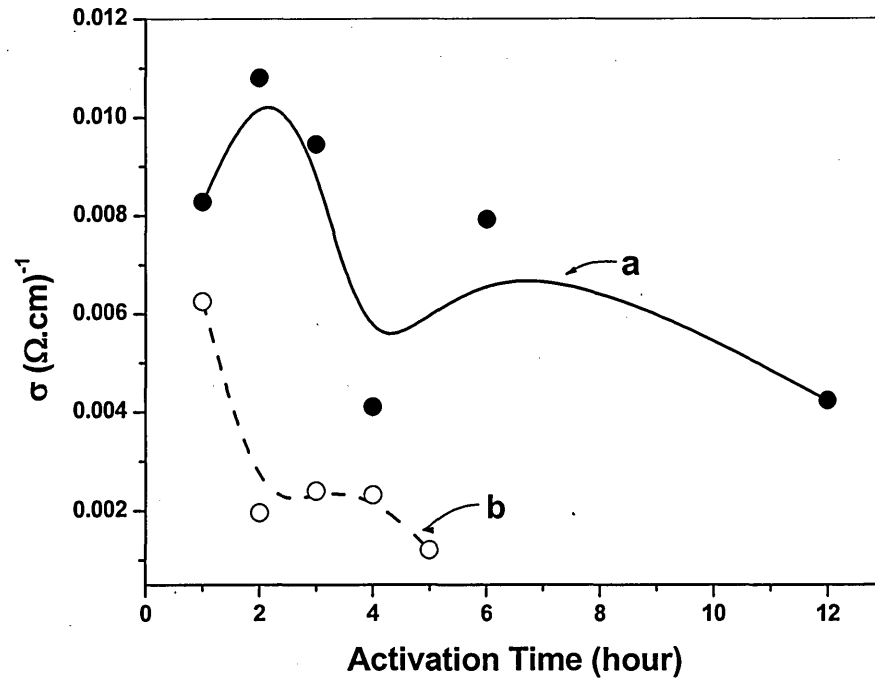


Figure 5.20: Conductivity as a function of activation time for cathodes activated at (a) 1125 K and (b) 1425 K.

On the other hand, the sharp increase in conductivity of the cathode activated at 1425 K with temperature has been associated with an equivalent circuit of σ_{oxide} and σ_{pore} connected in parallel with each other. [Due to Loosjes and Vink, 1949]. In temperature range lower than $T=450 K$, the oxide conductivity is affected by σ_{Ba} due to the contaminated Ba in a number of parts inside the oxide layer which is most likely to be in parallel with σ_{oxide} .

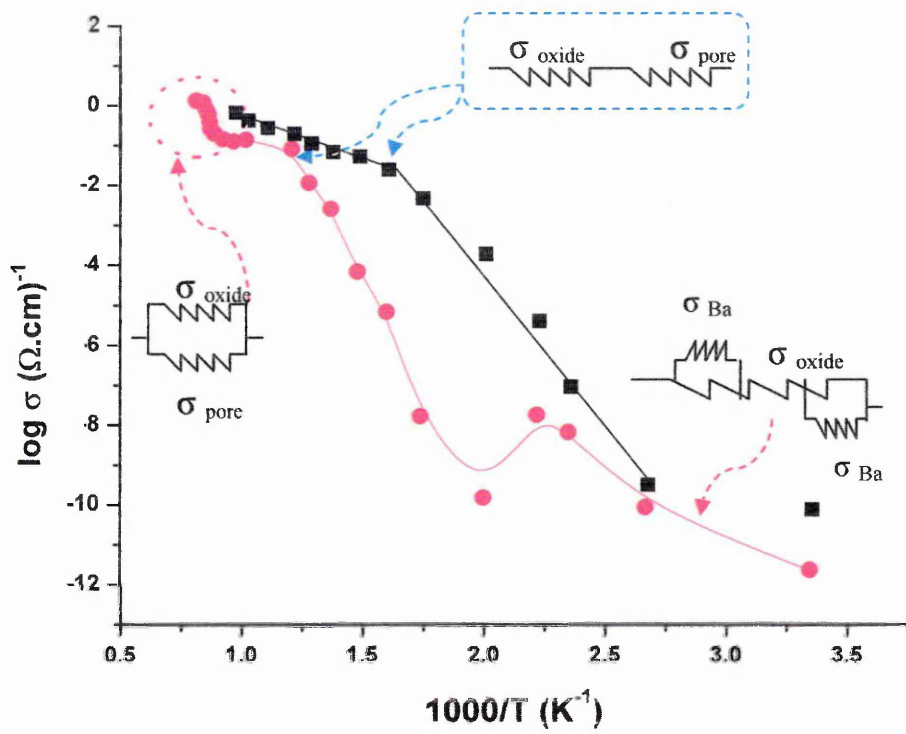


Figure 5.21: The conductivity of the oxide cathode activated at (a) 1125 K for 12 hrs (marked as ■) (b) 1425 K for 5 hrs (marked as ●).

Electron conduction associated with chemical transport of reducing elements in the oxide cathode

6.1 Introduction

One approach to investigate the interface layer which grows between the oxide material and the nickel cap surface is to reduce the existing cathode coating by the incorporation of an activator phase.

Understanding the nickel-oxide interface properties is key to understanding the mechanism of operation in oxide cathodes. The interface layer formed by the reaction products grows with time and also sets limits on the cathode performance. This line of investigation has been studied in different ways, but there is always a big problem to remove the oxide material without affecting the interface layer with a view to examining underneath the oxide coating.

XPS, AES and SIMS are unable to chemically depth profile through 50–100 μm of porous emissive layer, particularly without several treatments, lacking the depth resolution and analytical sensitivity required to analyze the interface.

In recent years, a few researchers have tried to discuss this key point. The buried interface could be exposed in a number of different ways [Jenkins et al, 2001]:-

- The moisture sensitivity is used in a positive manner to remove the bulk of the oxide layer and expose the interface. Removing the majority of the emissive layer improves the depth resolution for all of the chemical depth profiling techniques.
- Model cathodes may be produced with a flat thin carbonate coating prior to conversion. This will improve the depth resolution of the sputtering profiling technique.
- The porous layer can be impregnated with an organic resin to remove the emission layer intact. This of course contaminates the interface with organic resin. Interpretation of data, therefore, must reflect this contamination concern.
- The nickel and emissive layer could be analyzed in a polished cross-section provided it is encapsulated in a mounting material. However these materials tend to be organic resin based, and do not conduct. This will cause problems for both SEM/EDX and particularly AES.
- A combination of FIB (Fast Ion Bombardment) and AES/SAM (or SEM/EDX) is becoming common practice in the semiconductor industry to look at buried interfaces and for characterising defects [von Creigern et al, 1999]. FIB could be used to produce microscopic cross-sections through the oxide and interface for analysis with AES.

In the investigations of Eisenstein [Fineman et al, 1946 and Eisenstein, 1949] and others, the oxide was scraped off from the Ni base, and due to the better adhesion of the interface layer, a film with colour characteristics of the interface phases remained on Ni. This could be analyzed via XRD and the line intensity could be used as a measure of the respective thickness. In some cases this

surface was covered with a protective wax. XRD is still a reasonable method for a sufficiently large surface area and has recently been applied by T. Aida [Aida, 1982] as described above. Instead of XRD micro-Raman Spectroscopy may be used for the Raman active oxide compounds.

To investigate the depth view of interface layer and the mobility of the activator elements, Jenkins [Jenkins et al, 2003] used adhesive tape to remove the bulk of the emissive layer, followed by scratching with a metallic knife to enable areas of interest to be examined by AES.

In addition, the study of Roquais [2002] from Thomson used different methods such as SEM+EDX, AES and TEM to characterise cathode Ni surfaces, but without oxide coating. Their intention was to study activator diffusion and activator compound formation. Glow Discharge Optical Emission Spectroscopy (GDOES) was used to obtain the depth concentration and hence diffusion profiles of the activators Mg and Si, which were present in an amount of a few 100 ppm, and also Al as an impurity of about 100 ppm in Ni of 90 μm thickness.

After annealing the Ni cathode for a few minutes above 1000°C in a damp hydrogen flow, tiny crystallite remnants with dimensions between 100 and 500 nm were detected, decorating (transient) grain boundaries. By diffraction analysis in a TEM, the compounds percales MgO, spinel MgAl₂O₄ and spinel-type γ -Al₂O₃ were identified.

The aim of this chapter is to study the effect of the interface layer on the oxide cathode conductivity over a lifetime of a thousand hours plus by using the new dummy tube method as was explained in chapter three (section 3.7.3).

6.2 The metal-semiconductor junction and Schottky effect

Metal-to-semiconductor contacts are of great importance since they are present in every semiconductor device. They can behave either as a Schottky barrier or as an ohmic contact dependent on the characteristics of the interface. This chapter contains an analysis of the electrostatic of the M-S junction followed by a derivation of the current voltage characteristics due to diffusion, thermionic emission and tunnelling and a discussion of the non-ideal effects in Metal-Semiconductor junctions.

The current-voltage (I/V) characteristics of an M-S interface which were forming a Schottky junction can be expressed as:-

$$I = I_s \left[\exp\left(\frac{eV}{nkT}\right) - 1 \right] \quad (6.1)$$

The ideality factor (n) and the reverse saturation current (I_s) can be determined from the slope and the intercept of $\ln I$ against V respectively.

The device area offers a series resistance R_s and so a significant voltage drop occurs at a large forward current [Chand and Kumar, 1996]. This amounts to a reduction of the voltage across the barrier region from that actually applied to the electrodes of the device. Therefore, the voltage across the barrier region should be reduced from V to $V - IR_s$, and the I/V characteristic becomes:-

$$I = I_s \exp\left(\frac{e(V - IR_s)}{nkT}\right) \left[1 - \exp\left(\frac{-e(V - IR_s)}{kT}\right) \right] \quad (6.2)$$

6.3 Result and discussion

6.3.1 Morphological and elemental analysis

After the LG Philips activation procedure and following the process steps, all the cathodes were converted and activated as shown in table 3.1. The nickel cap surface was changed from being a clean rough surface to being decorated by a spotty coverage of small crystallites having a grain boundary like pattern, as shown in micrography, Figure 6.1.

Figure 6.1a, shows the micrography of the nickel cap surface of the coated cathode, confirming that there is no indication of activators that have diffused to the surface. It also shows the pattern and EDX spectrum of the uncoated cathode after activation, and accelerated by 850 hrs (Figure 6.1b).

The surface is initially free of compounds. The mobile species surface distribution indicates a pronounced preferential diffusion path through grain boundaries. Under magnification, the image shows that the oxide activators are composed of tiny crystallites in the size range from about $(1-3.5)\mu m$. X-ray spectroscopy analysis detected Al, W and O on most of the crystallites, and Mg and O on some of them.

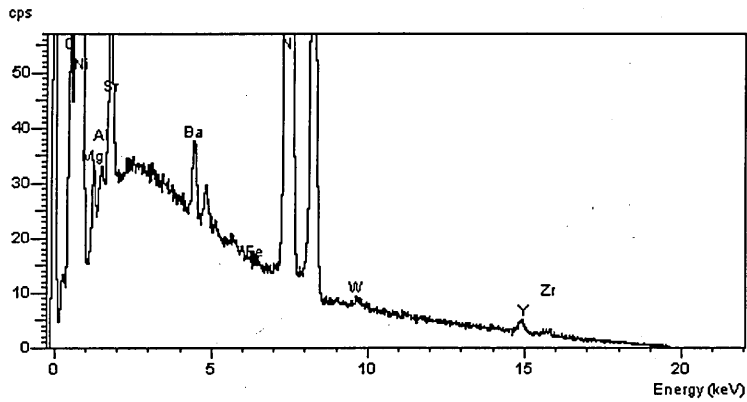
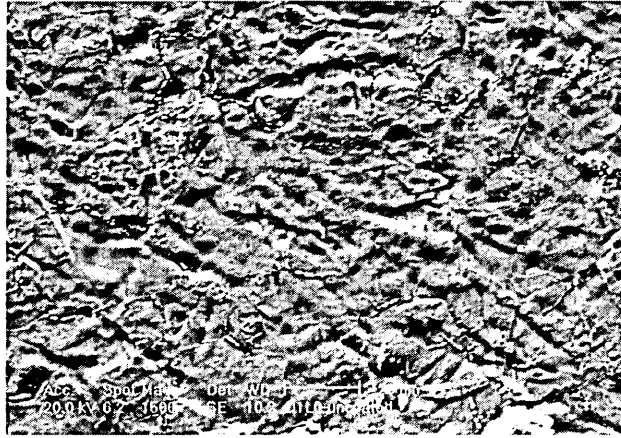
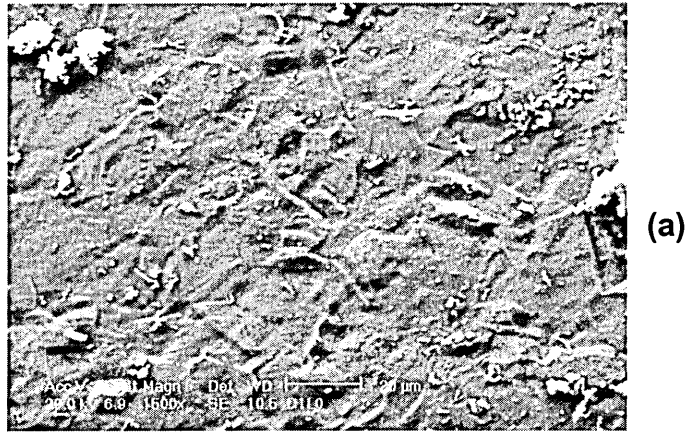
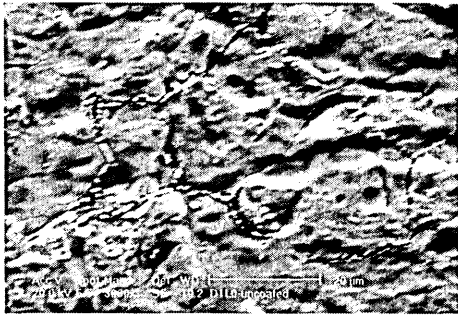


Figure 6.1: SEM images for the Ni cap surface (a) inactivated coated cathode (b) activated uncoated cathode and the EDX spectrum.

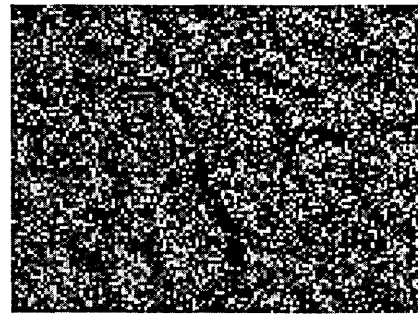
The EDX mapping of heterogeneous distribution revealed aluminum scattered all over the surface, as shown in Figure 6.2, while magnesium oxide is preferentially located at the grain boundaries of the base metal [Poret, 2000]. The EDX mappings observed a small amount of yttrium, iron and zirconium distributed on the surface.

A well localized area on the nickel cap surface of the uncoated cathode (Figure 6.2) shows a variation in the grain size through the lifetime. The initial average changes in the grain size are about $(20-18)\mu m$, when the acceleration lifetime is between $(0-144)hrs$ and the grain boundaries extend from $(1-1.5)\mu m$ for the same period of lifetime.

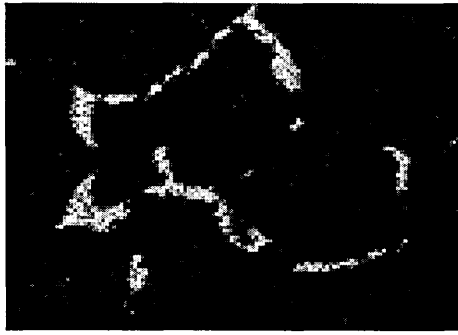
Figure 6.3 displays the morphology of the inactivated oxide cathode coated surface and the EDX spectrum. The X-ray spectrum indicates some Al and Zr elements diffused on the surface of the oxide. This may be explained later in terms of the influence of the interface layer in the pores space between the grain boundaries. As no Al and Zr were detected in the emissive layer prior to activation and ageing, this suggests that both activators have been able to diffuse over distances of $(65\pm 5)\mu m$ (most probably along the surface of the porous oxide network). This indicates that the interaction between the activator elements and emissive oxide is not restricted only to the nickel-oxide interface but is more complex and these elements may also be influencing the chemistry of cathode operation [Jenkins, 2003].



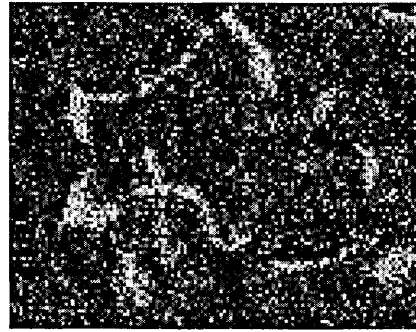
Localized SEM image



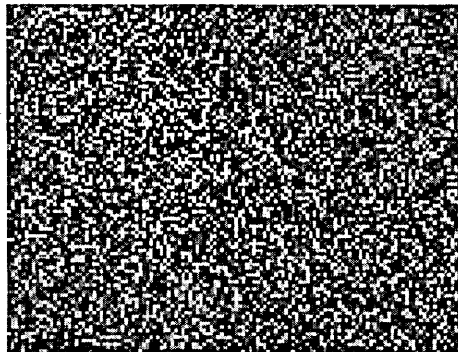
Aluminum



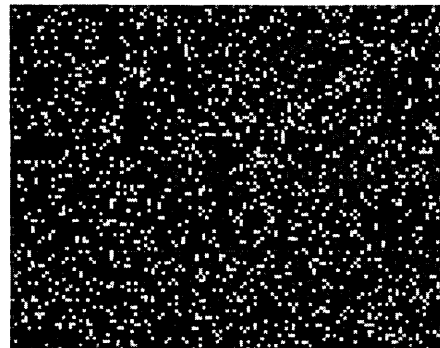
Magnesium



Oxygen



Iron



Yttrium

Figure 6.2: SEM micrography for the chosen area magnified 3000 times.

6.3.2 D.C. Electrical characterization

The dc electrical measurements were made for the same assembly and for different samples. Figure 6.4, displays typical I/V characteristics of coated-uncoated cathodes at 1075 K . The characteristics are found to be reversible and reproducible, and show a rectifying behavior with a rectification ratio close to 76, for the zero run hour samples. This ratio approached 100 when the samples were operated for 144 hrs .

Figure 6.5, shows a set of typical I/V characteristics at three different lifetimes. The reverse current appears almost saturating in the voltage range $(2-5)\text{ V}$, which may be explained as a limiting charge carrier transport through the junction. Between the zero run hour and 1896 hr , the rectification ratio had different values. This rectification capability depends on the influence of the interface layer in both the oxide material and the Ni cap grains. The ideality factor which has been calculated using Equation 6.2, gives a consistent value of about (≈ 9.6), as shown in Figure 6.6 for reverse bias. The higher value of n was ascribed to the tunneling in the junction area [Shah et al, 2003 and Mandal et al, 1997] as a result of the increase in the electron space charge (thermionic emission) and the increase in the Schottky effect. The values of n and I_s are given in table 6.1.

By substituting the values of n and I_s into Equation 6.2, an approximate value of R_s is obtained and it's found to approach an average value of $1.88\text{ M}\Omega$. The resistivity of activated (Ba,Sr)O coating is reported to be of the order of

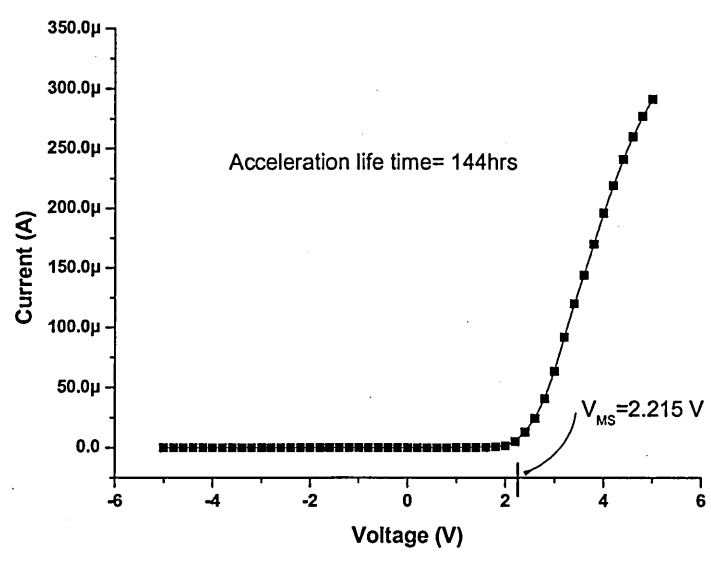
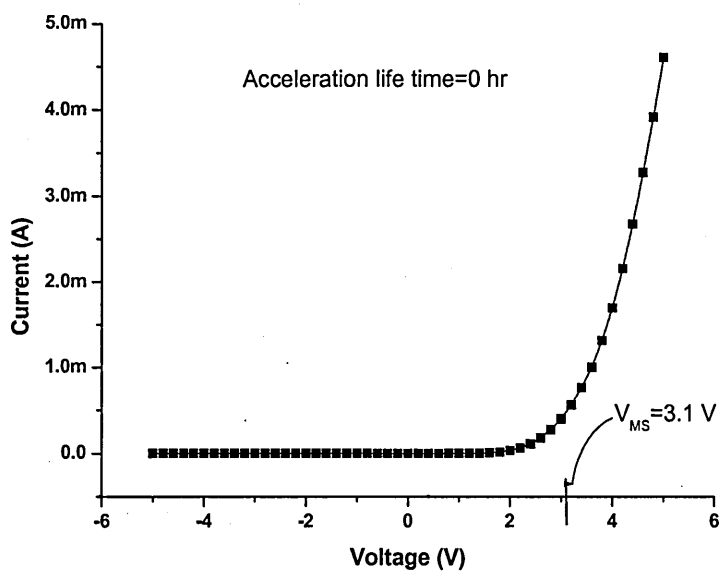


Figure 6.4: Dependence of the current (I) on the applied voltage (V) at operation temperature 1075 K .

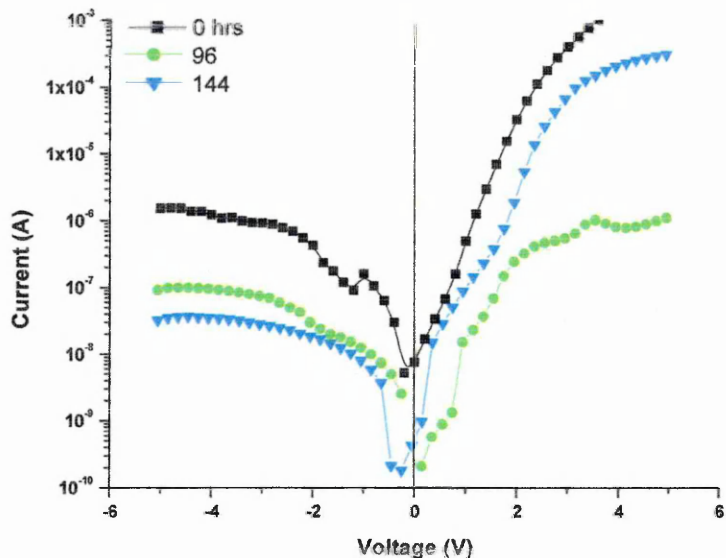


Figure 6.5: Current-voltage characteristics of cathode assembly at different acceleration lifetimes.

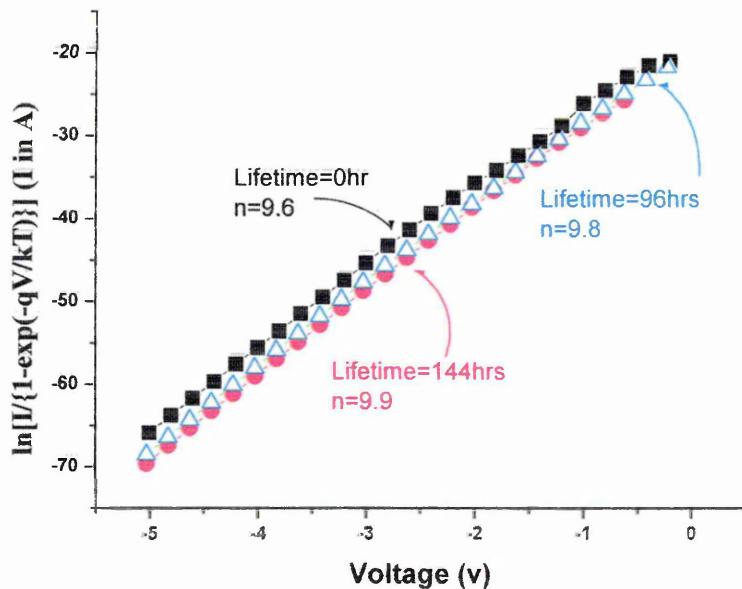


Figure 6.6: Logarithmic plot of $I/[1 - \exp(-qV/kT)]$ for the same samples in Fig (6.5).

Table 6.1: The rectification parameters of the dummy tube test

| Lifetime (hours) | n Ideality factor | (r) rectification ratio | I_s μA |
|---------------------|------------------------|--------------------------------|---------------|
| 0 | 9.6 | 77.7 | 1.6 |
| 48 | 9.6 | 13.61 | 0.05 |
| 96 | 9.8 | 8.21 | 0.088 |
| 144 | 9.9 | 100 | 0.03 |
| 330 | 9.96 | 1.519 | 0.5 |
| 834 | 9.93 | 1.4 | 1.4 |
| 1196 | 9.8 | 32 | 7.8 |
| 1890 | 9.78 | 1 | 20 |

$10^3 (\Omega.cm)^{-1}$ [Gätner et al, 2002], but the value for this new cermet oxide cathode with 2.5% Ni powder addition is decreased to $10^2 (\Omega.cm)^{-1}$ at the operating temperature. The comparison result shows that the resistivity of the interface is dominated by the device resistivity at the reverse bias.

The effect of the interfacial layer growth may be understood in term of a series resistance R_i due to an interface layer in series with the resistance R_o of activated oxide layer. The effective conductivity σ for this two resistor network can be calculated using equation 5.3. Where $\left(\eta = \frac{t_i}{t_o}\right)$ is the ratio of the interface

layer thickness to that of the oxide coating. Using the approximate values of $\sigma_o = 10^{-2} (\Omega.cm)^{-1}$, $\sigma_i = 10^{-8} (\Omega.cm)^{-1}$, $t_o = 65 \mu m (0 hrs)$ and $t_o = 50 \mu m (1896 hrs)$ the value of t_o can be estimated. The calculated values are $\sim 250 nm$ at zero run hours and $\sim 6 \mu m$ at 1896 hrs. This high value indicates non uniform shape of interfacial layer. This may prove the interface layer grows inside the Ni cap grain boundaries and penetrates in between oxide grains, as shown in Figure 6.7. This value seems to be an effective thickness which may increase the contact reaction reduction area between the surface cap and the oxide grains. The increase in the reaction reduction area increases the tunnelling reverse bias saturation current as shown in Figure 6.8.

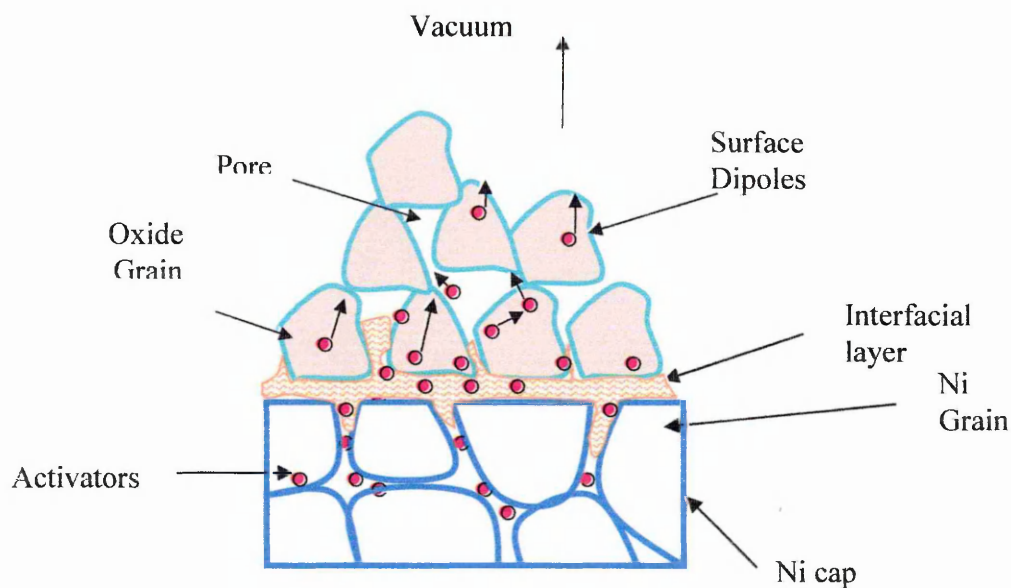


Figure 6.7: The non uniform interfacial layer.

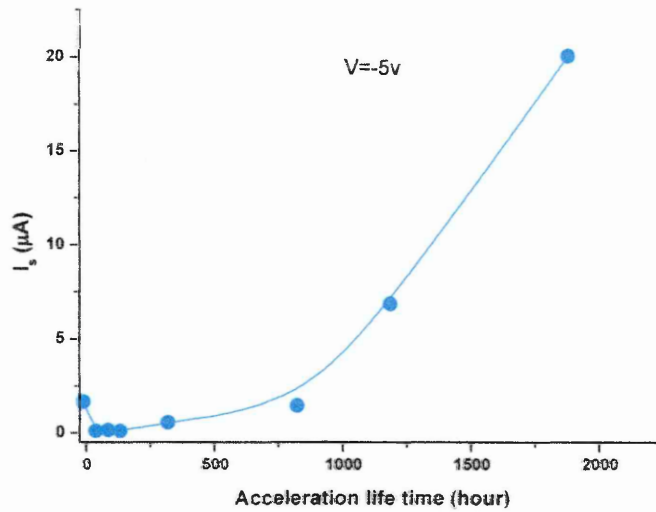


Figure 6.8: Variation in the reverse current saturation

The turn-on voltage taken from Figure 6.4, decreases in the range of $(3.1 - 2.2) eV$ within the short life of about $(0 - 144) hrs$ and $(2.2 - 1.03 eV)$ in the long term of about $(144 - 1896) hrs$, as shown in Figure 6.9. The difference between the two line slopes is the influence of the free Ba in the long life up to real time which is considered to be a very effective factor on the conductivity characteristics [Chin et al, 1974].

Figure 6.10, shows the measured $1/C^2 - V$ plot of the Ba/SrO: Ni cap structure. Because of the high free electron concentration in the Ni cap, band bending should mainly occur on the Ba/SrO side of the junction [D. Song et al, 2002]. Therefore, the $1/C^2 - V$ intercept of $6.27 V$ on the x-axis is essentially equal to

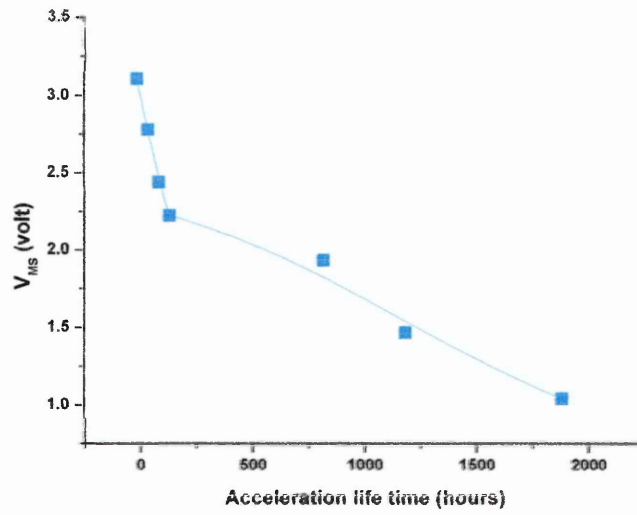


Figure 6.9: The variation of the turn-on voltage with the acceleration lifetime.

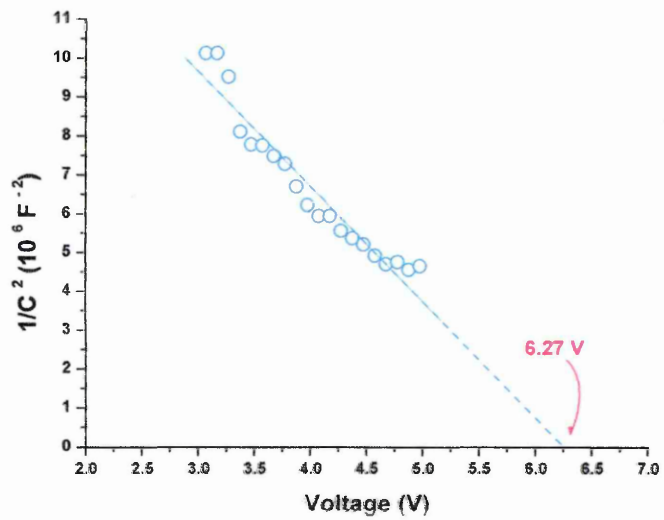


Figure 6.10: $1/C^2$ vs. voltage plot of the Ba/SrO: Ni cap M-S junction sample.

the diffusion potential at the Ba/SrO surface. The Ba/SrO Fermi level E_F was calculated to be 1.4 eV below the conduction band edge [Nergaard, 1952]. As a result, the potential barrier for electrons in the Ni cap conduction band is 7.65 eV . This value is approximately in agreement with the activation energy of this M-S junction, which was calculated by using equation 2.11 and is equal to 7.23 eV .

A supporting result for Figure 6.7, has been reported by Jenkins from L.G.Philips [Jenkins et al, 2003]. Jenkins investigated the outer surface of emissive layer by using in-situ sSIMS. Aluminum was found on the emitter surface after conversion and a significantly high level of a Mg-Ba compound was also formed after ageing as well as the predictably high level of surface free barium. This suggests that both activators have been able to diffuse over some distance, most probably along the surface of the porous oxide network. This indicates that the interaction between the activator elements and emissive oxide is not restricted only to the nickel-oxide interface but is more complex and these elements may also be influencing the chemistry of cathode operation.

Roquais reported that the enrichment of the Ni surface with Mg and Al caused by annealing is very remarkable. It is not only at the Ni surface but also a near surface region of the nickel about $5\text{ }\mu\text{m}$ that is affected by the creation of Mg and Al diffusing mainly through grain boundaries [Roquais et al, 2000].

Chapter 7

Conclusions, Further Work and Resistivity network model

7.1 Oxide cathode characteristics for CRT application

The aim is to enhance the emission current density by reducing the cathode coating resistivity by the incorporation of a conductive metallic phase. This is the main idea of the LG Philips new generation of oxide cathodes. One of the significant advances in recent times has involved the work of L.G. Philips Display Components on the development of new compositions for the emissive layer of their oxide cathodes. The oxide cathode comprises a top layer of Ba\SrO mixed with a Ni 5% (oxide cathode) or 2.5% (oxide cathode plus) powder cermets with surface area of 0.0165 cm^2 and layer thickness of approximately $(65\pm 10)\mu\text{m}$ deposited onto a Nickel alloy cap. This Ni cap (oxide cathode plus) contains low levels of *W* (2.98%), *Mg* (0.125%) and *Al* (0.1%) as activators in addition to small amounts of Yttrium, Zirconium and Iron.

Different assemblies have been fabricated to study their structural and electrical properties. Two different methods have been used to study the electrical properties and the formation of the interface layer. A special dummy tube was designed for this purpose. Numerous theories have been used for the conduction mechanisms of the oxide cathode in terms of the electron percolation and the MS junction.

Scanning electron microscopy (SEM) and EDX analysis of oxide cathode samples with different treatments have been performed. SEM micrographic images show the cathode conductivity type dependence (S or N types). EDX analysis shows that the conductivity is dependent on the amount of the Ba contaminate in the oxide layer. The analysis showed the penetration of the activators through the oxide, specifically the Al agents.

7.2 Electrical measurement and conduction properties

Current-voltage characteristics of the face to face cathode structure of oxide cathode utilising different kinds of cathodes in different methods and in vacuum chamber have been measured in the temperature range between $(300-1200)K$.

The experimental results can be summarizing as follows:

- Long term operation of this semi-closed system accumulated Ba as layers on the surface grains and involved another resistance to the resistivity network of the cathode. The effect of the Ba layers can be viewed in the low temperature range $(300-600)K$ and high temperature range $(1000-1200)K$ very clearly after several hundreds of operation hours.
- The conductivity of activated (Ba,Sr)O coating is reported to be of the order of $10^{-3}(\Omega cm)^{-1}$ [Gärtner et al, 2002] but the value for this new cermet oxide cathode with $(5-2.5)\%$ Ni powder addition is increased to $10^{-2}-10^{-1}(\Omega cm)^{-1}$ at the operating temperature.

- The cathode activation energy strongly depended on the cathode type structure (S or N type) due to the activation temperature and time.
- The D.C electrical characteristic shows very strong rectifying behaviour through the M-S junction due to the I/V curves, particularly after 144 *hrs* lifetime inside a dummy tube life test.
- The characteristics of the coated-uncoated cathode assembly are found to be reversible and reproducible, and showed a rectification ratio (r) of 100. The calculated ideality factor shows a value of $n = 9.6$ which is evidence for the tunnelling conduction at low temperature.
- The interface layer thickness grows from $\sim 250\text{nm}$ at zero run hours to $\sim 6\mu\text{m}$ after accelerating the cathode to 1896 *hrs* (real time $\sim 14200\text{hrs}$). This value seems to be an effective thickness which may increase the reaction reduction area between the surface cap and the oxide grains. The increase in the reaction area increases the tunnelling reverse bias saturation current, as shown in Figure 6.8.

7.3 Morphological and elemental analysis

The cathode assemblies were mounted, face to face in pairs in a specially designed holder inside a glass chamber, which was evacuated prior to and during all measurements, to a vacuum of about 3×10^{-7} *mbar*. The cathode that decomposed and activated under this condition (with enough compression

between the two attached cathodes and a very high temperature) is most likely to be an "S" type cathode. The morphological analysis shows:

- The Ba lost by this system is much less than the open system and contaminates are present inside the pores and between the grains. Ba atoms cover the grains surface as an adsorbed mono layer in some places and as a multi-layer in other places.
- As it became more sintered, the grain size increased from approximately $6\ \mu m$ to $10\ \mu m$ after twelve hours of activation at $1200\ K$. It was also apparent that the porosity decreased with the increasing activation time.
- The EDX analysis of the interface layer on the Ni cap shows that tungsten was the first element to diffuse through the Ni boundary grains to the Ni surface, forming one of the tungsten oxide compositions.
- The presence of Al was observed in an appreciable quantity after 3 hours of activation. Magnesium was found in a small proportion only after a long time of activation of about 12 hours at $1200\ K$. These particles are believed to remain in their respective oxide forms (e.g. Al_2O_3 for Al and MgO for Mg) distributed on the surface of the cap, concentrated in the Ni grain boundaries. Mg may also be present in the $MgAl_2O_4$ form.
- The decrease in the Al agents on the Ni cap surface indicates that the Al particles left the interface and were transported through the oxide layer. These particles can reduce the oxygen from the oxide grains directly and cause a Ba

adsorption layer on the grain surface. The evidence for this description is the Al element which was found to be distributed on the oxide layer.

Additional conclusions due to the dummy tube test:

- X-ray spectrum indicates some Al and Zr elements are diffused on the surface of the oxide. The high value of the interface layer thickness indicates a non uniform shape of interfacial layer. This may prove the interface layer grows inside the Ni cap grain boundaries and penetrates in between oxide grains, diffused on the surface of the oxide. This may be explained in term of the influence of the interface layer in the pores space between the grain boundaries, as shown in Figure 6.7.
- Mg was found to be diffused on the Ni cap surface initially very clearly, as shown in Figure 6.2. Actually, this is in contradiction with the EDX and SEM results for the cathode activated to 1200 K in section 5.3.1.

These results can be accepted if it is supposed that the Mg was initially diffused to the surface and then transported through the oxide quickly but with a very short path. This explains the disappearance of the Mg from the Ni cap surface images and EDX test.

7.4 Resistivity network model

By highlighting some points from chapter two and using the conclusions above, it helps to build a new network model for the new generation of oxide cathode. The highlighted points can be summarized as:

1. According to the Loojese and Vink experiments in the oxide coating, there is a dependence of conduction on temperature given by equation 2.12. If these two conduction mechanisms are connected in series, the resultant conductivity will at every temperature be determined mainly by the mechanism with the lowest conductivity. If, however, these mechanisms are connected parallel to each other the resultant conductivity will at every temperature be determined mainly by the mechanism with the highest conductivity. One mechanism, the "low-temperature" mechanism, dominates at low temperatures and the other, the "high-temperature" mechanism, dominates at high temperature. The resultant conductivity is in that case the sum of the conductivities of the separate mechanisms, as shown in Figure 2.11.

2. Narita [1953] suggested two structural types due to the decomposition and activation processes and another type of conduction due to the barium contamination. These types are S-type, N-type and M-type. He also suggested a new model for oxide-coated cathode, which must be introduced to overcome the differences in the evaluation of the activation energy and work function due to the experimental resultants.

The Narita theory produced a new classification of the structures of the oxide coated cathodes. This classification included four different types ($\alpha, \beta, \gamma, \delta$) based on the energy band structure and their subtypes as illustrated in Figures (2.22- 2.25).

3. In oxide-coated cathodes, Dearnaley [1969] proposed that the presence of reducing agents at the activation temperature results in the removal of some oxygen from the coating. At certain favorable points on the metal-oxide interface the oxygen may locally become conducting, perhaps owing to an aggregation of oxygen vacancies, which may occur particularly at grain boundaries in the polycrystalline structure. If an electric field is applied during activation, the filament will then tend to grow through the oxide coating.

That oxygen evolved from the structure may be understood from the fact that the Debye temperature of the alkaline earth oxides is quite low, despite their refractory nature: thus θ_D for barium oxide is about $525 K$. Owing to their low mass the oxygen atoms will undergo violent thermal agitation at $T \sim 2\theta_D$ and may be ejected from the structure while the far heavier barium atoms remain relatively undisturbed. In the conducting chain created by a high concentration of oxygen vacancies and terminating at the metal base, the applied field will cause a very large electric stress at the other end, extending as it does into the insulating oxide. Under such a stress, and at the activation temperature, he supposes that further oxygen vacancies migrate to this tip and cause it to grow until the chain penetrates the oxygen layer. The increased conductivity of the layer will eventually reduce the electric field and filament growth will come to an end.

4. Barium adsorption serves not only to increase the electron emission at the cathode surface but also to enhance the electron conductivity between the oxide crystallites. With the above assumption it is conceivable that the rate of barium-

ion adsorption at the interfaces is equal to that at the emitting surfaces. This would explain the linear relation of electron emission and conduction. Since the electron conductivity of BaO crystals cannot be increased through this adsorption process, the relationship of the thermionic emission with the electron conductivity is not expected to be linear.

Conclusion can be drawn using the experimental data of the theories discussed earlier, concerning the structure of the oxide cathode through the activation and operation process.

The low Debye temperature of the BaO ($\theta_D = 525 K$) leads to decomposed Ba/SrO. Low decomposition temperature compared with the normal cathode operation temperature creates a high oxygen contaminant concentration on the grain surface and inside the pores.

By the effect of the electrical field, the free oxygen formed a filament chain percolated in the oxide layer and ended at the Ni cap surface and oxide top layer. At the high operation and activation temperature, the activators such as Al, W and Mg move to the Ni cap surface. These activators reach the oxygen filament depending on their reactions-reduction activities to be oxidized. The high oxygen concentration encourages these elements to follow the high activity points. Because of that, the activators move away from the Ni cap surface and transport through the oxide layer creating different kinds of oxides. This is also the reason for the existence of the Al or W on the top surface of the Ba/SrO.

Also, the free Ba and oxygen vacancies move to the grain surface creating conduction or emission electron and an adsorbed mono or multi-layer of Ba.

All these processes form resistances which are connected with each other in a way more complicated than the resistance network explained in Figure 5.8.

It is believed that the conductivity changes occurring during the activation process can be attributed to this structural re-arrangement and coarsening of the Ni phase between the Ba/SrO grains and in between these oxide activators to make a short pathway for the electron to transport in between these chains following the lower resistance and the number of continuous electrical pathways will be reduced after this process.

Figure 7.1 shows this new model taking into account all these processes and the experimental results in this thesis.

On this occasion, it's very difficult to analyze this new generation of oxide cathode through the classification of Narita models.

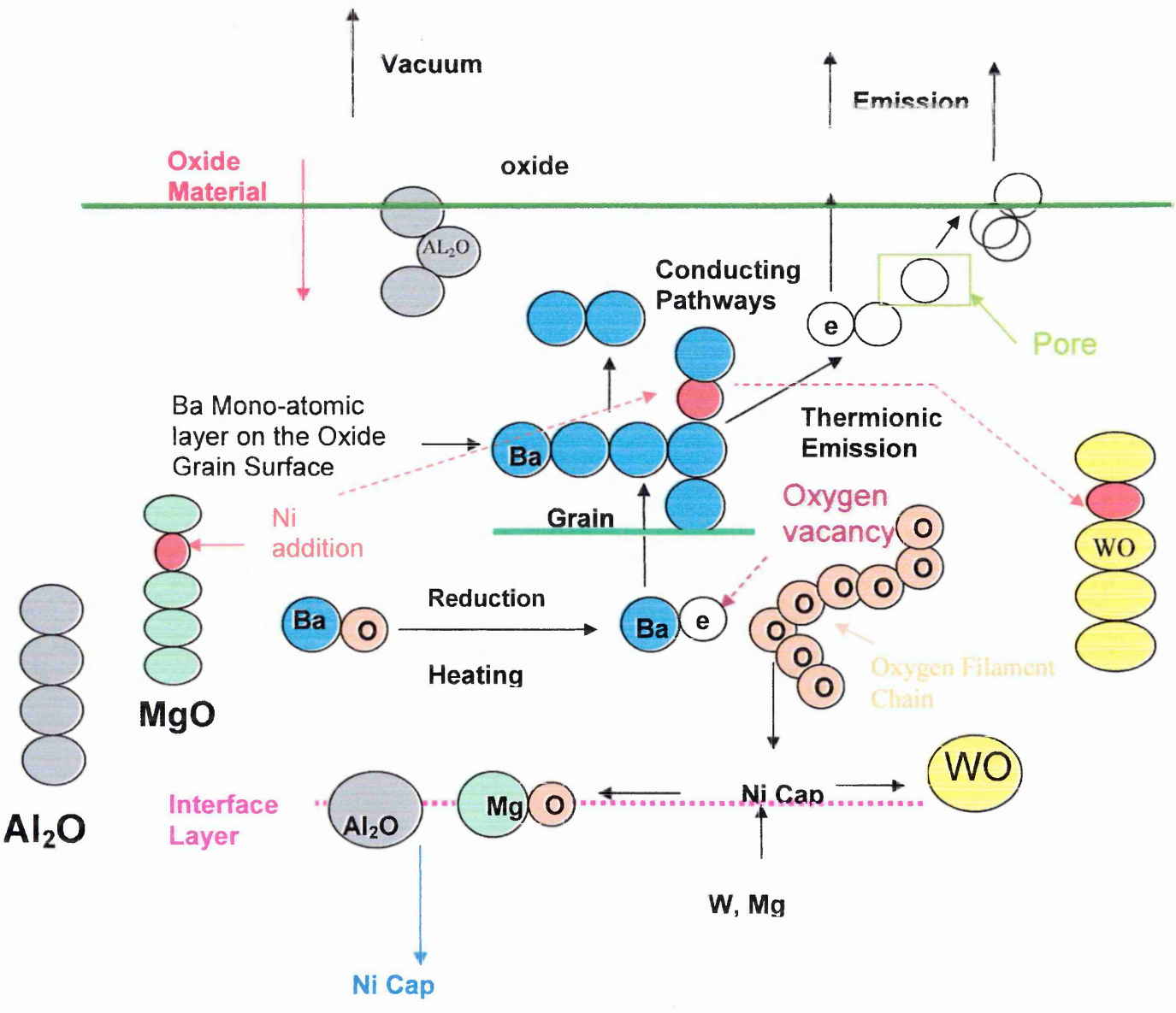


Figure 7.1: The new structural model

7.5 Suggestions and future work

1. Repeat the dummy tube test under load voltage (diode voltage).
2. Further use of morphology analysis to observe the transportation of the chemical activators elements through the cathode layers.
3. Study the effect of the additional elements in the new generation of oxide cathode plus two.
4. Study the rectification electrical properties of the oxide cathode plus in a dummy tube test to confirm the interpretation of the rectification results. .

(A)

- Allison H. and Samelson H.**, J. Appl. Phys., 30/9, 1419-1424, 1959.
- Aleksandrov E.M., Prik K. E. and Sirolkin G.D.**, Zvestiya VUZ. Fizika, 11, 10, 159, 1968.
- Aida T., Taguchi S., Yamamoto S. and Fukushima H.**, J. Appl. Phys., 53, 12, 1982.
- Aida T., Tanuma H., Sasaki S., Yanguchi T., Taguchi S., Koganezawa N. and Nonaka Y.**, J. Appl. Phys., 74, 11, 1993.
- Al-Ajili A., Ray A.K., Travis J.R., Hodgson S.N.B., Baker A.B. and Goodhand C.J.**, J. Mater. Sci., Mater. Elec., 11, 489, 2000.
- Al-Ajili A., Hodgson S.N.B., Baker A.B., Ray A.K., Travis J.R. and Goodhand C.J.**, J. Mater. Sci., Mater. Elec., 12, 99, 2001.
- Al-Ajili A. N. H., Ray A. K., Hassan A. K., Hodgson S. N. B. and Goodhand C. J.**, Materials Letters, 57 (2), 513-517, 2002.
- Aki A. A., Kamal H. and Abdel-Hady K.**, Physica B, 325, 65, 2003.

(B)

- Becker J. A.** , Phys. Rev, 34, 1929.
- Becker J.A.**, Trans. Electrochem. Soc. 59, 15 pp., 1931.
- Becker J.A. and Sears R.W.**, Phys. Rev., 38, 1931.
- Becker J.A.**, Rev. Mod. Phys., 7, 95, 1935.
- Balas W., Dempsey J. and Rexer E.F.**, J. Appl. Phys., 26, 9, 1955.
- Beynar K.S. and Nikonov B.P.**, Radio Eng. Elec., 9, 1518, 1964.
- Beynar K.S. and Nikonov B.P.**, Radio Eng. Elec., 10, 408, 1965.
- Bennet G.A.G.**, "Electricity and Modern Physics". 2nd Ed. (Edward Arnold. London), 1974.
- Barratt D. and Gärtner G.**, Appl. Surf. sci., 215, 65-71, 2003.

(C)

Chin T. N., Cohan R.W. and Coutts M.D., RCA Rev., Vol 35, 1974.

Chand S. and Kumar J., J. Appl. Phys., 80, 288, 1996.

Cortenraad R., Denier van der Gon A.W., Brongersma H.H., Gärtner G. and Manenschijn A., Appl. Surf. Sci., 146, 69, 1999.

Cortenraad R., Gon A.W. denier van der, brongersma H.H., Gärtner G., Raasch D. and Manenschijn A., Appl. Surf. Sci., 215, 1-4, 2003.

(D)

Dolloff R.T., J. Appli. Phys., 27, 1418, 1956.

Dearnaley G., phys. Letters, 25A,760, 1967.

Dearnaley G., Thin Solid Films, 3, 161, 1969.

Dieumegard D., Tonnerre J.C, Brion D. and Shroff A.M., Appl. Surf. Sci., 111, 84, 1997.

Dakhel A.A., J. Phys. Chem. Soli., 65,1765-1771, 2004.

(E)

Eisenstein A., J. Appl. Phys., 20/8, 776, 1949.

(F)

Fineman A.and Eisenstein A., J. Appl. Phys.,17/8, 663, 1946.

Forman R., Phys. Rev., 96, 6, 1954.

(G)

Gärtner G.F. and Houweligen D. van, "Electron emission cooling of thermionic thoriated tungsten cathodes under high dc-loads, Elektronenröhren u. Vakuumelektronik, NTG-Fachbericht 95, VDE-Verlag, pp. 224-229, 1986.

Gärtner G.F., European Patent Number EP0560 436 B1, Philips Ltd, 1992.

Gärtner G., Geittner P., Lydtin H. and Ritz A., Appl. Surf. Sci., 111, 11, 1997.

Gärtner G., Res Rep., PFL-Aachen Report, Philips Company, 1999.

Gärtner G., Raasch D., Janiel P., Schlageter K., Heide P. van der and Jenkins S., Dis. Vac. Elec. 165 237, 2002.

Gärtner G. and Clausen C., Res Rep., PFL-Aachen Report, Philips Company, 2002.

Gärtner G., Janiel P. and Raasch D., Appl. Surf. Sci., 201, 35, 2002.

Gärtner G., Raasch D., Barratt D. and Jenkins S., Appl. Surf. Sci., 215, 72-77, 2003.

Gillet M., Lemire C., Gillet E. and Aguir K., Surf. Sci., 532-535, 519, 2003.

(H)

Heinze W. and Wagener S., Z. Tech. Phys., 20, 17, 1939.

Hannay N.B., MacNair D. and Whitt A.H., J. Appl. Phys., 20, 669, 1949.

Herrmann G. and Wagener S., The Oxide-coated Cathode, Vols. I and II, Chapman and Hall, 1951.

Hensley E.B., J. Appl. Phys., 23, 10, 1952.

Hensley E.B., J. Appl. Phys., 27, 3, 1955.

Higginson G.S., British J. Appl. Phys., 9, 1958.

Hutson A.R., "Semiconducting properties of some oxide and sulphides", p 543 In semiconductors, Reinhold Pup. Corp. 1959.

Haas G.A., Shih A. and Thomas R.E., Appl. Surf. Sic., 2, 293, 1979.

Haas G.A. and Shih A., Applications. Surf. Sic., 8, 145-170, 1981.

Haas G.A., Shih A. and Marrian C.R.K., Appl. Surf. Sci., 16, 139, 1983.

Hodgson S.N.B., Baker A.B., Goodhand C.J., Heide P.A.M. van der, Lee T., Ray A.K. and Al-Ajili A., Appl. Surf. Sci., 146, 79, 1999.

Hayashida Y., Ozawa T. and Sakurai H., Appl. Surf. Sci., 146, 7, 1999.

Higuchi T., Matsumoto S., Koyama K., Hara A. and Hamamoto H., Appl. Surf. Sci., 146, 109, 1999.

Hodgson S.N.B., baker A.P., Goodhand C. J., Heide P.A.M. van det, Lee T., Ray A.K. and Al-Ajili A., Appl. Surf. Sci., 146, 79, 1999.

(J)

Jonscher Andrew K., Thin Solid Films, 100 (4), 329-344, 1983.

Jenkins S., Johnstone W., Heide P.A.M. van der, Rommers P., Straaten M. van der and Gärtner G., Disp. Vac. Elec., 165, 231, 2001.

Jenkins S., Barber D.K., Whiting M.J. and Baker M.A., Appl. Surf. Sci., 215, 78, 2003.

(K)

Koller L.R., Phys. Rev., 25,671,1925.

Kasap S.O., "Principles of Electrical Engineering Materials and Devices", McGraw-Hill, 1997.

(L)

Lowry E.F., Phys.Rev. 35, 1367-1378, 1930.

Loosjes R. and Vink H.J., Philips Res. Rep., 4, 449, 1949.

Leblond B. and Rejaonera G., Nucl. Instr. Meth. Ohys. Res., A 340, 1994.

(M)

Mecklenburg W., Z. Tech. Phys., 120, 21, 1942.

Müller Wolfgang, J. Vac, Technol., A6, 3, 1988.

Müller Wolfgang, IEEE Trans. Elec. Devi., 36, 1, 1989.

Makovicka C., Gärtner G., Hardt A., Hermann W. and Wiechert D.U., Appl. Surf. Sci., 111, 70, 1997.

Mandal S.K., Maity A.B., Dutta J., Pal R., Chaudhuri S. and Pal A.K., Phys. Stat. Sol. (a) 163, 433, 1997.

(N)

Narita S. and arizumi T., J. Phys. Soc. japan, 3, 356, 1948.

Nergaard L. S., RCA Rev., 13, 464, 1952.

Narita Shin-ichiro, J. Appl. Phys., 23, 5, 1952.

Narita Shin-ichiro, J. Phys. Soc. Japan, Vol 8, No. 3, 1953.

Norman D., Tuck R.A., Skinner H.B., Wadsworth P. J., Gardiner T.M.,

Narita M., European patent Number Ep 0685 868 A1, NEC Corporation, 1995.

Nakai H., Shinohara J., Sassa T. and Ikegami Y., Nucl. Instru. Meth.: Phys. Res. B, 121, 125, 1997.

(O)

Owen I.W., Richardson C.H. and Thornton G., Phys. Rev. Let., 58, 5, 1987.

Ohring M., "Engineering Materials Science", (Academic Press, New York), 1995.

Ohira T., Teramoto H., Saito M. and Shinjo T., Appl. Surf. Sci., 146, 47, 1999.

Ortiz-López J. and Gómez-Aguilar R., REVISTA MEXICANA DE FISICA 49, (6) 529-536, 2003.

Ondo-Ndong R., Ferblantier G., Pascal-Delannoy F., Boyer A. and Foucaran A., Microelectronics J., 34, 1087-1092, 2003.

(P)

Peterson R., Anderson D. and Shepherd W., J. Appl. Phys., 28/1, 22-33, 1957.

Pikus G.Ya. and Shnyukov V.F., Radiotekhnika i Elektronika, 10, 1, 124, 1964.

Poret F., Dufour P., De Rosa B., Roquais J.M. and Steinbrunn A., Sol. Sta. Phen., 72, 35, 2000.

Poret F., Roquais J.M., Le Doze R., Pual M., Dufour P. and Steinbrunn A., Appl. Surf. Sci., 215, 1-4, 2003.

(R)

Rothe H., Z. Physik, 36, 737, 1926.

Redington R.W., Phys. Rev., 87, 6, 1952.

Roquais J.M., Poret F., Le Doze R., Dufour P. and Steinbrunn A., Appl. Surf. Sci., 201, 85, 2002.

(S)

Shepherd A.A., British J. Appl. Phys., 4, 70, 1953.

Saum G.A. and Hensley E.B., Phys. Rev., 113, 1019, 1959.

Shih A. and Haas G.A., Applications. Surf. Sic.,8, 125-144, 1981.

Saito M., Suzuki R., Fukuyama K., Watanabe K., Sano K. and Nakanishi H., IEEE Trans. Elect. Dev., 37, 12, 1990.

Sasaki S., Amano I., Yaguchi T., Matsuzaki N., Yamada E., Taguchi S. and Shibata M., Appl. Surf. Sci., 111, 18, 1997.

Shih A., Yater J.E. and Abrams R., Appl. Surf. Sci., 146, 1, 1999.

Sasaki S., Yaguchi T., Mori N., Taguhi S. and Shibata M., Appl. Surf. Sci., 146, 17, 1999.

Song D., Neuhaus D., Xia J. and Aberle A.G., Thin Solid Films, 422, 180-185, 2002.

Shah Jay M., Li Y.-L., Gessmann Th. and Schubert E.F., J. Appl. Phys., 94, 2627, 2003.

(T)

Tomloinson T.B., J. Appl. Phys., 25, 6, 1954.

Tomlinson T.B. and King R.E.j., British J. Appl. Phys,7, 1956.

(U)

Uda E., Nakamura O., Matsumoto S. and Higuchi T., Appl. Surf. Sci., 146, 31, 1999.

(W)

Wehnelt A.H., Ann. der Phys., 14, 425, 1904.

Wilson A.H., Proc. Roy. Soc. London, 133,458, 1931.

Wright D.A., Proc. Roy. Soc. A190, 394-417, 1947.

Wright D.A., Nature, 164, 714, 1949.

Whited R.C. and Walker W.C., "Exciton and interband spectra of crystalline CaO", Phys. Rev., 188, 1380, 1969.

(Y)

Yamamoto S., J. Vac. Soc. Japan, 40, 5, 1997.

(Z)

Zalm P., "Thermionic Cathodes", p. 211 In advances in Electronics and Electron Physics, Acadmic Press, Inc., New York 1968.

Appendix

The derivation of the equation 5.3

From the series connections shown in Figure 5.8, the resistivity is given by:

$$\rho = \rho_o + \rho_i$$

These resistances are affected by the material layer thickness:

$$(t_o + t_i)\rho = t_o\rho_o + t_i\rho_i$$

In the case of the oxide cathode $t_o \gg t_i$, because t_o is in the range of $\sim 65 \mu m$ and t_i is in the range of few micrometers.

$$t_o\rho = t_o\rho_o + t_i\rho_i$$

By substituting conductivity for resistivity, the formula becomes:

$$\frac{t_o}{\sigma} = \frac{t_o}{\sigma_o} + \frac{t_i}{\sigma_i}$$

hence:

$$\frac{1}{\sigma} = \frac{\sigma_i + (t_i/t_o)\sigma_o}{\sigma_o\sigma_i}$$

and then:

$$\sigma = \frac{\sigma_o\sigma_i}{\eta\sigma_o + \sigma_i}$$

Where $\eta = \frac{t_i}{t_o}$.